

**DOCKET NO: A-93-02  
V-B-7**

**TECHNICAL SUPPORT DOCUMENT FOR  
§194.23: GROUND WATER FLOW AND CONTAMINANT  
TRANSPORT MODELING AT WIPP**

**U.S. ENVIRONMENTAL PROTECTION AGENCY  
Office of Radiation and Indoor Air  
Center for the Waste Isolation Pilot Plant  
401 M. Street, S.W.  
Washington, DC 20460**

**MAY 1998**

Technical support for this document was provided by Sandy Cohen and Associates, Inc. and/or its subcontractors under EPA Contract 68D70073.

Contents

1. Introduction .....	1-1
2. Objectives .....	2-1
3. Problem Conceptualization .....	3-1
3.1 1992 PA Conceptual Model .....	3-1
3.2 Conceptual Model for STAFF3D .....	3-3
3.3 STAFF3D Capabilities .....	3-4
4. Model Formulation .....	4-1
4.1 Spatial Discretization .....	4-1
4.2 Parameterization - Source Term .....	4-9
4.3 Parameterization - Single Porosity Base Case .....	4-14
4.3.1 Borehole .....	4-14
4.3.2 Repository .....	4-16
4.3.3 Salado .....	4-23
4.3.4 Culebra .....	4-29
4.4 Data Input - Dual Porosity Base Case .....	4-34
4.4.1 Culebra - Fracture Properties .....	4-35
5. Description of Model Simulations and Discussion of Results .....	5-1
5.1 Modeling Results - General Discussion .....	5-2
5.1.1 Single Porosity Simulations .....	5-5
5.1.2 Dual Porosity Simulations .....	5-17
5.2 Issue Specific - Results and Conclusions .....	5-18
5.2.1 Issue 1 - Solubility Limited Assumptions .....	5-21
5.2.2 Issue 2 - Castile Brine Reservoir/Multiple Intrusions (E1E2) .....	5-22
5.2.3 Issue 3 - Decoupling of Repository from Culebra .....	5-28
5.2.4 Issue 4 - Mass Balance and Discretization .....	5-29
5.2.5 Issue 5 - Treatment of Fracture Hydraulic Conductivities .....	5-35
5.2.6 Issue 6 - Travel Time Analysis .....	5-37
5.2.7 Issue 7 - Permeability of Culebra Specified in BRAGFLO .....	5-39
5.2.8 Issue 8 - Borehole Permeability .....	5-42
6. References .....	6-1

Appendix S- Supplemental STAFF3D Modeling

Appendix Kd- Assessment of Selected Distribution Coefficients used in CCA

## Tables

Table 1.1.	Summary of Computer Models Used in the 1992 WIPP Performance Assessment To Calculate Scenario Consequences . . . . .	1-3
Table 4.1.	Model Parameterization--Single Porosity Base Case . . . . .	4-11
Table 4.2.	Culebra Fracture Properties . . . . .	4-35
Table 5.1.	Input Parameters for Single Porosity Simulations . . . . .	5-6
Table 5.2.	Input Parameters for Dual Porosity Simulations . . . . .	5-8
Table 5.3.	Hydraulic Property Data for the Culebra Dolomite . . . . .	5-38

## Figures

Figure 1.1	Models used in 1992 WIPP performance assessment. The names for computer models (i.e., computer codes) are shown in capital letters. . . . .	1-4
Figure 4.1	WIPP land withdrawal boundary . . . . .	4-2
Figure 4.2	Model layout in three Dimensions . . . . .	4-3
Figure 4.3	Diagram of repository with respect to geology . . . . .	4-4
Figure 4.4	Pore Volume waste (m <sup>3</sup> ) . . . . .	4-5
Figure 4.5	System conceptualization . . . . .	4-6
Figure 4.6	Identification of pathways within Culebra Dolomite from release points above the corners and center of the waste-panel layout . . . . .	4-8
Figure 4.3.1.	Volume average gas pressure in waste (Pa) . . . . .	4-17
Figure 4.3.2.	Calculated lithostatic and hydrostatic pressures with depth (SAND93-00700, Vol 3 p. 2-40). . . . .	4-19
Figure 4.3.3.	E1E2 scenario, intrusion at 1000 yr: cumulative brine flow up the borehole (m <sup>3</sup> ). . . . .	4-20
Figure 4.3.4.	SANCHO results: porosity as a function of time for various constant gas-generation rates (f values), porosity based on BRAGFLO definition of porosity (ratio of void volume to initial room volume). . . . .	4-22
Figure 4.3.5	Pore volume in waste (m <sup>3</sup> ). . . . .	4-22
Figure 4.3.6.	Steady-State Flow Simulation, Non-Intrusion Scenario . . . . .	4-25
Figure 4.3.7.	Steady-State Flow Intrusion Scenario . . . . .	4-26
Figure 4.3.8.	Adjusted potentiometric surface of the Culebra Dolomite Member of the Rustler Formation in the WIPP vicinity (Brinster, 1991). . . . .	4-30
Figure 4.3.9.	Culebra freshwater heads at the WIPP - area boreholes . . . . .	4-31
Figure 5.1.	Plan view of the head distribution (m) in the Salado before borehole the intrusion. . . . .	5-3

Figures (Continued)

Figure 5.2. Plan view of the Steady-state potentiometric surface for Culebra Dolomite 5-4

Figure 5.3. Potentiometric surface for Culebra Dolomite after borehole intrusion (Pus.k20) ..... 5-4

Figure 5.4. Potentiometric surface of the Culebra Dolomite after borehole intrusion ..... 5-11

Figure 5-5. Pressure within the repository with respect to time ..... 5-12

Figure 5-6. Pressure within the Culebra at intrusion borehole with respect to time after intrusion ..... 5-12

Figure 5.7. Areal representation of plutonium plume ..... 5-15

Figure 5-8. Breakthrough curve of Pu-239 Concentration at the well in Culebra (Single Porosity Simulations) ..... 5-16

Figure 5-9. Cumulative curies exiting out of the well and into the Culebra (single porosity simulations). ..... 5-16

Figure 5-10. Breakthrough Curve of Pu-239 Concentration at the well in Culebra (dual porosity simulation) ..... 5-19

Figure 5-11. Cumulative curies exiting out of the well into Culebra (dual porosity simulations) ..... 5-20

Figure 5-12. Breakthrough of the hydraulic head in the repository (dual porosity simulation) ..... 5-21

Figure 5-13. Breakthrough curve of Pu-239 concentration at the well in Culebra (dual porosity simulations) ..... 5-23

Figure 5-14. E2 scenario, intrusion at 1000 yr: cumulative brine flow up borehole (m<sup>3</sup>). ..... 5-25

Figure 5-15. Nodal flux locations and cumulative curies exiting from the well into Culebra. .... 5-26

Figure 5-16. Breakthrough curve of Pu-239 concentration at the well in Culebra (single porosity simulations) ..... 5-30

Figures (Continued)

Figure 5-17. Breakthrough concentration of Pu-239 at the Boundary of the WIPP site for steady-state and transient flow runs. . . . . 5-30

Figure 5.18. Breakthrough curve of Pu-239 concentration at the well in the repository (single porosity simulations) . . . . . 5-33

Figure 5.19. Breakthrough curve of Pu-239 concentration at the well repository (dual porosity simulations) . . . . . 5-33

Figure 5.20. Breakthrough concentration of Pu-239 at the boundary of WIPP site (single porosity simulations) . . . . . 5-40

Figure 5.21. Travel time results with Culebra hydraulic conductivity at 20 m/y . . . . . 5-41

Figure 5.22. Cumulative volume of water exiting out of the well (single porosity simulations) . . . . . 5-43

Figure 5.23. Cumulative volume of water exiting out of the well into culebra (dual porosity simulations) . . . . . 5-44

Figure 5.24. Cumulative curies exiting out of the well into culebra (single porosity mode with 10 boundary flux nodes) . . . . . 5-44

Figure 5.25. Cumulative curies exiting out of the well into culebra (dual porosity mode with 10 boundary flux nodes) . . . . . 5-45

## 1. Introduction

DOE's submittal of their 1992 PA (Docket: A-93-02, Ref# 563) raised a number of issues in which EPA identified potential concerns. With the exception of the distribution coefficient analyses presented in Appendix Kd, all of the modeling described in this report is focused on addressing issues that EPA identified during their review of the 1992 PA. In some instances, DOE has changed their 1992 PA modeling approach for the CCA or modified the assumptions upon which the modeling was based. In many of these situations the Agency's original concerns are no longer relevant; and in other cases the issues have been resolved through other means (e.g., additional data). In order to place EPA's modeling work in context with the CCA, this report has recently been edited and areas that are particularly relevant to the CCA are noted.

The 1992 WIPP Performance Assessment (PA) addresses a series of scenarios that could potentially result in contaminant releases to the accessible environment. These scenarios in the 1992 PA (A-93-02, Ref# 563) were obtained by Sandia National Laboratories using the following nine computer codes as indicated in Figure 1-1; CUTTINGS, BRAGFLO, PANEL, SECOFL2D, SECOTP2D, GRASP\_INV, CCDFPERM (this code was replaced by CCDFGF for the CCA, see Section 5.4.12 of the Technical Support Document (TSD) for Models and Computer Codes, A-93-02, V-B-6), GENII-S AND SANCHO (this code was replaced by SANTOS for the CCA, see Section 5.4.11 of the TSD for Models and Computer Codes, A-93-02, V-B-6). In the 1992 PA, radionuclide transport in the repository and along the marker beds was not simulated, however, for the CCA, DOE used the computer code BRAGFLO\_DBR and NUTS to simulate transport of radionuclides within the repository and marker beds (see Sections 4.5.1 and 5.4.4 of the TSD for Models and Computer Codes, A-93-02, V-B-6). Brief descriptions of the 1992 PA models are given in Table 1.1.

In both the 1992 PA and CCA, all of these codes are interlinked by their input and output requirements, for example, SANTOS/SANCHO is used to calculate porosity values of the waste contained in the repository. These values are used as input to BRAGFLO and BRAGFLO\_DBR which, in turn, models the brine and gas movement into, and out of the repository to the Culebra Dolomite. The output of BRAGFLO or BRAGFLO\_DBR, which is in the form of gas and brine fluxes is input into NUTS or PANEL (see Section 4.6 of the TSD for Models and Computer Codes, A-93-02, V-B-6). PANEL subsequently performs a series of solubility calculations to estimate the curies of each respective radionuclide that are

released to the Culebra Dolomite. NUTS uses the velocity field calculated from BRAGFLO or BRAGFLO\_DBR to calculate the releases up an intrusion borehole and along the anhydrite marker beds. These radionuclide concentration data are used in SECOTP2D as a boundary condition for the prediction of flow and transport to the accessible environment.

Ideally, a single computer code would be used to simulate all of the physical and chemical processes that affect the radionuclide transport rates and release concentrations from the repository to the Culebra Dolomite. However, this type of fully integrated approach is simply not feasible given the constraints of the software and hardware technology in conjunction with the computational intensity of the Performance Assessment simulations. Therefore, many of the physical processes have been decoupled from one another by using the output from one code as the input to a complementary code.

This decoupling of the physical system via the linking of the input and output from the various models has raised concerns pertaining to the loss of continuity in the overall modeling approach and in the representativeness of the modeling results to the actual system. Furthermore, the 1992 PA placed a heavy reliance on Latin Hypercube Sampling to reflect uncertainty in the cumulative probability distribution functions. This statistical approach makes it difficult to isolate the effects caused by either a single parameter or a suite of constructed parameters. To address some of these concerns an independent modeling effort has been initiated and is focused on using the computer code STAFF3D (Solute Transport And Fracture Flow in 3 Dimensions)(Huyakorn et. al.1992) to perform a number of bounding analyses to isolate key parameters and processes. The STAFF3D modeling fully couples the flow and transport processes from the repository to the Culebra Dolomite. STAFF3D is a descendent of STAFF2D which was used by DOE in the 1991 PA to predict flow and transport within the Culebra to the accessible environment.

Table 1.1. Summary of Computer Models Used in the 1992 WIPP Performance Assessment To Calculate Scenario Consequences

Model	Description
BRAGFLO	Describes the multiphase flow of gas and brine through a porous, heterogenous reservoir. BRAGFLO solves simultaneously the coupled partial differential equations that describe the mass conservation of gas and brine along with appropriate constraint equations, initial conditions, and boundary conditions. Additional information: Chapters 4 and 5 (A-93-02,Ref# 563).
CCDFPERM	Constructs probabilities and consequences for various computational scenarios associated with human intrusion by exploratory drilling. Also constructs CCDF's. Additional information: Section 1.4.2 of Volume 3 (A-93-02,Ref# 563).
CUTTINGS	Calculates the quantity of radioactive material brought to the surface in cuttings and cavings generated by an exploratory borehole that penetrates a waste panel. Additional information: Chapter 7. (A-93-02,Ref# 563)
GENII-S	Estimates potential radiation doses to humans from radionuclides in the environment. Additional information: Leigh et al., 1993.
GRASP_INV	Generates transmissivity fields (estimates of transmissivity values) conditioned on measured transmissivity values and calibrated to steady-state and transient pressure data at well locations using an adjoint sensitivity and pilot-point technique. Additional information: (A-93-02,Ref# 390).
PANEL	Calculates rate of discharge and cumulative discharge of radionuclides from a repository panel through an intrusion borehole. Discharge is a function of fluid flow rate, elemental solubility, and radionuclide inventory. Additional information: WIPP PA Division 1991b, Section 5.3. (A-93-02,Ref# 563)
SECO-FLOW	Calculates single-phase Darcy flow for groundwater-flow problems in two dimensions. The formulation is based on a single partial differential equation for hydraulic head using fully implicit time differencing. Additional information: Chapter 6. (A-93-02,Ref# 563)
SECO-TRANSPORT	Simulates fluid flow and transport of radionuclides in fractured porous media. Additional information: Chapter 6. (A-93-02,Ref# 563)
SANCHO	Solves quasistatic, large deformation, inelastic response of two-dimensional solids with finite element techniques. Used in the 1992 performance assessment to determine porosity of the waste as a function of time and cumulative gas generation. Additional information: Section 1.4.7 of Volume 3 (A-93-02,Ref# 563).

STAFF3D is ideally suited for predicting flow and transport through fractured media, and therefore is primarily used as an analog to the SECO codes. Neither STAFF3D nor the SECO codes simulate multiphase flow and transport or rock consolidation behavior. This limitation, however, is not a major concern in that the STAFF3D analyses are primarily of a scoping nature and are focused on the Castile brine-intrusion scenarios (E1) and the accompanying effects on flow and transport in the Culebra dolomite. The intention of this modeling was not

only to evaluate the sensitivity of the results to various suites of parameters but also to provide a framework from which additional scenarios and bounding analyses can be performed. Additional analyses are found in Appendices A and B which explore more in

depth some of the main repository

the issue of the near

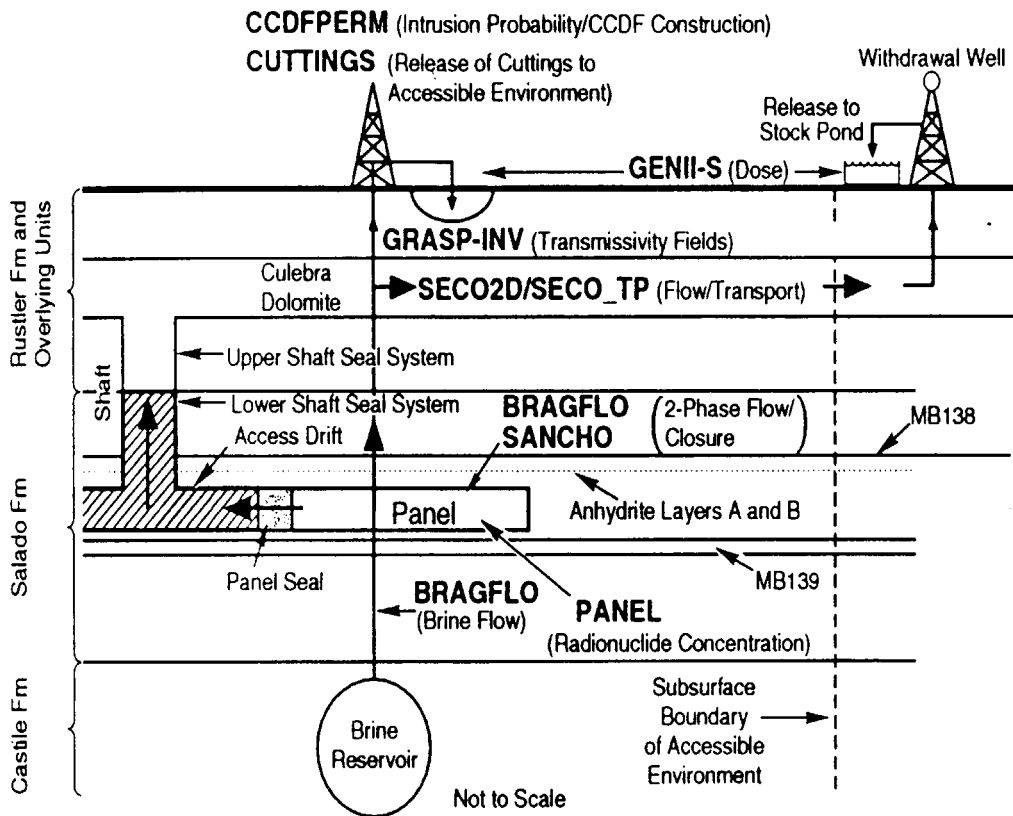


Figure 1.1 Models used in 1992 WIPP performance assessment. The names for computer models (i.e., computer codes) are shown in capital letters. (A-92-03, Ref #563). (Note that SANTOS is now used instead of SANCHO and NUTS performs radionuclide transport within the repository and Salado).

## 2. Objectives

The primary objective of the STAFF3D modeling was to develop a means by which components of the conceptual model presented in the 1992 PA and CCA could be independently tested. It is not the objective of this modeling to predict the number of curies that would reach the WIPP Land Withdrawal Boundary, but rather to identify the parameters and processes that most influence the modeling results. To accomplish this goal, this modeling study focuses on the construction of an analogous system to that presented in the 1992 PA, by which the sensitivity of the results to various parameters and assumptions can be evaluated.

This approach should provide a better understanding of the system behavior, and of the appropriateness of both the formulation of the 1992 conceptual models and of their implementation in the 1992 PA. All of the objectives of the STAFF3D modeling are focused on the disturbed case scenarios performed in the 1992 PA, specifically, the E1 and E2 scenarios. The E2 scenario evaluates the effects that an exploratory borehole would have on the radionuclide release if the borehole were to intercept the repository. Alternatively, the E1 scenario assumes that the repository has been breached by a borehole, but also simulates the effects on groundwater flow and radionuclide transport if the borehole were to penetrate a Castile brine reservoir that is assumed to reside approximately 240 meters beneath the repository. (The E1 Scenario is shown in Figure 1.1).

To facilitate the presentation of the modeling results, the specific modeling objectives have been arranged into a series of issues that have direct relevance to the 1992 PA and CCA. These issues are briefly described below and are discussed in greater detail in Section 5.0, and essentially all of these issues have been resolved in the CCA.

### 1992 PA - Issue 1

The 1992 PA assumes that the release of radionuclides from the repository will be controlled by their solubility. However, Sandia used an inventory limited approach until more data became available. Therefore, one of the objectives of the STAFF3D modeling was to estimate at what rate the wastes would be released under various flow and transport scenarios if their release

was inventory limited.<sup>1</sup> Now that the CCA contains reliable predictions regarding radionuclide solubilities the releases are not necessarily controlled by the inventory release limits (see A-93-02, II-G-1, Volume XVII, Appendix SOTERM).

Time-dependent release rate calculations performed with STAFF3D indicate in an E1-type scenerio almost all of the curies that are ultimately released from the repository up the intrusion borehole and into the Culebra are released within 500 years after the intrusions occur. It would be expected that the most conservative PANEL results would also predict comparable release rates. Time dependent results from PANEL, however, are not currently available for comparison.

#### *RELEVANCE TO CCA*

EPA performed a detailed review of the means in which DOE treated the actinide source term (see EPA's Technical Support Document for DOE's Actinide Source Term, A-93-02, V-B-17). As discussed in that document, EPA has concluded that DOE has adequately treated the actinide source term for performance assessment.

#### 1992 PA - Issue 2

The 1992 PA does not explicitly model radionuclide transport within the repository. The computed flux from BRAGFLO is input into PANEL which determines a release rate to the Culebra. One of the enhancements currently planned for BRAGFLO is the coupling to a transport code for the repository. Therefore, the assumed intrusion location(s) for any borehole(s) which penetrate the Castile brine reservoir will have an effect on the release rates. The effect of multiple intrusions on the flow and transport is termed an E1E2-type scenerio in the 1992 PA. One of the STAFF3D modeling objectives is to estimate the sensitivity to the number of boreholes and the intrusion location(s) relative to the radionuclide release values.

Both the number of intrusions (simulated as prescribed flux nodes) in the repository and their respective locations were found to have considerable impact on the quantity of radionuclides that move out of the repository through the borehole. When two flux nodes are placed vertically along the borehole, the brine contributed to the flow system by these nodes rushed up through the borehole, immediately after it was opened, leaving behind radionuclides that are located further away from the borehole. On the other hand, with 4 flux nodes placed at corners of the repository, the brine is in

---

<sup>1</sup> Inventory limited assumes that all of the waste is in solution and consequent releases are not based on solubility limits.

contact with larger portions of the waste and is able to drive greater quantities of radionuclides up the borehole. One consequence of the 4 corner nodal arrangement is that the radial flow originating from the flux nodes transports some of the brine and radionuclides into the adjacent parts of the Salado, thereby increasing the travel time for these radionuclides to reach the Culebra Dolomite. Distributing the brine flux uniformly in 10 nodes (4 m<sup>3</sup>/y each) allows brine to be in contact with the largest surface area of the waste, of the three nodal distributions examined. Thus, maximizing the migration of radionuclides from the repository. All of the remaining STAFF3D simulations that assume the borehole penetrates the Castile brine reservoir use the 10 node arrangement.

#### *RELEVANCE TO CCA*

As indicated above, the computer simulations performed in the 1992 PA did not account for radionuclide transport within the repository. However, for the CCA, DOE did couple the flow fields calculated with BRAGFLO to the transport mechanisms simulated with the computer code NUTS (see Section 4.4.10 of EPA's TSD for 194.23: Models and Computer Codes, A-93-02, V-B-6). EPA's conclusions regarding DOE's work, with respect to this issue, is that it is adequate to support the CCA.

#### 1992 PA - Issue 3

In the 1992 PA, the flow and transport processes active in the repository were effectively decoupled from those in the Culebra. That is, the output from PANEL consists of radionuclide concentrations which are subsequently input into SECO codes, which in turn simulates flow and transport through the Culebra to calculate cumulative releases at the WIPP Land Withdrawal Boundary. The flux, however, that is calculated to move up the borehole by BRAGFLO is not introduced into the Culebra. Therefore, the influence of water flowing out of the borehole on the ambient flow field of the Culebra is not considered in the 1992 PA analysis. The effect that this perturbation may have on the groundwater gradients could impact the estimates made in the 1992 PA regarding the cumulative mass reaching the accessible environment over the 10,000 year simulation.

The STAFF3D analyses indicate that if the flux from the repository is introduced to the Culebra there is a significant increase in radionuclide velocities to the WIPP Land Withdrawal Boundary. Additional analyses are presented in the Supplemental Report that also supports these preliminary findings.

#### *RELEVANCE TO CCA*

As indicated above the computer simulations performed in the 1992 PA decoupled the flow fields of the repository and the Culebra. EPA's initial concern was that the volume of flow up the borehole would perturb the Culebra flow system. However, the volume of water predicted to flow up the borehole in a human intrusion scenario is relatively small and is significantly less in the CCA, than that which was predicted in the 1992 PA. Therefore, steady-state assumptions on the flow field appear to be reasonable because the volume of flow up the borehole and therefore in the Culebra member will be relatively small with respect to the flow field (Docket: A-93-02, II-G-1, Reference # 542, Reeves et al 1991, page 3-12). Furthermore, the contaminant introduced into the Culebra is immediately dispersed into the fractures over a grid block that is 50 m<sup>2</sup>. DOE's approach artificially introduces instantaneous advection over this area which should approximate the initial fast advection adequately (Docket: A-93-02, II-G-11, *Analysis Package for Culebra Flow and Transport*, WPO #40516, page 26).

#### 1992 PA - Issue 4

In the 1992 PA, the model domain for BRAGFLO had what appeared to be a relatively coarse discretization. To provide some perspective on the mass balance problems to which BRAGFLO may be subject, a general discussion of the STAFF3D mass-balance results with respect to the model domain discretization is presented.

The grid that was ultimately used for STAFF3D that resulted in reasonable mass balance errors (less than 5%) was far more finely discretized than the grid used for BRAGFLO in the 1992 PA. The STAFF3D grid used 528 nodes to define the waste region in a panel, whereas, BRAGFLO incorporated 256 nodes to discretize the entire panel. These results do not indicate that BRAGFLO has experienced mass-balance difficulties, but only suggest that this is an area that should receive additional attention.

#### *RELEVANCE TO CCA*

To address this issue of whether the grid used for BRAGFLO was fine enough to attain a converged solution, EPA requested that DOE perform a detailed grid convergence study on the same grid as that used for the CCA calculations (A-93-02, II-I-16). DOE completed this work ( "Sensitivity of Flow, Transport, and Direct Brine Release to Grid Refinement Using the BRAGFLO and NUTS Computer Models") and a subsequent review by EPA indicated that the grid spacing used in the CCA will adequately characterize the problem and the numerical solution produced adequate results.

#### 1992 PA - Issue 5

The SECO flow and transport modeling performed in the 1992 PA appears to have randomly adjusted the effective porosities of the fractures, independent of the fracture spacing or of the Culebra transmissivity (aquifer thickness multiplied by hydraulic conductivity). The failure for the fractures to properly account for a change in transmissivity could significantly bias the modeling results.

In the 1992 PA, a series of transmissivity fields were used for modeling the Culebra Dolomite. Each of these fields is divided into a number of regions of varying hydraulic conductivities. The thickness of the Culebra is held constant at 7.7 m, therefore, the hydraulic conductivity is heterogeneous within each of the transmissivity fields. To conserve mass, each of the various transmissivity regions would need different fracture properties depending on the hydraulic conductivity assigned to the region. Not only does the 1992 PA not take this approach but it also assumes a single fracture hydraulic conductivity (i.e., effective porosity/ aperture) regardless of the Culebra transmissivity. Furthermore, the fracture aperture is sampled independently from the fracture spacing which means that single fractures could have very small apertures or many fractures could have very large apertures. This approach to the assignment of fracture properties and the effect of this random sampling on dependent variables was further reviewed in Appendix S to this TSD.

#### *RELEVANCE TO CCA*

As indicated by EPA's concern, one might suspect the possibility of some correlation between sampled Culebra transport parameters. Culebra physical transport parameters for which values are used in performance assessment consist of Culebra thickness, matrix tortuosity, diffusive porosity, advective porosity, matrix block length, and dispersivity. To test this possibility of correlation, DOE prepared scatter plots of interpreted results from the hydopad test sites which yielded the physical transport parameters used to develop the PA parameters distributions (H-3, H-11, and H-19) (Docket: A-93-02, II-G-1, Volume X, Appendix MASS, Attachment MASS 15-10, Figures 1 and 2). Figure 1 shows plots, constructed using transmissivity and physical transport parameters inferred from hydraulic and tracer test results at the H-3, H-11 and H-19 hydopads Beauheim 1987, Beauheim 1989, Docket: A-93-02, II-G-1, Reference #41, Reference #44 and Holt (1997). A review of the plots presented in Figure 1 of MASS Attachment 15-10 reveal no obvious correlations between transmissivity and the physical transport parameters. It has been noted that in some cases plotting scattergrams of the serial ranks of the parameters can reveal correlations which are unapparent from scattergrams of parameter values Helton et. al., (1992) - (Docket: A-93-02, II-G-1, Reference # 563, Volume 4). Therefore, DOE also plotted the serial rank of both the advective porosity and the matrix block length against

the serial rank of transmissivity and against each other. These scatter plots are presented as Figure 2 in MASS Attachment 15-10, and again no correlations are apparent. Furthermore, no trends or zoning patterns are apparent in the distribution of physical transport parameters across the WIPP site. Based on these results DOE and EPA have concluded that no correlations exist between transmissivity and physical transport parameters for the Culebra dolomite. EPA also required DOE to ensure that the uncertainty ranges placed on the parameters would not result in unrealistic combinations (Docket: A-93-02, II-G-1, Volume XI, Appendix PAR, page PAR-189). EPA believes that the work documented by DOE has adequately evaluated potential correlations between porosity and transmissivity and that none exist.

#### 1992 PA - Issue 6

In the 1992 PA, travel times in the Culebra to the accessible environment are presented. The modeling results for single porosity non-fractured media in the 1992 PA are summarized by the following. "...90 percent of the travel times were longer than 12,000 yr., 50 percent of the travel times were longer than 18,000 yr., and 10 percent of the travel times were longer than 27,000 yr." The STAFF3D modeling provides a method to determine whether these travel times are realistic and in accordance with the available field data.

The transmissivity field(s) used for the 1992 PA are comprised of multiple blocks (or zones) of various dimensions which are assigned uniform permeability values within each block. The 1992 PA assumes that the mean hydraulic conductivity for the Culebra Dolomite is 7 m/y. STAFF3D travel-time analyses suggest that the overall combined effect of these composite permeabilities yield travel times far shorter than that which would be expected had the mean hydraulic conductivity of 7 m/y been used over the entire field. Furthermore, the assumption that 7 m/y is the mean value of hydraulic conductivity is not supported by the measured field data over the travel path of the radionuclides.

#### *RELEVANCE TO CCA*

To address these issues the Agency asked DOE to perform the following end-to-end-test in order to address EPA's concerns (A-93-02, II-I-17, bottom of page 3):

- Generate a synthetic data set that is statistically similar to the WIPP-site data to be used to evaluate the statistical validity of GRASP\_INV results.
- Process the synthetic data with GRASP\_INV to produce 100 calibrated transmissivity fields, input the fields to SECOFL2D to produce velocity fields, and input the velocity fields to TRACKER to produce travel paths

from 20 release points to a compliance boundary.

The response to the need for an end-to-end functional requirement and test is provided by the test presented in Lavenue, 1997 (A-93-02, II-I-19; WPO #44199). The response presented in Lavenue, 1997, addressed the issues raised above. As discussed in detail in Section 5.6 of the TSD for Section 194.23: Models and Computer Codes (A-93-02, V-B-6), EPA finds that the results of this test indicate that DOE's treatment of the transmissivity fields is adequate.

#### 1992 PA - Issue 7

The modeling that was performed with BRAGFLO in the 1992 PA included flow into the Culebra. The Culebra was assigned a hydraulic conductivity of 7 m/y. However, this value was not statistically sampled as part of the LHS procedures and no analyses were presented to demonstrate the sensitivity of the modeling results to this parameter.

STAFF3D results indicate that the brine volumes predicted by BRAGFLO to move up the borehole are insensitive to the value of permeability assigned to the Culebra over the range of tested values. This conclusion supports the approach taken in the 1992 PA.

#### *RELEVANCE TO CCA*

As noted above, the STAFF3D modeling indicated that DOE's approach in the 1992 PA was adequate. Furthermore, since their approach has not fundamentally changed in the CCA, with respect to the treatment of the Culebra properties in BRAGFLO, EPA has determined that DOE's approach is appropriate and it is unnecessary to statistically sample the Culebra properties in the BRAGFLO simulations.

#### 1992 PA - Issue 8

The modeling in the 1992 PA indicated that the results were very sensitive to the assumed permeability of the borehole. This value may be assigned based on regulatory guidance rather than laboratory or field tests. Therefore, the effect on the results should be independently substantiated.

STAFF3D results demonstrate that the volume of brine flowing up the borehole, particularly for the E1 intrusion scenario, is sensitive to the borehole permeability. However, this STAFF3D sensitivity analysis was rather limited in scope. Furthermore, the amount of curies that were released to the Culebra was relatively insensitive to the borehole permeability because the inventory based approach allowed the majority of radionuclides to flow up the borehole at all of the permeabilities tested.

## RELEVANCE TO CCA

The EPA undertook several activities that investigated the effect that borehole permeability has on the CCAPA results. First, the EPA performed a parameter sensitivity analysis (A-93-02,V-B-13) and second the EPA required DOE to perform a Performance Assessment Verification Test (PAVT) in which the borehole permeability was one of the parameters that was varied (A-93-02,V-G-26). The Agency has determined that the combined results of these analyses indicate that DOE's approach is adequate.

### 3. Problem Conceptualization

As mentioned previously, all of the STAFF3D simulations were directed at evaluating two major scenarios. In the first scenario, flow and transport simulations were made without considering the effect of a brine source located below the repository (E2). The second scenario takes into account contribution of the brine source to the flow system (E1). Under each scenario, several simulations were made to examine the effects of various model input parameters and processes.

The primary pathways for the potential migration of the contaminants from the repository to the accessible environment considered in the E1 and E2 scenarios may be broken into two segments: (1) upward migration through the abandoned borehole, and (2) release of the contaminant into the Culebra dolomite and subsequent migration towards the site boundary. The number of curies that will be released and their migration rates will be dependent upon a number of factors which comprise the various components of the conceptual model.

The following subsections present the components of the 1992 PA conceptual model and compare the differences among the 1992 conceptual model and aspects of the conceptual model as it is simulated with STAFF3D. The most significant difference between the 1992 PA conceptual model of the Culebra, with that of the CCA, is that the effective thickness was reduced from 7.7 m to 4.0 m. This would, however, have essentially no impact on any of the conclusions drawn from the STAFF3D modeling results.

#### 3.1 1992 PA CONCEPTUAL MODEL

The primary components of the conceptual model presented in the 1992 PA consist of the following:

##### *Borehole*

- The borehole is not present until 1,000 years after the wastes have been emplaced.
- The borehole is uncased and filled with sediment.
- The borehole penetrates the repository in the E2 scenario, and penetrates both the waste and a Castile Formation brine reservoir in the E1

scenario.

- An impermeable plug seals the borehole immediately above the Culebra Dolomite.

### *Repository*

- The waste repository is situated 600 meters below land surface within the Salado formation. A disturbed rock zone completely surrounds the repository.
- Dimensions are equal to those of 1 (of 8) panel.
- Brine flow within the repository is described by Darcy's law, and the waste is assumed to be homogeneous and isotropic.
- The repository is depressurized over the operational period of the repository (i.e. initial conditions of the repository are set to atmospheric).
- Porosity of the waste changes with time as a function of gas generation rates and the porosity is calculated with SANCHO (rock creep characteristics)
- Permeability of the waste and panel dimensions remain fixed with time.
- The number of curies assumed to be in the repository are equivalent to those expected to be contained in one panel (or one-eighth the anticipated inventory).
- Brine is consumed and gas is generated from degradation of the wastes.

### *Castile*

- The Castile is impermeable and is situated 240 meters below the repository.
- A pressurized brine reservoir is assumed to lie beneath the repository in the Castile.

### *Salado*

- Brine flow within the Salado is described by Darcy's law, and the salt is assumed to be homogeneous and isotropic.
- Anhydrite marker beds of higher permeability are present in the Salado

which connect the repository to the far field.

- A disturbed rock zone of higher permeability immediately surrounds the repository.
- The Salado, in the vicinity of the waste, is depressurized over the operational period of the repository (i.e. initial conditions of the repository are set to atmospheric).
- Lateral boundary conditions are set to far field pressures.

#### *Culebra*

- Brine exiting the borehole essentially vanishes from the model domain and does not enter the Culebra.
- No areal recharge moves into the unit.
- Ground-water flow and transport within the unit is controlled by steady-state conditions.
- Ground-water flow and radionuclide transport are controlled by horizontally oriented parallel fractures which are described by a dual porosity approach.
- The unit is a uniform thickness of 7.7 meters.
- The heterogeneous nature of the unit is described by the 70 transmissivity fields obtained from GRASP\_INV and dispersion is a function of matrix block size.
- Lateral boundaries are set to constant head and no-flow values.

### 3.2 CONCEPTUAL MODEL FOR STAFF3D

Only the components of the 1992 PA conceptual model which have been altered for the STAFF3D modeling are described below. Additional clarification on how these differences are treated in the model, and the effects on the modeling results are provided in Sections 4 and 6.

#### *Borehole*

- Essentially identical to the 1992 PA conceptual model.

### *Repository*

- Radionuclide concentrations are assumed to be inventory limited.
- The repository is saturated with brine throughout the simulation.
- No gas is generated (i.e., all flow is in a single liquid phase).
- Initial pressures are assigned based on gas and brine pressures presented in the 1992 PA, after 1000 years of gas generation.
- The porosity of the wastes does not change with time.
- The repository volume only considers the volume for the wastes and not the backfill, seals, etc.

### *Castile*

- The influx of the Castile brine to the repository is simulated by a number of flux nodes placed directly within the repository.

### *Salado*

- The Salado is assumed to be homogeneous and isotropic (i.e., a disturbed rock zone and anhydrite marker beds are not modeled).
- The Salado is not assumed to become depressurized to atmospheric conditions during the operational phase in the repository history.

### *Culebra*

- Brine exiting the borehole enters the Culebra, and affects the flow field.
- The transmissivity is homogeneous (uniform thickness of 7.7 m and uniform hydraulic conductivity).

## 3.3 STAFF3D CAPABILITIES

Groundwater flow and transport modeling was performed using the numerical, three-dimensional model STAFF3D (HydroGeoLogic, 1992). STAFF3D is a finite element code for simulating groundwater flow and transport of dissolved chemical or radioactive species

in fractured or porous media. STAFF3D is a descendant of the public domain 2D model, TRAFRAP. The original model was extended to three-dimensions and other enhancements were added for simulating flow and transport through fractured formations underlying the Yucca Mountain, Nevada, proposed high level waste repository site.

The key assumptions of the STAFF3D computer code are summarized below:

- Flow in the rock matrix and fractures obeys Darcy's Law.
- Only single-phase flow is modeled. For variably saturated conditions, the air phase is assumed to be inactive.
- For fractured reservoir systems, the aperture of the fractures is assumed to be very small compared with other dimensions in the fracture plane.
- Temperature effects on the flow properties are assumed to be negligible.
- Transport in the porous medium is governed by Fick's Law. The hydrodynamic dispersion coefficient is defined in terms of the coefficients of mechanical dispersion and molecular diffusion. The medium dispersivity is assumed to correspond to that of an isotropic porous medium and hence related to two constants, longitudinal and transverse dispersivities.
- The adsorption and decay of chemical species are described by a linear equilibrium isotherm and a set of first-order constants.

## 4. Model Formulation

### 4.1 SPATIAL DISCRETIZATION

The size of the grid used for the STAFF3D model corresponds to the WIPP Land Withdrawal Boundary which is 4 miles  $\times$  4 miles (6437 m  $\times$  6437 m) (Figure 4.1). The five-layer numerical model consists of 48,070 nodes and 42,300 elements (Figure 4.2). The size of the grid blocks vary from 15 m in the vicinity of the borehole to 286 m at the extreme northern boundary of the model. Since flow in and out of the borehole is radial, a line of symmetry along the x-axis (longitudinal distance) and passing through the center of the well is conveniently drawn. Taking advantage of this symmetry, only half of the original domain is modeled, thus reducing the size of the grid and the computation time.

Various types of hazardous wastes and radionuclides may ultimately be placed into the WIPP repository which is at a depth of about 600 m ((Docket: A-93-02, Ref# 563; Vol3., p.3-17) (Figure 4.3). The total excavated volume in the disposal region is  $4.36 \times 10^5 \text{ m}^3$  (Docket: A-93-02, Ref# 563; Vol3., p.3-5). In the 1992 PA, BRAGFLO assumes a repository volume of  $46,064 \text{ m}^3$  for the repository modeling (Docket: A-93-02, Ref# 563; Vol 4., p.5-4). This volume represents one of the eight full-size waste emplacement panels excluding seals as described in Vol. 4 of the PA (Docket: A-93-02, Ref# 563) on Page 5-1:

" The volume of the equivalent panel equals one-tenth of the total storage volume of the repository. This smaller volume is based on the assumption that the panel seals will prevent fluid flow between each of the ten panels; therefore only one of the repository's ten panels is compromised by a borehole intrusion. The volume of this equivalent panel is assumed to equal the volume of one of the eight full-size waste-emplacement panels."

The reported design disposal volume is  $1.756 \times 10^5 \text{ m}^3$  or about 40% of the excavated volume. Therefore, the waste volume in one of the ten equivalent panels would equal  $17,566 \text{ m}^3$ .

STAFF3D also assumes a volume for the repository of approximately  $46,000 \text{ m}^3$ . However, the backfill is assumed to have the same permeability and porosity as the Salado. This assumption should have little affect on the modeling results in that the predominant source of brine in almost all of the analyses was from the Castile brine reservoir and not from the far-field in the Salado.

Image Not  
Available

Figure 4.1 WIPP Land Withdrawal Boundary (Docket: A-93-02, Ref# 563)

Image Not  
Available

Fig. 4.2 Model layout in three Dimensions. (Distance shown along the Y-axis is half of the domain).

Image Not  
Available

Fig. 4.3 Diagram of repository with respect to geology. ((Docket: A-93-02, Ref# 563)

Waste properties in STAFF3D were assigned to a volume of 17,566 m<sup>3</sup>, or ten percent of the total design disposal volume for the waste ((Docket: A-93-02, Ref# 563;Vol3., p.3-11).

As shown in Figure 4.4 the pore volume in the wastes, as predicted with SANCHO (Docket: A-93-02, Ref# 563) quickly decreases from a high value of 66 percent as a function of time, due to the decreasing porosity associated with the room closure. In STAFF3D a value of 20 percent porosity was used to describe the porosity of the waste.

As mentioned previously, the symmetry of the problem required that only half of the model domain to be modeled, however, to facilitate the interpretation of the analysis and to provide greater flexibility in future analyses the entire waste volume of 17,566 m<sup>3</sup> was included in the problem domain. As shown in Figure 4.5, vertical discretization of the repository in the Salado Formation was selected so that the height of the block containing the repository is equal to 3.96 m, the width is 36.4 m and the length is 122 m.



Fig. 4.4 Pore volume in waste (m<sup>3</sup>). (Docket: A-93-02, Ref# 563)

Image Not  
Available

Figure 4.5 System conceptualization

Three brine-yielding units are modeled in the 1992 PA. The uppermost is the Culebra and has a saturated thickness of 7.7 m (Figure 4.5). The height of the grid elements in the Culebra correspond to the thickness (7.7 m) of the unit. The lower brine-yielding formation is the Salado and the STAFF3D modeling assumes a saturated thickness of 18.4 m. As shown in Figure 4.5, this thickness of 18.14 m is considerably less than that which was modeled in the 1992 PA (218. m), and corresponds to the base of the Anhydrite Marker Bed 138 and to the base of Anhydrite Marker Bed 139. It is unlikely that the STAFF3D results are particularly sensitive to the thickness of the Salado, for the E1 scenario because the flow derived from the far-field of the Salado is insignificant when compared with that of the brine introduced to the repository from the underlying Castile reservoir. The E1 scenario would be more sensitive to the Salado thickness than the E2 Scenario, however, the 1992 PA modeling results suggest that the major source of far-field brine is derived from brine migration within the Salado interbeds beds. The STAFF3D modeling does not consider the effects of the interbeds, as the modeling was focused almost entirely on the E1-type scenario, where the interbeds should have limited effect on the modeling results. All the model elements in the material separating the Salado from the Culebra (431.25 m) are not given physical material values (i.e., no flow was assumed into or out of these units) and are not shown in Figure 4.5.

The 1992 PA and the STAFF3D modeling both assume that a human intrusion occurs after a simulated time period of 1000 years. The intrusion consists of a 0.355 m diameter borehole that connects the Culebra to the repository. The borehole in the STAFF3D modeling, is represented by 10 vertical line elements from 2.23 m below the repository to the top of Culebra. The height of the six elements of the borehole through the material between the two formations is 71.87 m each, for a total distance of 431.25 m. The location of the borehole is 2414 m from the WIPP Land Withdrawal Boundary. This distance was also assumed for the 1992 PA modeling (Docket: A-93-02, Ref# 563; Vol4., p.6-7), and is the shortest horizontal distance from the wastes to the accessible environment. However, this distance assumes that radionuclides will flow due south to the WIPP boundary. The 1992 PA and previous investigator's predict a more circuitous route which would result in a mean travel distance of 3600 m as shown by the travel path taken by particle C in Figure 4.1.6 (Docket: A-93-02, Ref# 542).

There are a number of factors which suggest that a more conservative analysis than that taken in the 1992 PA is more appropriate for evaluating the travel path within the Culebra

and



Image Not  
Available

Figure 4.6. Identification of pathways within Culebra Dolomite from release points above the corners and center of the waste-panel layout (Docket: A-93-02, Ref# 542).

includes: a considerable uncertainty regarding both the direction and magnitude of the groundwater gradients; the effect that density dependence may have on the flow field is essentially unknown (this issue is addressed in another TSD titled *Density Effects for Radionuclide Transport in the Culebra at the WIPP site*; A-93-02, V-B-9); low permeability values that are assigned south of the intrusion point cause a southeastern divergence in the flow field that is not substantiated by the field data. To address these concerns EPA reviewed and tested the means by which the transmissivity fields are being constructed in the CCA by GRASP\_INV (see Section 5.4.6 of the TSD for Section 194.23: Models and Computer Codes, A-93-02, V-B-9). Additional STAFF3D simulations were also performed that are designed to test the effect of flow-path lengths on travel times, and is included in the supplemental report in Appendix S.

#### 4.2 PARAMETERIZATION - SOURCE TERM

As discussed in Section 2, it is not the objective of this modeling exercise to predict the normalized releases at the WIPP Land Withdrawal Boundary, but rather to identify the parameters and processes that most influence the modeling results. Therefore, it is desirable to select a radionuclide that has a long half-life so that any decrease in concentrations may be attributed to the flow and transport processes under investigation. Pu-239 has a half-life of  $2.4 \times 10^4$  years and therefore was selected as an appropriate radionuclide. The waste is assumed to lie in the repository for 1000 years before the simulation is started. During this period, it is subject to radioactive decay.

The simulated source-term volume has the dimensions which are equal to one-tenth the total repository disposal volume ( $17,566 \text{ m}^3$ ). Therefore, the level of radioactivity of Pu-239 at the time of waste emplacement was assumed to be one-tenth of the total 1992 PA inventory of contact and remote handled Pu-239 (i.e.,  $3.44 \times 10^5$  curies, (Docket: A-93-02, Ref# 563; Vol 3 p. 3-24), and is, therefore, set to  $3.44 \times 10^4$  curies. The 1000 years of radioactive decay prior to the simulation decreases the curie content to  $3.34 \times 10^4$ . As will be described in Section 5.4.4, the concentration for Pu-239 is dependent upon the repository volume, porosity, specific storage, and change in hydraulic head over the simulation period. However, the assumptions regarding the initial curie content are easily modified without making additional STAFF3D simulations, in that the actual simulations are made by assigning a relative concentration of one to all of the nodes in the waste region of the repository.

### Pu-239 Properties

**Free water diffusion coefficient** - The free water diffusion coefficient is the measured rate at which radionuclides can diffuse from the fractures into and out of the rock matrix. It is this process that leads to the physical retardation of the radionuclides along their travel path.

There is very little discussion in the 1992 PA pertaining to the free water diffusion coefficient values. However, Reeves et. al. (Docket: A-93-02, Ref# 542, p. 236) indicate that diffusivity tends to decrease with increasing salinity and chose for their modeling, a base case value of  $1.7 \times 10^{-6} \text{ cm}^2/\text{sec}$  ( $1.7 \times 10^{-10} \text{ m}^2/\text{sec}$ ) which was based on relatively limited data. The diffusion coefficient range for Pu-239 that is presented in the 1992 PA is  $4.8 \times 10^{-11} - 3 \times 10^{-10} \text{ m}^2/\text{sec}$  with the median at  $1.74 \times 10^{-10} \text{ m}^2/\text{sec}$  (Docket: A-93-02, Ref# 563; Vol 3 p. 3-37).

This median value was used as input into STAFF3D after it was converted to m<sup>2</sup>/yr (Table 4.1.):

**Distribution coefficient.** The transport of radionuclides is affected by a wide range of chemical processes. Many of these reactions are poorly understood and are the subject of on-going research. From a practical view, the important aspect is the removal of solute from solution irrespective of the process. For this reason, STAFF3D and most computer codes, including the SECOTP code used for the transport simulations in the 1992 PA, simply lump all of the cumulative effects of the geochemical processes into a single term (i.e., the distribution coefficient-  $K_d$ ) which describes the degree to which the radionuclide is retarded relative to the groundwater. Thus, the distribution coefficient relates the radionuclide concentration in solution to concentrations adsorbed on the rocks.

The 1992 PA assumes that chemical and physical retardation occur only in the Culebra and assigns a range for Pu distribution coefficients in the matrix of the Culebra at  $1 \times 10^{-4}$  -  $1 \times 10^2$  m<sup>3</sup>/kg (Table 4.1). The median value is assigned  $2.61 \times 10^{-1}$  m<sup>3</sup>/kg. The range for the distribution coefficient in the clay lined fractures of the Culebra is  $1 \times 10^{-4}$  -  $1 \times 10^3$  m<sup>3</sup>/kg, with the median at  $2.04 \times 10^2$  m<sup>3</sup>/kg.

In the 1992 PA radionuclide transport is not explicitly performed in the repository, Salado or borehole, therefore distribution coefficients are not required. Essentially, in the 1992 PA no credit is taken for physical or chemical retardation until the radionuclides enter the Culebra.

Although transport was performed in the repository with STAFF3D, no physical or chemical retardation was assumed.

Table 4.1. Model Parameterization--Single Porosity - E2 Scenario (Base Case)

Parameter	1992 PA Range	Median Value	Reference (SAND92-0700)	STAFF3D-E2 (Base Case)
RADIONUCLIDE PROPERTIES - Pu-239				
Diffusion Coefficient	$4.8 \times 10^{-11}$ - $3 \times 10^{-10}$ m <sup>2</sup> /s.	$1.74 \times 10^{-10}$ m <sup>2</sup> /sec	Vol. 3 p. 3-37	$5.4873 \times 10^{-3}$ m <sup>2</sup> /yr
Distribution Coefficient (Matrix)	$1 \times 10^{-4}$ - $1 \times 10^2$ m <sup>3</sup> /kg	$2.61 \times 10^{-1}$ m <sup>3</sup> /kg	Vol. 3 p. 2-93	0.0
Distribution Coefficient (Fractures)	$1 \times 10^{-4}$ - $1 \times 10^3$ m <sup>3</sup> /kg	$2.04 \times 10^2$ m <sup>3</sup> /kg	Vol. 4 P. 3-3	0.0
Half Life	$2.4 \times 10^4$ yr	—	Vol. 3 p. 3-33	$2.407 \times 10^4$ yr
BOREHOLE				
Permeability	$1 \times 10^{-14}$ - $1 \times 10^{-11}$ m <sup>2</sup>	$3.16 \times 10^{-12}$ m <sup>2</sup>	Vol. 3 p. 3-1	1200 m/y
Effective Porosity	—	—	—	0.25
Diameter	0.267 - 0.444 m	0.355 m	Vol. 3 p. 3-3	0.355 m
REPOSITORY				
Dimensions-Panel (Waste region only)	17,556 m <sup>3</sup>	—	Vol. 3 p. 3-5	17,556 m <sup>3</sup>
Initial Pressure	7-22 MPa (581. - 1826. m)	—	Vol. 4 p. 5-28	1,246 m (15 MPa)
Permeability	$1. \times 10^{-13}$ m <sup>2</sup>	—	Vol. 4 p. 5-5	37.9 m/y
Total Porosity	Variable	Unknown		0.2
Specific Storage	—	—	—	$0.001 \text{ m}^{-1}$
Effective Porosity	—	—		0.2

Table 4.1. Model Parameterization--Single Porosity - E2 Scenario (Base Case) - Continued

Parameter	1992 PA Range	Median Value	Reference (SAND92-0700)	STAFF3D-E2 (Base Case)
SALADO				
Permeability	$1 \times 10^{-24}$ - $1 \times 10^{-19}$ m <sup>2</sup>	$2 \times 10^{-21}$ m <sup>2</sup>	Vol. 4 P. 3-25	$7.59 \times 10^{-7}$ m/y
Specific Storage	$2.8 \times 10^{-8}$ - $1.4 \times 10^{-6}$ m <sup>-1</sup>	$9.5 \times 10^{-8}$ m <sup>-1</sup>	Vol. 3 p. 2-11	$9.5 \times 10^{-8}$
Porosity	$1 \times 10^{-3}$ - $3 \times 10^{-2}$	$1 \times 10^{-2}$	Vol. 3 p. 2-11	$1 \times 10^{-2}$
Effective Porosity	—	—		$1 \times 10^{-2}$
Tortuosity	$1 \times 10^{-2}$ - $6.67 \times 10^{-1}$	$1.4 \times 10^{-1}$	Vol. 3 p. 2-11	$1.4 \times 10^{-1}$
Dispersivity (longitudinal)	1-40 m	15 m	Vol. 3 p. 2-11	15 m
Dispersivity Ratio ( $\partial_I/\partial_T$ )	3-25 m	10 m	Vol. 3 p. 2-11	10 m
CULEBRA				
Boundaries	935.3 m and 913 m	—	Figure 4.3.7	—
Hydraulic conductivity	From Transmissivity Fields	7.1 m/y	Vol. 4 p. 5-5	7.1 m/y
Specific Storage	$6.5 \times 10^{-7}$ - $6.5 \times 10^{-4}$ m <sup>-1</sup>	$2.6 \times 10^{-6}$ m <sup>-1</sup>	Vol. 3 p. 2-76	$2.6 \times 10^{-6}$ m <sup>-1</sup>
Porosity	—	—	—	—
Effective Porosity	$5.8 \times 10^{-2}$ - $2.53 \times 10^{-1}$ $9.6 \times 10^{-2}$ - $2.08 \times 10^{-1}$	0.139	Vol. 4 p. 3-3 Vol. 3 p. 2-76	0.139
Tortuosity	$3 \times 10^{-2}$ - $3.3 \times 10^{-1}$	$1.2 \times 10^{-1}$	Vol. 3 p. 2-76	$1.2 \times 10^{-1}$
Dispersivity (longitudinal)	$5 \times 10^1$ - $3 \times 10^2$ m	$1 \times 10^2$	Vol. 3. p. 2-76	$1 \times 10^2$ m
Dispersivity Ratio ( $\partial_I/\partial_T$ )	1 - 25. m	10	Vol. 3 p. 2-76	10

The distribution coefficient is used to calculate a retardation factor as determined from the following equation:

where  $R_F$  is the Retardation Factor;  $K_d$  is the distribution coefficient;  $P_b$  is the bulk density of the aquifer material; and  $n$  is the aquifer porosity. The retardation factor is the ratio between the groundwater and radionuclide velocities. A retardation factor of 2, therefore indicates that the groundwater moves at twice the rate of the radionuclide.

In this study, the distribution coefficient for all of the simulations for all of the materials was set to 0.0 (Table 4.1). That is, no chemical retardation was assumed. The rationale for this assumption is that chemical retardation had not been verified at the time of the 1992 PA and therefore, no credit for retardation was taken for the transport analysis. In the CCA, however, DOE demonstrated that chemical retardation would occur as discussed in the Technical Support Document titled *Assessment of Kd's used in the CCA* (Docket:A-93-02,V-B-4).

**Half life.** The time required for the radioactive decay of one-half the amount of parent material is called the half-life. For Pu-239 the half life is  $2.4 \times 10^4$  years. As mentioned previously, the half-life was used to determine the number of curies present after 1000 years of radioactive decay. The following equation is used:

Where:

$C$  = Number of curies remaining after accounting for radioactive decay (Ci)

$C_0$  = Initial number of curies (Ci)

$e$  = 2.712

$\lambda$  =

$t$  = Time of interest

$C = 3.44 \times 10^4 \text{ Ci} \cdot e^{-2.879 \times 10^{-5} \cdot 1000}$

$$\lambda =$$

$$C = 3.3424 \times 10^4 \text{ Ci}$$

STAFF3D also allows radionuclides to decay in transit as a function of their half-life. One of the reasons Pu-239 was selected for this modeling analysis, however, is that it has a longer half life than most of the other radionuclides that will potentially make up the repository inventory, which facilitates the data analysis. The decrease in Pu concentration along the flow path due to radioactive decay is approximately 25 percent over a 10,000 year time frame.

### 4.3 PARAMETERIZATION - SINGLE POROSITY BASE CASE (E2)

Two general types of simulations were performed with STAFF3D: 1) those that assume a matrix only approach in which fractures are not present, and 2) those based on a dual porosity approach which include fractures. The median parameter values taken from the 1992 PA are used as the STAFF3D base case.

#### 4.3.1 Borehole

**Borehole Permeability.** The borehole permeability used in the 1992 PA modeling ranged from  $1 \times 10^{-14}$  -  $1 \times 10^{-11} \text{ m}^2$ , with a median value of  $3.16 \times 10^{-12} \text{ m}^2$  (Table 4.1). The following relationship is used to translate permeability to hydraulic conductivity for input into STAFF3D:

where  $K$  is hydraulic conductivity (m/s),  $\kappa$  is intrinsic permeability ( $\text{m}^2$ ),  $\mu$  is fluid viscosity (Pa•s),  $\rho$  is fluid density ( $\text{kg}/\text{m}^3$ ), and  $g$  is the gravitational constant ( $\text{m}/\text{s}^2$ ).

The fluid density of the Salado brine is  $1230 \text{ kg}/\text{m}^3$  (Docket: A-93-02, Ref# 542, Vol. 3 p. 4-1), therefore this value is used as the density of the brine in the borehole. For a more rigorous treatment the brine density could have been changed to equal that of the Castile

(i.e., 1215 kg/m<sup>3</sup>) for the E1 scenario. However, the borehole hydraulic conductivity is relatively insensitive to such a small change in fluid density. The median value of the borehole hydraulic conductivity is 667 m/y as calculated by the following:

$$\kappa = 3.16 \times 10^{-12} \text{ m}^2$$

$$\rho = 1230 \text{ kg/m}^3$$

$$g = 9.79 \text{ m/s}^2$$

$$\mu = 1.8 \times 10^{-3} \text{ (Docket: A-93-02, Ref# 542, Vol 3, p. 4-1)}$$

As mentioned above, the 1992 PA assumed borehole hydraulic conductivities range from 2 - 2109.0 m/y, with a median of 667 m/y. However, the viscosity value that was used for these determinations ( $1.8 \times 10^{-3}$  Pa•s) was obtained from a reference by Kaufman (1960). In the absence of more recent, site specific data a value of viscosity was assigned that is equal to the Culebra brine viscosity of  $1.0 \times 10^{-3}$  Pa•s. This assumption leads to a more conservative borehole hydraulic conductivity of 1200 m/y. The sensitivity of the STAFF3D results to borehole permeability is discussed later in Section 5.

**Borehole Diameter.** The borehole diameter in the 1992 PA was assumed to range from 0.267 - 0.444 m, with a median value of 0.355 m (Table 4.1). This median value was input into STAFF3D and is not altered for any of the simulations.

**Borehole Effective Porosity.** Transport up the borehole is not explicitly modeled in the 1992 PA, therefore a value of effective (i.e. interconnected) porosity was not required. A value of 0.25 was assigned for the STAFF3D modeling and is representative of a silty sand. The effective porosity is used in the velocity calculation as follows:

Where:

V = Groundwater velocity (m/y)

K = Hydraulic conductivity (m/y)

I = Gradient

$n$  = Effective porosity

Neither the STAFF3D modeling or the 1992 PA assume that the hydraulic conductivity of the borehole decreases with time as a result of salt creep. However, the majority of the release is shown to occur in the first five hundred years after intrusion and therefore the effect of borehole closure on the release does not appear to be significant in the STAFF3D simulations.

#### 4.3.2 Repository

In the STAFF3D conceptualization all of the wastes are initially assumed to be confined inside the repository under pressure and the connecting borehole is closed (i.e., no contaminant migration takes place). Radionuclides are assumed to be uniformly distributed inside the repository. The waste remains under this condition for 1000 years during which it is subject to radioactive decay and physical degradation. After 1000 years, the connecting borehole is opened and upward migration through the borehole is allowed. Radionuclides released into the Culebra are subsequently carried by the ambient groundwater flow towards the downgradient (southern) boundary of the site.

**Repository Dimensions.** In the STAFF3D modeling, the volume of the repository was assumed to be that of a panel or approximately 46,000 m<sup>3</sup>. Waste properties in STAFF3D were assigned to a volume of 17,566 m<sup>3</sup>, or ten percent of the total design disposal volume for the waste (Docket: A-93-02, Ref# 542; Vol 3., p.3-11).

**Repository Initial Conditions.** The maximum pressure observed in the 1992 PA is 22 MPa (Figure 4.3.1). The far field pressure in the Salado is between 12 and 13 MPa. The lithostatic pressure at the repository horizon is approximately 15 MPa. Above this value hydrofracturing may occur which neither STAFF3D nor the 1992 version of BRAGFLO can



Figure 4.3.1. Volume average gas pressure in waste (Pa).

accommodate. Therefore, a value of 15 MPa appears to be a reasonable value to assign as initial conditions for the waste in STAFF3D. This initial pressure will dissipate very quickly with time once the borehole connects the repository to the Culebra. In the CCA, DOE did account for pressure induced permeability increases in the anhydrite marker beds (see Section 4.4 of the TSD for 194.23: Models and Computer Codes). Pressures of 15 MPa were at the high end of the range of pressures reported in the CCA. The conversion from MPa to head for input into STAFF3D is shown below:

$$P = \rho gh$$

Where:

P = Pressure (MPa)

g = Gravitational constant (m<sup>2</sup>/s)

$h$  = Head (m)  
 $\rho$  = Fluid Density ( $\text{kg}/\text{m}^3$ )

$h$  =

$P = 1.5 \times 10^7 \text{ Pa}$  (1 MPa =  $1 \times 10^6 \text{ Pa}$ )

$\rho = 1230 \text{ kg}/\text{m}^3$  (Salado brine density)

$g = 9.79 \text{ m}/\text{s}^2$

$h = 1.246 \times 10^3 \text{ m}$

As shown below, the repository pressure that is required to provide a sufficient driving force to allow flow from the Salado to the Culebra is approximately 5 MPa. This is provided that the brine in the borehole does not experience a significant pressure loss in transit due to pressures and permeabilities of the intervening formations.

This calculation indicates that far field pressures in the Salado (12.5 MPa) are more than sufficient to drive the brine/wastes upward from the repository to the Culebra Dolomite.

Culebra Elevation  $\approx 816 \text{ m}$   
WIPP Repository Elevation  $\approx \underline{380 \text{ m}}$   
436 m

Salado brine =  $1230 \text{ kg}/\text{m}^3$

$P = h\rho g$

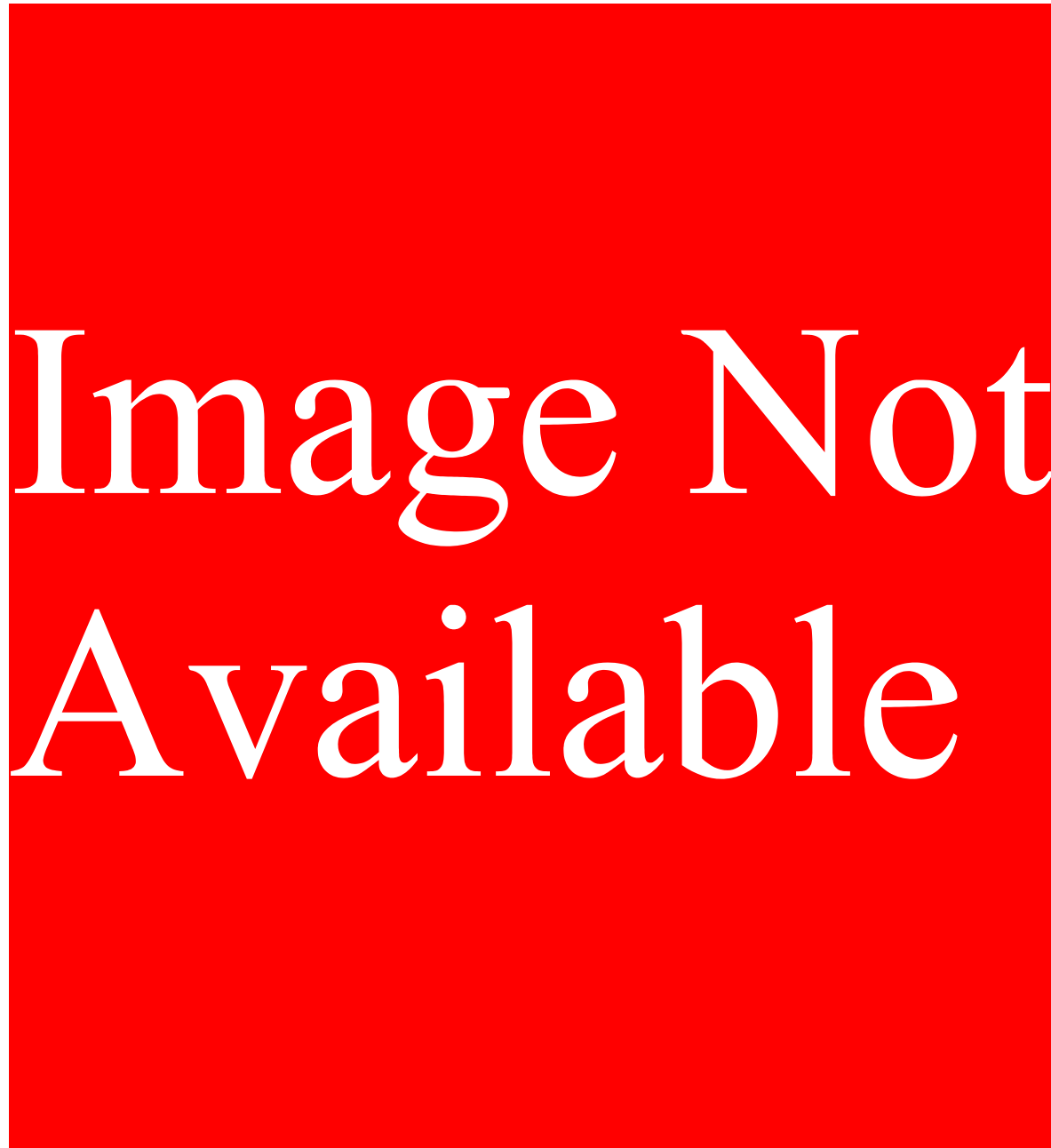
$P = (436.0)(1230.0)(9.79)$

$P = 5.25 \text{ MPa}$

A similar calculation indicates that it would take a pressure of approximately 10.0 MPa to allow brine to flow from the Castile to the Culebra. Hydrostatic pressures are shown in Figure 4.3.2. Note that the application of these equations requires the pressure in the repository to be about 7.9 Mpa in order to move brine to the surface.

**Repository Boundary Conditions.** As will be discussed in more detail in Section 5, the introduction of the Castile brine into the repository for the E1 and E1E2 scenarios is treated as a flux-type boundary condition. That is, a specified amount of brine was injected directly into the repository. The volume of brine that was injected in the STAFF3D simulations was

derived from the 1992 PA BRAGFLO results which indicate brine volumes flowing up the borehole in the E1E2 scenarios (Figure 4.3.3). A volume of 40 m<sup>3</sup>/yr was selected which yields a total brine flow over a 9,000 time period of 3.6 x 10<sup>5</sup> m<sup>3</sup>.



4.3.2. Calculated lithostatic and hydrostatic pressures with depth (Docket: A-93-02, Ref# 542, Vol 3 p. 2-40).

Figure

As shown in Figure 4.3.3, almost all of the 1992 PA simulations are below this value, however, a few of the simulations are considerably above it. STAFF3D simulations were also performed with a injection rate of 20 m<sup>3</sup>/y for a total brine volume of 1.8 x 10<sup>5</sup> m<sup>3</sup>.



Figure 4.3.3. E1E2 scenario, intrusion at 1000 yr: cumulative brine flow up the borehole (m<sup>3</sup>). (Docket: A-93-02, Ref# 542).

**Repository Permeability.** In the 1992 PA, a permeability of  $1.0 \times 10^{-13} \text{ m}^2$  is assigned to the waste and this value is not altered for any of the simulations. This permeability value is converted to hydraulic conductivity as follows:

where  $K$  is hydraulic conductivity (m/s),  $\kappa$  is intrinsic permeability (m<sup>2</sup>),  $\mu$  is fluid viscosity (Pa•s),  $\rho$  is fluid density (kg/m<sup>3</sup>), and  $g$  is the gravitational constant (m/s<sup>2</sup>).

The fluid density of the Salado brine is  $1230 \text{ kg/m}^3$ , therefore this value is used for the density of the brine contained within the wastes. The value of hydraulic conductivity for input into STAFF3D is calculated by the following:

The disturbed rock zone and backfill in the STAFF3D model domain is assigned the same permeability as the Salado as presented in Section 4.3.3. As mentioned previously, the viscosity value that was used for these determinations ( $1.8 \times 10^{-3} \text{ Pa}\cdot\text{s}$ ) was obtained from a reference by Kaufmann (1960). In the absence of more recent, site specific data a value of viscosity was assigned that is equal to the Culebra brine viscosity of  $1.0 \times 10^{-3} \text{ Pa}\cdot\text{s}$ . This leads to a more conservative hydraulic conductivity for the waste of 38 m/y.

**Repository Total Porosity.** In the 1992 PA the total porosity of the waste was bounded with SANCHO and changed with time based on the gas generation rates (Figure 4.3.4). BRAGFLO uses the porosity distribution from SANCHO to make predictions regarding the final porosity of the waste. These BRAGFLO results from the 1992 PA are shown in Figure 4.3.5. In the STAFF3D modeling the porosity must be held constant with time. The 1992 PA results suggest that the porosity does not change significantly after several hundred years. From Figure 4.3.5 it appears that a value of 20 percent would be a reasonable approximation for porosity after 1000 years and was therefore used for the STAFF3D modeling.

**Repository Specific storage.** The value of specific storage varies with the porosity of the material. Therefore, because the porosity of the waste changes with time in the 1992 PA, the specific storage also varies with time. To calculate a value of specific storage for input into STAFF3D the following approach is used:

Where  $S_s$  is specific storage (1/m),  $\theta$  is porosity,  $\beta$  is fluid compressibility (1/Pa),  $\alpha$  is waste compressibility 1/Pa),  $\rho$  is fluid density (kg/m<sup>3</sup>), and  $g$  is the gravitational constant (m/s<sup>2</sup>).



Image Not Available

Figure 4.3.4. SANCHO results: porosity as a function of time for various constant gas-generation rates ( $f$  values), porosity based on BRAGFLO definition of porosity (ratio of void volume to initial room volume).(Docket: A-93-02, Ref# 542)



Image Not Available

Figure 4.3.5 Pore volume in waste (m<sup>3</sup>).(Docket: A-93-02, Ref# 542).

$$\rho = 1230 \text{ kg/m}^3$$

$$g = 9.79 \text{ m/s}^2$$

$$\theta = 0.2$$

$$\beta = 0.43 \times 10^{-9} \text{ Pa}^{-1} \text{ (compressibility of water)}$$

$$\alpha = 1.53 \times 10^{-7}$$

$$S_s = 1230 \cdot 9.79 [1.53 \times 10^{-7} (1.0 - 0.2) + 0.2 (0.43 \times 10^{-9})]$$

$$S_s = 0.001$$

**Repository Effective Porosity.** Transport within the repository is not explicitly modeled in the 1992 PA, therefore a value of effective porosity was not required. A value of 0.20 was assigned for the STAFF3D modeling, primarily to keep the analysis more straightforward by assigning total porosity and effective porosity the same values.

#### 4.3.3 Salado

**Salado Boundary Conditions.** The 1992 PA assumes a far field pressure for the Salado at 12 - 13 MPa with a median value at 12.5 MPa. This pressure was translated to a head of 1038 m in the following manner:

$$P = \rho gh$$

Where:

P = Pressure (MPa)

g = Gravity (m<sup>2</sup>/s)

h = head (m)

$\rho$  = Fluid Density (kg/m<sup>3</sup>)

h =

$$P = 1.25 \times 10^7 \text{ Pa}$$

$$\rho = 1230 \text{ kg/m}^3$$

$$g = 9.79 \text{ m/s}^2$$

$$h = 1038 \text{ m}$$

Both the northern and the southern boundaries were assigned this value. There is currently no justification for assigning an ambient gradient within the Salado and, therefore, the same approach was taken in the STAFF3D modeling as in 1992 PA in that the only gradient is caused from the pressure build-up and subsequent release from the repository.

**Salado Initial Conditions.** The initial conditions for the Salado are obtained by allowing the system to equilibrate under steady-state conditions. That is, the boundary conditions, rock properties, and initial conditions of the wastes will equilibrate to a pressure surface prior to the intrusion of the borehole. Figure 4.3.6. is an illustration of how the steady-state potentiometric surface of the Salado and the Culebra may look prior to the borehole penetration. In this example, the initial pressure in the waste is set to 15 MPa and the far - field pressure in the Salado to 12.5 MPa (1038 m). Figure 4.3.7 shows the potentiometric surfaces once the borehole connects the Culebra to the repository. As shown in Figure 4.3.7, when the borehole connects the repository to the Culebra Dolomite, the higher heads in the repository cause the hydraulic head in the Culebra to rise. Eventually, the pressures in the Culebra will equilibrate with the far-field Salado pressures as the pressure pulse dissipates.

**Salado Permeability.** In the 1992 PA, the permeability range for the intact halite is  $1 \times 10^{-24}$  -  $1 \times 10^{-19} \text{ m}^2$ . The median is  $2 \times 10^{-21} \text{ m}^2$ . The translation of the median permeability value to hydraulic conductivity for input into STAFF3D is as follows:

where  $K$  is hydraulic conductivity (m/s),  $\kappa$  is intrinsic permeability ( $\text{m}^2$ ),  $\mu$  is fluid viscosity (Pa•s),  $\rho$  is fluid density ( $\text{kg/m}^3$ ), and  $g$  is the gravitational constant ( $\text{m/s}^2$ ).

The fluid density of the Salado brine is  $1230 \text{ kg/m}^3$ , and this value is used for the density of the brine contained within the wastes. The median value of hydraulic conductivity of the halite that was input into STAFF3D is  $4.22 \times 10^{-7} \text{ m/y}$  as calculated by the following:

Image Not  
Available

Figure 4.3.6. Steady-State Flow Simulation, Non-Intrusion Scenario (Shaded area is waste region)(Note: these contours are only conceptual in nature and are not actual simulation results).

Image Not  
Available

Figure 4.3.7. Steady-State Flow Intrusion Scenario. (Note these contours are only conceptual in nature and are not actual simulation results.)

$$\kappa = 2 \times 10^{-21} \text{ m}^2$$

$$\rho = 1230 \text{ kg/m}^3$$

$$g = 9.79 \text{ m/s}^2$$

$$\mu = 0.0018 \text{ Pa}\cdot\text{s}$$

As mentioned previously, the value of viscosity that was assigned to the Salado brine for the 1992 PA, is not site-specific. Therefore, the viscosity of the Culebra brine was used to calculate hydraulic conductivities which yielded a value that was almost double the median value ( $4.22 \times 10^{-7} \text{ m/y}$ ) or  $7.59 \times 10^{-7} \text{ m/y}$ . Furthermore, the domain of the STAFF3D model does not include the higher permeability anhydrite marker beds; which suggests that for these scoping calculations a permeability higher than the Salado halite is appropriate.

**Salado Specific Storage.** In the 1992 PA, the range for specific storage is  $2.8 \times 10^{-8}$  -  $1.4 \times 10^{-6} \text{ m}^{-1}$ . The median of  $9.5 \times 10^{-8} \text{ m}^{-1}$  was input directly into STAFF3D.

**Salado Porosity.** In the 1992 PA, the range for porosity of undisturbed halite is  $1 \times 10^{-3}$  -  $3 \times 10^{-2}$ . The median value is  $1 \times 10^{-2}$  and is input directly, without modification, into STAFF3D.

**Salado Effective porosity.** Transport within the Salado is not explicitly modeled in the 1992 PA, therefore a value of effective porosity was not required. A value of  $1 \times 10^{-2}$  is assigned for the STAFF3D modeling, primarily to keep the analysis more straightforward by assigning total porosity and effective porosity the same values.

**Salado Tortuosity.** The tortuosity is a measure of how tortuous the travel path of the radionuclide is at the molecular level. In the 1992 PA, the range for tortuosity is  $1 \times 10^{-2}$  -  $6.67 \times 10^{-1}$ . The median value is  $1.4 \times 10^{-1}$  and is input directly, without modification, into STAFF3D. Tortuosity is used to estimate the total amount of diffusion occurring as described by the following:

$$D^o = \tau D^*$$

Where:

$D^{\circ}$  = Apparent molecular diffusion coefficient  
 $\tau$  = Tortuosity  
 $D^*$  = Free water diffusion coefficient

Diffusion in solutions is the process whereby ionic or molecular constituents move under the influence of their kinetic activity in the direction of their concentration gradient. Molecular diffusion is a relatively slow process but contributes to the overall dispersion process, primarily through micro-scale mixing within individual pores or fracture channels which leads to large-scale bulk dilution and spreading in very slow moving groundwater.

**Salado Dispersivity (longitudinal).** The process by which solutes are transported by the bulk motion of water is known as advection. There is a tendency, however, for the solute to spread out from the path that it would be expected to follow according to the advective hydraulics of the flow system. This spreading phenomenon is called hydrodynamic dispersion. It causes dilution of the solute and occurs because of spatial variations in groundwater flow velocities and mechanical mixing during fluid advection; molecular diffusion, due to the thermal-kinetic energy of the solute particles also contributes to the dispersion process.

Dispersion can result from diffusion, channeling, and turbulent flow, but dispersion by itself does not affect the average rate at which the transported material moves. It can, however, cause some of the contaminant (in a diluted state) to move faster than the average groundwater flow velocity. The range of longitudinal dispersivity assigned to the Salado in the 1992 PA is 1. - 40. m. The median value of 15 m is used in the STAFF3D modeling.

**Salado Dispersivity Ratio** (longitudinal/transverse). The range of the dispersivity ratios assigned to the Salado in the 1992 PA is 3 - 25. The median which is used in the STAFF3D modeling is 10.

#### 4.3.4 Culebra

The Culebra Dolomite is simulated both as a single and dual porosity medium in the STAFF3D flow and transport runs. In the dual porosity mode, the Culebra is assumed to be made of porous matrix blocks with a single horizontal open fracture separating them. Advective flow into the porous material blocks is neglected, which means that transport in the fractures is by advection and dispersion, while molecular diffusion is the only mechanism whereby mass can enter and exit the matrix. The 1992 PA indicated that the modeling results are very sensitive to the number of fractures present. The greater the number of fractures the more matrix diffusion is allowed which in turn, leads to greater physical retardation. Therefore, a very conservative approach was undertaken for the STAFF3D modeling in that a single fracture of constant aperture is assumed to be present in the Culebra for the flow and transport simulations. Calculations of fracture hydraulic conductivities are provided in the next section.

**Culebra Boundaries.** The potentiometric surface map used in the 1992 PA to determine a groundwater gradient in the Culebra was apparently obtained from Brinster (1991) and is shown in Figure 4.3.8. This map indicates a gradient of an 18.4 meter drop over 6.64 km. Cauffman et. al., (Docket: A-93-02, Ref# 115), however, presents a potentiometric surface map that indicates a much steeper gradient of 22.3 m over 6.64 km (Figure 4.3.9).

A lower gradient will result in slower groundwater velocities and lower release rates. Therefore, the gradient that was assumed for the STAFF3D modeling was based on the Cauffman et. al., (Docket: A-93-02, Ref# 115) data.

The hydraulic heads along the northern and southern boundaries of the Culebra remain constant throughout the simulation and are set to 935.5 and 913 m respectively. In the 1992 PA the data are presented as head data making it unnecessary to convert pressure (MPa) to head (m) as is done for the boundary conditions for the repository and the Salado.

**Culebra Initial Conditions.** The initial conditions for the Culebra are obtained in a similar fashion to those of the Salado by allowing the system to stabilize under steady-state conditions. That is, the boundary conditions and the rock properties will equilibrate to a potentiometric surface prior to the intrusion of the borehole. Figure 4.3.6 is an illustration of how the

Image Not  
Available

Figure 4.3.8. Adjusted potentiometric surface of the Culebra Dolomite Member of the Rustler Formation in the WIPP vicinity (Brinster, 1991). Contours based on head data from indicated wells.

Image Not  
Available

Figure 4.3.9. Culebra freshwater heads at the WIPP - area boreholes.  
(Docket: A-93-02, Ref# 115)

steady-state potentiometric surface of the Culebra (and Salado) may look prior to the borehole penetration. Figure 4.3.7 shows a potential response to the potentiometric surfaces once the borehole connects the Culebra to the repository. (Note: these contours are only conceptual in nature and are not actual simulation results).

**Culebra Hydraulic Conductivity.** In the 1992 PA, the hydraulic conductivity is simulated as one of 70 transmissivity fields (transmissivity is equal to the hydraulic conductivity multiplied by the thickness of the unit).

The transmissivity fields were determined by conditioning the transmissivities against data collected from field-stress tests and from hydraulic head measurements. The 1992 PA does, however, also estimate a median value of permeability of  $2.1 \times 10^{-14} \text{ m}^2$ . The translation of this median permeability value to hydraulic conductivity for input into STAFF3D is as follows:

where  $K$  is hydraulic conductivity (m/s),  $k$  is intrinsic permeability ( $\text{m}^2$ ),  $\mu$  is fluid viscosity (Pa s),  $\rho$  is fluid density ( $\text{kg}/\text{m}^3$ ), and  $g$  is the gravitational constant ( $\text{m}/\text{s}^2$ ).

The fluid density of the Culebra brine is  $1090 \text{ kg}/\text{m}^3$ ; therefore this value is used for the hydraulic conductivity calculations for the Culebra brine contained within the wastes. The value of hydraulic conductivity that was input into STAFF3D is  $7.1 \text{ m}/\text{y}$  as calculated by the following:

**Culebra Specific Storage.** The modeling performed in the 1992 PA assumes that the flow field in the Culebra remains constant with time. Therefore, a value for specific storage is not required. However, as mentioned previously, the STAFF3D modeling allows the flow from the repository to enter the Culebra creating a transient flow field. To properly capture these effects, a specific storage value must be assigned to the Culebra. The 1992 PA presents storage coefficient values that range from  $5 \times 10^{-6} \text{ m}^{-1}$  -  $5 \times 10^{-4} \text{ m}^{-1}$ , with a median at  $2 \times 10^{-5} \text{ m}^{-1}$ . The storage coefficient divided by the Culebra thickness (7.7 m) results in a median specific storage value of  $2.6 \times 10^{-6} \text{ m}^{-1}$  which is input into STAFF3D.

**Culebra Porosity.** The availability of a specific storage value eliminates the need for a porosity value from which specific storage could be estimated.

**Culebra Effective Porosity.** In the 1992 PA, there is a discrepancy in the range for effective matrix porosities. In Vol. 4 p. 3-3 (Docket: A-93-02, Ref# 542) the range is given as  $5.8 \times 10^{-2}$  -  $2.53 \times 10^{-1}$ , whereas in Vol. 3 p. 2-76 (Docket: A-93-02, Ref# 542) the range is specified as  $9.6 \times 10^{-2}$  -  $2.08 \times 10^{-1}$ . The median is the same in both references ( $1.39 \times 10^{-1}$ )

and is input directly into STAFF3D.

**Culebra Tortuosity.** The tortuosity is a function of how tortuous the travel path of the radionuclide is at the molecular level. In the 1992 PA, the range for tortuosity for the Culebra is  $3 \times 10^{-2}$  -  $3.3 \times 10^{-1}$ . The median value is  $1.2 \times 10^{-1}$  and is input directly into STAFF3D. Tortuosity is used to estimate the total amount of diffusion occurring as described by the following:

$$D^o = \tau D^*$$

Where:

$D^o$  = Apparent molecular diffusion coefficient

$\tau$  = Tortuosity

$D^*$  = Free water diffusion coefficient

**Culebra Dispersivity (longitudinal).** The longitudinal dispersivity range specified in the 1992 PA is  $5 \times 10^1$  -  $3 \times 10^2$  m, with the median at  $1 \times 10^2$  m. Dispersion (neglecting molecular diffusion) is not significantly affected by laminar eddy currents. If molecular diffusion is momentarily disregarded, dispersion in porous or fractured media is caused by five principal phenomena: anisotropic permeability, varying pore sizes, varying path length, variation in the velocity gradient across pore space, and flow splitting around soil particles with mixing within the pore space. These five phenomena all contribute to longitudinal dispersion; anisotropic permeability and flow splitting around the soil particles can also cause lateral dispersion. In nearly all groundwater systems, longitudinal dispersion effects are much larger than lateral dispersion effects. Researchers have reported longitudinal dispersivity values ranging from about 1 to 25 times higher than transverse dispersivity values (Gelhar et al. 1985). In fractured systems, such as WIPP, it would be expected that the longitudinal dispersivity would be greater than the transverse.

A radionuclide that is introduced into a fractured porous medium will migrate through the fracture openings by means of advection as well as hydrodynamic dispersion. The radionuclide may also diffuse slowly into the porous matrix. If molecular diffusion is

occurring it will dominate flow and transport within the porous matrix because the fluid velocity in the porous matrix is usually very small. Upon introduction of the radionuclide into a fractured aquifer, the radionuclide moves rapidly within the fracture network. As time progresses, the zone of contamination will diffuse farther into the porous matrix. Since the

porous matrix has a very large capacity to store the contaminant, it plays a significant role in retarding the advance of the concentration front in the fractures. If the source of contamination is discontinued and the water-bearing unit is flushed by non-contaminated water, the contaminant mass in the fractures will be removed relatively quickly, whereas the contaminant in the porous matrix will be removed very slowly via diffusion back into the fracture openings.

**Culebra Dispersivity Ratio** (longitudinal/transverse). The range of the dispersivity ratios assigned to the Salado in the 1992 PA is 1 - 25. The median which is used in the STAFF3D modeling is 10 m (i.e., the longitudinal dispersivity was set to 100 m, and the transverse dispersivity was set to 10 m).

#### 4.4 DATA INPUT - DUAL POROSITY BASE CASE (E2)

In the dual porosity scenarios, in which a fracture is added to the Culebra Dolomite, the STAFF3D boundaries, initial conditions and flow and transport parameters for the borehole, repository, Salado and matrix properties of the Culebra are the exact same as those assigned to the single porosity STAFF3D E2 scenario (base case). Therefore, the following discussion will only focus on the fracture properties assigned to the Culebra Dolomite (Table 4.2.).

**Culebra Fracture spacing.** The 1992 PA uses a range for fracture spacing of  $6 \times 10^{-2}$  to 8 (m). The assumed median value is 0.4 m. The STAFF3D dual porosity modeling assumes one fracture which dictates a spacing of 3.85 m (7.7 m divided by 2).

**Culebra Specific Storage.** Field tests of the Culebra Dolomite suggest that a specific storage of  $1.96 \times 10^{-7} \text{ m}^{-1}$  is a reasonable value for the fractures (LAV90).

**Culebra Tortuosity.** The tortuosity of the fractures is assigned an identical value to that of the matrix (i.e., 0.12).

Table 4.2. Culebra Fracture Properties

Parameter	1992 PA Range	Median Value	Reference	STAFF3D - Base Case
Fracture Spacing	$6 \times 10^{-2} - 8 \text{ m}$	.4 m	Vol. 4 p. 3-2	3.85 m
Specific Storage	—	—	LAV90	$1.96 \times 10^{-7} \text{ m}^{-1}$
Tortuosity	—	—	—	0.12
Fracture Porosity	$1 \times 10^{-4} - 1 \times 10^{-2}$	$1 \times 10^{-3}$	Vol. 3 p. 2-76	See $K_f$ calculation
Permeability	-	-	-	See $K_f$ calculation
Dispersivity (Longitudinal)	-	-	-	100 m
Dispersivity ( $\partial_1/\partial_1$ )	-	-	-	10

#### 4.4.1 Culebra - Fracture Properties (1992 PA)

**Culebra Fracture porosity** - The 1992 PA assigns a fracture porosity range of  $1 \times 10^{-4}$  to  $1 \times 10^{-2}$  (dimensionless). The porosity value (i.e., derived from fracture aperture) for STAFF3D is calculated to determine the fracture permeability as described in the STAFF3D permeability input.

**Culebra Hydraulic Conductivity.** Fracture hydraulic conductivity in the Culebra used in the dual porosity flow simulations was calculated using the equation given by Snow (1969):

where

$K_f$  is the hydraulic conductivity of the fracture (m/y)

$b$  is the fracture half aperture (m)

$g$  is the gravitational acceleration ( $\text{m/s}^2$ )

$\mu$  is the dynamic viscosity (Pa•s)

$\rho$  is the fluid density ( $\text{kg/m}^3$ )

$b$  is given by the following expression:

where

$\bar{K}$  is the equivalent hydraulic conductivity of a porous medium (m/y)

L is half the distance between fractures

From the equations above, the STAFF3D fracture hydraulic conductivity was calculated as follows for a matrix hydraulic conductivity of 7.1 m/y.

Single Fracture:

**Dispersivity.** A value of dispersivity for the fractures was not presented in the 1992 PA. therefore, it was assumed that the dispersivity was the same as that of the matrix (100m). The ratio of longitudinal/transverse was also kept the same at 10.

## 5. Description of Model Simulations and Discussion of Results

As mentioned earlier, all model runs were divided into two general scenarios. The first scenario is referred to as "Repository Intrusion Without a Castile Brine Source" or E2 and the second is referred to as "Repository Intrusion With a Castile Brine Source" or an E1 scenario. The major emphasis, however, was placed on the E1 scenario, both because the components of this conceptual model make it more difficult for the repository to meet the compliance criteria, and because the E1 scenario leads quickly to the flooding of the repository, in which case, single-phase flow (i.e., brine) would predominate. STAFF3D is incapable of modeling a mobile gas phase and therefore, the prediction of brine flow is more conducive to STAFF3D modeling.

These general scenarios were further subdivided into either single porosity or dual porosity simulations. The single porosity simulations were performed primarily to provide a means to evaluate the travel time analyses that were presented in the 1992 PA. Alternatively, the dual porosity simulations were focused more broadly on the various components of the conceptual model.

To facilitate the presentation of the STAFF3D results, the discussion has been divided into two major components. First there is a general discussion on the overall response of the system to various assumptions in the selected parameters and processes (Section 5.1). The second major part of the discussion is more focused and pertains to how STAFF3D modeling results meet specific issues related to WIPP (Section 5.2). In each case, a description of the simulations, input parameters, and discussion of the results is provided.

All flow runs of STAFF3D are carried out in two steps. The first step is a steady-state simulation that represents a period of 1000 years without an open borehole connecting the repository to the Culebra. The purpose of this run is to generate initial conditions for the second step of the analysis that involves the transient simulations which last for a period of 10,000 years during which the borehole is open. (This results in a total simulation time of 11,000 years). The transient flow simulations describe the effects of the borehole intrusion on the groundwater flow field over time. This information is subsequently input into the transport simulations to provide velocity vectors from which the direction and migration rates of the contaminants are predicted.

As presented in Section 4.3.3, the initial and boundary conditions assumed for the Salado are not changed for any of the STAFF3D simulations. Furthermore, the low permeability of the Salado Formation, in conjunction with the separation distance from the Culebra (440 m), hydraulically isolates the Culebra from any perturbances originating in the Salado. The distribution of the potentiometric surface in the Salado prior to the borehole intrusion is shown in Figure 5.1. This surface is derived from the equilibration of initial waste pressures of 15 MPa and the far field pressure of 12.5 MPa (1038). The waste pressure of 15 MPa (1246 m) is maintained as a constant pressure boundary condition for the first 1000 years. After 1000 years, it is changed to an initial condition and allowed to dissipate. Figure 5.1 represents the initial conditions in the Salado for all of the simulations presented in this section. Since the borehole is absent, the initial waste pressure of 15 MPa (1246 m), which is higher inside the repository than the Salado far field pressures 12.5 MPa, has dissipated into the adjacent parts of the Salado Formation. However, since the pressure is constantly applied for the first thousand years it has not dropped from its initial value of 15 MPa. Furthermore, due to the extremely low conductivity in the Salado Formation the pressure gradient is very steep in the immediate vicinity of the repository prior to the intrusion.

Figure 5.2 shows the potentiometric surface of the Culebra at steady-state conditions. The boundary conditions for the Culebra remain unchanged among all of the E1 and E2 scenarios (Section 4.3.3). However, the rock properties (e.g., permeability) of the Culebra are changed between the various simulations, which dictates that a new steady-state flow field be established prior to each transient simulation. The gradient for each of the steady-state flow fields will be the same, the flux or volume of groundwater moving through the system however, will vary considerably depending upon the specified permeability of the Culebra (i.e. high hydraulic conductivities will result in high flow volumes).

## 5.1 MODELING RESULTS - GENERAL DISCUSSION

After a simulated time of 1000 years, the hydraulic head of 1246 m in the repository is changed from a fixed boundary condition to an initial condition and subsequently dissipates as a function of time. Brine flow in the Salado Formation is driven by the head difference between the repository and the far field boundaries. Upward flow through the borehole is driven by the head difference between the repository and Culebra where the hydraulic head at the location of the borehole under ambient conditions is 921.4 m. Groundwater flow in the Culebra is controlled by the regional hydraulic gradient plus the head build-up at the

Image Not  
Available

borehole.

Figure 5.1. Plan view of the head distribution (m) in the Salado before the borehole intrusion.

Image Not  
Available

Figure 5.2. Plan view of the Steady-state potentiometric surface for Culebra Dolomite

Figure 5.3. Potentiometric surface for Culebra Dolomite after borehole intrusion (Pus.k20)



Image Not  
Available

In the conceptual model, the borehole is filled with a silty-sand material and in the E1 scenario fully penetrates the Culebra, repository and Castile; whereas, the E2 Scenario(s) assume that the borehole only penetrates the Culebra and the repository as shown in Figure 4.3.6. In the STAFF3D modeling, flow is not permitted through the eastern and western boundaries of the model as is also the case in the 1992 PA modeling (i.e., no flow boundaries).

#### 5.1.1 Single Porosity Simulations

The data input for the single porosity simulations are presented in Table 5.1. The shaded parameter values in the table indicate which parameter was changed from the previous simulation. Transport simulations are for Pu-239 and it was assumed that there was no chemical retardation in any of the units. The Base Case, shown in Table 5.1, is the only E2 Type scenario performed with STAFF3D. The borehole does not penetrate the Castile brine as shown by a brine water flux rate of 0.0 entered in Table 5.1. The only difference between the Base Case (E2) and Pus-k20 is that Pus-k20 is an E1 type scenario and assumes that the Castile brine has been intercepted at a specified brine inflow rate of 40 m<sup>3</sup>/y. Pus-k7 is identical to Pus-k20 with the exception that the hydraulic conductivity of the Culebra in Pus-k20 has been lowered from 20 m/y to 7.1 m/y. Finally, Pus-k20a is the same as Pus-k20 except that the Castile brine inflow rate is reduced from 40 m<sup>3</sup>/y to 20 m<sup>3</sup>/y.

Figures 5.2 and 5.3 show the potentiometric surfaces of the Culebra Dolomite both before and after the borehole penetrates the repository. In Figure 5.3, there is a slight bending of the contour line at the location of the borehole indicating a small amount of water is coming out of the well in comparison with the ambient flow in the Culebra. It is unlikely that the amount of water entering the Culebra under this scenario (i.e., Pus-k20) has much effect on the transport of radionuclides to the WIPP boundary. However, as is further discussed in Section 5.2, and shown in Figure 5.4 certain assumptions regarding the initial pressures in the repository and hydraulic conductivities in the Culebra may have a significant impact on the flow field in the Culebra. In Figure 5.4, the flow field in the Culebra is shown to be very disturbed from the ambient flow field. This effect is caused by higher repository pressures and greater fluxes exiting the borehole, due to the added flux from the Castile brine reservoir.

Figure 5.5 shows the hydraulic head in the repository throughout the simulation period; whereas Figure 5.6 is a graph of the head at the borehole in the Culebra over the same period. The results (i.e., circles on the graphs) from the E2 Scenario (Base Case) indicate

that the equilibration between the far field pressures in the Salado and the head in the

Table 5.1. Input Parameters for Single Porosity Simulations (Shaded areas indicate changes from previous simulations)

	Base Case	Pus-k20.dat	Pus-k7.dat	Pus-k20a.dat
<b>RADIONUCLIDE — Pu-239</b>				
Kd (m <sup>3</sup> /kg)	0.0	0.0	0.0	0.0
Diff. Coeff. Pu-239 (m <sup>2</sup> /y)	5.55E-03	5.55E-03	5.55E-03	5.55E-03
Half life Pu-239 (y)	24070	24070	24070	24070
<b>BOREHOLE</b>				
Retardation	1	1	1	1
Hyd. Conductivity (m/y)	1200	1200	1200	1200
Effective Porosity	0.25	0.25	0.25	0.25
Fluid Density (kg/m <sup>3</sup> )	1230	1230	1230	1230
Long. Dispersivity (m)	10	10	10	10
Diameter (m)	0.355	0.355	0.355	0.355
<b>REPOSITORY</b>				
Retardation	1	1	1	1
Initial Pressure (M Pa)	15	15	15	15
Fluid Density (kg/m <sup>3</sup> )	1230	1230	1230	1230
Hydraulic Conductivity (m/y)	37.9	37.9	37.9	37.9
Specific Storage (m <sup>-1</sup> )	0.001	0.001	0.001	0.001
Effective Porosity	0.2	0.2	0.2	0.2
Castile Brine flux rate (m <sup>3</sup> /y)	0	40	40	20
No. of prescribed flux nodes	0	10	10	10
Long. Dispersivity (m)	10	10	10	10

Table 5.1. Input Parameters for Single Porosity Simulations ( Shaded areas indicate changes from previous simulations) (Continued)

	Base Case	Pus-k20.dat	Pus-k7.dat	Pus-k20a.dat
Ratio of (long/transverse) Disp.	10	10	10	10
<b>SALADO</b>				
Retardation (Pu-239/)	1	1	1	1
Fluid Density (kg/m <sup>3</sup> )	1230	1230	1230	1230
Hyd. Conductivity (m/y)	7.59E-07	7.59E-07	7.59E-07	7.59E-07
Specific Storage (m <sup>-1</sup> )	9.58E-08	9.58E-08	9.58E-08	9.58E-08
Tortuosity	0.14	0.14	0.14	0.14
Effective Porosity	0.01	0.01	0.01	0.01
Long. Dispersivity (m)	15	15	15	15
Ratio of (long/transv.) Dispersivity	10	10	10	10
<b>CULEBRA</b>				
Hyd. conductivity (m/y)	20	20	7.1	20
Fluid Density (kg/m <sup>3</sup> )	1090	1090	1090	1090
Tortuosity	0.12	0.12	0.12	0.12
Specific Storage (m <sup>-1</sup> )	1.96E-07	1.96E-07	1.96E-07	1.96E-07
Effective Porosity	0.139	0.139	0.139	0.139
Retardation	1	1	1	1
Long. Dispersivity (m)	100	100	100	100
Ratio of (long/transv.) Disp.	10	10	10	10

Table 5.2. Input Parameters for Dual Porosity Simulations (Shaded areas indicate changes from previous simulations)

	Base Case	Pud-nd2.dat	Pud-nd4.dat	Pud-nd10.d	Pud-1.dat	Pud-2.dat	Pud-3.dat	Pud-4.dat
<b>RADIONUCLIDE — Pu-239</b>								
Kd (m <sup>3</sup> /kg)	0.0	0.0	0.0	0.0	0.0	0.0	0.0	0.0
Diff. Coeff. Pu-239 (m <sup>2</sup> /y)	5.48E-03	5.48E-03	5.48E-03	5.48E-03	5.48E-03	5.48E-03	5.48E-03	5.48E-03
Half life Pu-239 (y)	24070	24070	24070	24070	24070	24070	24070	24070
<b>BOREHOLE</b>								
Retardation	1	1	1	1	1	1	1	1
Hyd. Conductivity (m/y)	1200	1200	1200	1200	1200	1200	1200	1800
Effective Porosity	0.25	0.25	0.25	0.25	0.25	0.25	0.25	0.25
Density (kg/m <sup>3</sup> )	1230	1230	1230	1230	1230	1230	1230	1230
Long. Dispersivity (m)	10	10	10	10	10	10	10	10
Diameter (m)	0.355	0.355	0.355	0.355	0.355	0.355	0.355	0.355
<b>REPOSITORY</b>								
Retardation	1	1	1	1	1	1	1	1
Initial Pressure (M Pa)	15	15	15	15	15	15	15	15
Density (kg/m <sup>3</sup> )	1230	1230	1230	1230	1230	1230	1230	1230
Hyd. Conductivity (m/y)	37.9	37.9	37.9	37.9	37.9	37.9	37.9	37.9
Specific Storage (m <sup>-1</sup> )	0.001	0.001	0.001	0.001	0.001	0.001	0.001	0.001
Effective Porosity	0.2	0.2	0.2	0.2	0.2	0.2	0.2	0.2
Brine water flux rate	0	40	40	40	20	40	40	40
No. of prescribed flux nodes	0	2	4	10	10	10	10	10

Table 5.2. Input Parameters for Dual Porosity Simulations (Shaded areas indicate changes from previous simulations)  
(Continued)

	Base Case	Pud-nd2.dat	Pud-nd4.dat	Pud-nd10.d	Pud-1.dat	Pud-2.dat	Pud-3.dat	Pud-4.dat
Long. Dispersivity (m)	10	10	10	10	10	10	10	10
Ratio of (long/transverse) Dis.	10	10	10	10	10	10	10	10
<b>SALADO</b>								
Retardation	1	1	1	1	1	1	1	1
Fluid Density (kg/m <sup>3</sup> )	1230	1230	1230	1230	1230	1230	1230	1230
Hyd. Conductivity (m/y)	7.59E-07	7.59E-07	7.59E-07	7.59E-07	7.59E-07	7.59E-07	7.59E-07	7.59E-07
Specific Storage (m <sup>-1</sup> )	9.58E-08	9.58E-08	9.58E-08	9.58E-08	9.58E-08	9.58E-08	9.58E-08	9.58E-08
Tortuosity	0.14	0.14	0.14	0.14	0.14	0.14	0.14	0.14
Porosity	0.01	0.01	0.01	0.01	0.01	0.01	0.01	0.01
Long. Dispersivity (m)	15	15	15	15	15	15	15	15
Ratio of (long/transv.) Disp.	10	10	10	10	10	10	10	10
<b>CULEBRA</b>								
Matrix Properties								
Retardation	1	1	1	1	1	1	1	1
Effective Porosity	0.139	0.139	0.139	0.139	0.139	0.139	0.139	0.139
Specific Storage (m <sup>-1</sup> )	1.96E-07	1.96E-07	1.96E-07	1.96E-07	1.96E-07	1.96E-07	1.96E-07	1.96E-07
Hyd. conductivity (m/y)	7.1	7.1	7.1	7.1	7.1	7.1	20	20
Tortuosity	0.12	0.12	0.12	0.12	0.12	0.12	0.12	0.12
Fluid Density (kg/m <sup>3</sup> )	1090	1090	1090	1090	1090	1090	1090	1090
<b>FRACTURE PROPERTIES</b>								



Image Not  
Available

Figure 5.4. Potentiometric surface of the Culebra Dolomite after borehole intrusion of repository and Castile brine reservoir

Image Not  
Available

Figure 5-5. Pressure within the repository with respect to time after intrusion

Figure 5-6. Pressure within the Culebra at intrusion borehole with respect to time after intrusion

Culebra results in a very slight upward gradient. That is, as the initial head of 1246 m dissipates to equilibrate with the far-field head of 1038 m the head in the borehole at the Salado levels out to about 922.0 m, while the head in the Culebra equilibrates back to initial conditions at 921.4 m. This indicates that the far-field pressures in the Salado allow just enough water to flow into the repository to maintain a relative equilibrium with the Culebra. This same phenomena would be observed if the borehole were to penetrate the Salado but not the repository. This also suggests that if the borehole is uncased, the ambient pressure gradients would be insufficient to allow flow from the repository to the land surface unless additional pressures are applied (e.g., drilling, Castile brine pocket, gas generation). Salado pressures of about 8.0 MPa (750 m) would be sufficient to drive the brine to the land surface in a cased borehole. The remaining simulations which all include a Castile brine source indicate, as would be expected, stronger upward gradients from the repository to the Culebra.

In Figure 5.1 a steep pressure gradient is indicated between the repository and the Salado in that the values of head just outside the repository do not change significantly. This large initial difference in head between inside and outside the repository prevents water from flowing from the Salado into the repository. As the water in the repository flows quickly up through the borehole and pressure within the repository dissipates, additional flow into the repository and up the borehole is controlled mainly by the permeability of the Salado Formation. This effect is also shown in Figures 5.5 and 5.6 in which the pressures are shown to drop and equilibrate to a constant value within the first 100 years of the simulation.

Figure 5.7 is an areal representation of the plutonium distribution in the Culebra Dolomite at some specified time. A more revealing depiction of the modeling results, however, is the time dependence of the concentrations. Therefore, the remaining figures are all of breakthrough curves which present the parameter of interest as a function of time.

Figures 5.8 and 5.9 indicate that in all of the simulations where Castile brine is introduced to the repository (E1), the majority of the curies in the panel are released to the Culebra over the first thousand years after intrusion, the remaining curies are slowly released over the 10,000 years. Figure 5.9 indicates that in all but the base case (E2) simulation about 25,000 curies are released in the first one thousand years following the intrusion of the borehole. There are 33,424 curies present in the panel immediately prior to the intrusion. Therefore,

75 percent of the curies are released, when the following assumptions were used 1) borehole hits the repository and a Castile brine pocket; 2) the solubility is inventory limited; and 3) no retardation was assumed in the wastes or borehole. The results from the base case (E2) simulation indicate that the release is smaller (i.e. 15,000 Ci) and much slower as the releases are controlled by the inflow of Salado brine to the repository and the slight upward gradient to the Culebra. Furthermore, the releases would be even lower in the E2 type scenario, than those predicted by STAFF3D, if it takes longer than 1000 years for the repository to fill with the brine.



Figure 5.7. Areal representation of plutonium plume

# Image Not Available

Fi

Figure 5-8. Breakthrough curve of Pu-239 Concentration at the well in Culebra (Single Porosity Simulations).

Figure 5-9. Cumulative curves exiting out of the well and into the Culebra (single porosity simulations).

### 5.1.2 Dual Porosity Simulations

In all dual porosity simulations, the Culebra dolomite is treated as a dual porosity medium consisting of porous matrix blocks separated by a single open fracture. Advective flow through the porous material blocks is neglected, this means that transport towards the WIPP boundary is only in the fractures and is controlled by advection and dispersion, while molecular diffusion is the only mechanism whereby mass can enter into the matrix. A single fracture of constant aperture is assumed to be present in Culebra in the flow simulations. Input parameters for these data files are presented in Table 5.2.

All of the dual porosity simulations deal solely with the transport of Pu-239 and assume no chemical retardation in any of the units (Table 5.2). As in the single porosity base case simulations, the dual porosity base case (E2-type scenario) does not consider the introduction of Castile brine to the repository. The remaining dual porosity simulations are all E1-type scenarios.

Data files Pud-nd2, Pud-nd4, and Pud-nd10 are all identical to the base case, except that all three of these simulations assume a Castile brine source (Table 5.2). The difference among these simulations is the number of nodes in the repository over which the Castile brine flux was distributed (i.e., 2, 4 or 10). This aspect of the modeling is further discussed in Section 5.2.

Data file Pud-1 is identical to Pud-nd10 except that the volume of Castile brine assumed to enter the repository is reduced from 40 m<sup>3</sup>/y to 20 m<sup>3</sup>/y. Pud-2 is identical to Pud-nd10 and has been included in the table and figures only to facilitate the discussion and presentation of the results. Pud-3 is essentially identical to Pud-2 except for that the hydraulic conductivity of the Culebra has been increased from 7.1 m/y to 20 m/y. Similarly, Pud-4 is identical to Pud-3 except that the hydraulic conductivity of the borehole has been increased from 1200 m/y to 1800 m/y. The statistical range used in the 1992 PA assigned an upper bound on the borehole hydraulic conductivity of approximately 2100 m/y. Figures 5.10 and 5.11 indicate that, as is the case in the single porosity STAFF3D simulations, about 75 percent of the initial curies are released from the repository in all of the Castile brine scenarios, but the majority of the curies are released to the Culebra within the first 200 years after the borehole intrusion. The radionuclide release for the dual porosity E2-Scenario (base case) is also very rapid and driven by the initial pressure differential between the repository and the Culebra.

However, after the initial pressure dissipates (within the first several hundred years), only the ambient pressure gradients established between the repository and the Culebra drive brine flow from repository to the Culebra, therefore the release continues much more slowly for the remainder of the simulation, as is shown by the slight upward slope of the base case release curve in Figure 5.11. As was previously discussed, this same phenomenon was observed in the single porosity simulations.

A comparison between Figures 5.12 and 5.5 indicate that the dissipation curves for hydraulic head in the repository have nearly identical trends for comparable simulations between the single porosity and the dual porosity scenarios. The results from simulation Pud-4 are interesting in that although the Castile brine injection rate is identical to that in simulations Pud-2 and Pud-3, the hydraulic head is lower by about 65 m and 20 m, respectively. This is because the hydraulic conductivity in the borehole is higher in Pud-4 (i.e., 1800 m/y versus 1200 m/y in Pud-2 and Pud-3) and allows a better communication with the Culebra. This essentially decreases the gradient between the repository and the Culebra, which in turn, reduces the driving force which is responsible for transporting the radionuclides from the repository. Although the driving force is decreased, the higher permeability results in a greater flux and therefore the overall release may be greater when the borehole permeability is higher. The importance of this is that as is indicated in the 1992 PA that the modeling results are very sensitive to the borehole permeability. Furthermore, high initial pressures in the repository in conjunction with low borehole permeabilities may significantly alter the gradient in the Culebra.

## 5.2 ISSUE SPECIFIC - RESULTS AND CONCLUSIONS

The following discussion focuses the modeling results to address a number of specific issues pertaining to the flow and transport modeling in the 1992 PA.

Image Not  
Available

Figure 5-10. Breakthrough Curve of Pu-239 Concentration at the well in Culebra (dual porosity simulations)

Image Not  
Available

Figure 5-11. Cumulative curies exiting out of the well into Culebra (dual porosity simulations)



Image Not  
Available

Figure 5-12. Breakthrough of the hydraulic head in the repository (dual porosity simulations).

#### 5.2.1 1992 PA Issue 1 - Solubility Limited Assumptions

The 1992 PA assumes that the release of radionuclides from the repository will be controlled by their solubility. However, until more data was to become available DOE used an inventory limited approach. Therefore, one of the objectives of the STAFF3D modeling was to determine at what rate the wastes would be released under various flow and transport scenarios if their release was inventory limited, instead of solubility limited. Now that the CCA contains reliable predictions regarding radionuclide solubilities the releases are not necessarily controlled by the inventory release limits (see A-93-02, II-G-1, Volume XVII, Appendix SOTERM).

The best means of evaluating this objective is to review the modeling results with respect to the breakthrough curve of the curies exiting out the borehole into the Culebra shown in Figures 5.8 and 5.13 for the single and dual porosity simulations, respectively. These

figures indicate that almost all of the curies that are eventually transported out of the repository and into the Culebra are released within the first one thousand years after the intrusion of the borehole. Figures 5.9 and 5.11 indicate that very few curies are leaving the borehole after 1000 years, and that for the E2 scenario, approximately 50 percent of the initial curies are released from the repository to the Culebra, whereas in the E1 scenarios approximately 85 percent of the repository inventory is released over this time period.

The time-dependent release concentrations to the Culebra (i.e., the output of PANEL) are not presented in the 1992 PA. However, because STAFF3D explicitly simulates radionuclide transport from the repository to the Culebra it should provide a relatively good approximation of the most conservative release histories to the Culebra, particularly for the E1 scenario. Therefore, these STAFF3D breakthrough curves could be compared against the PANEL output when it becomes available.

#### *RELEVANCE TO CCA*

EPA performed a detailed review of the means in which DOE treated the actinide source term (see EPA's Technical Support Document for DOE's Actinide Source Term, A-93-02, V-B-17). As discussed in that document, EPA has concluded that DOE has adequately treated the actinide source term for performance assessment.

#### 5.2.2 1992 PA Issue 2 - Castile Brine Reservoir/Multiple Intrusions (E1E2)

In the 1992 PA, the wastes are released at a rate calculated with PANEL by using repository inflow rates and volumes determined with BRAGFLO/SANCHO. However, the STAFF3D modeling analysis places the wastes directly within the repository and relies upon the inflow of

Salado (E2) and Castile (E1) brine to physically transmit the waste from the repository up the borehole to the Culebra. Therefore, the manner (i.e. location and volume) in which brine enters the repository, particularly for the Castile intrusion scenario, will have a direct impact on the volume and rate at which the radionuclides migrate from the repository. The placement of multiple flux nodes within the repository is analogous to the 1992 PA E1E2-type scenario in which multiple intrusions of the Castile brine reservoir are assumed. This approach allows a bounding type analysis in that all of the Castile brine entering the

repository is only allowed to

flow up a single borehole to the Culebra. However, the current STAFF3D analysis does divide the total brine assumed in the 1992 PA for the E1E2 scenarios among the various flux nodes (i.e., intrusion points) so that it is not a true bounding approach.



Figure 5-13. Breakthrough curve of Pu-239 concentration at the well in Culebra (dual

porosity simulations).

In order to investigate the sensitivity of the assumptions regarding the placement and number (i.e., multiple intrusions) of Castile brine entry points and volumes, a series of STAFF3D simulations were performed. These simulations will also provide insight for reviewing the future modeling that is planned to support the PA.

To account for the brine introduced by the borehole penetration into the Castile, the 1992 PA explicitly models a borehole that connects the repository to the Castile. The modeling in the 1992 also makes a conservative assumption in that all of the Castile brine that moves up the borehole is assumed to enter the repository prior to completing its path to the Culebra. A significant amount of work has been performed which investigates the expected volumes of brine that could potentially be derived from a Castile reservoir (Docket:A-93-02, Ref#540). Therefore, rather than explicitly simulate the Castile brine reservoir in the STAFF3D analyses, which would dramatically increase simulation times and computer storage requirements, a modified approach was undertaken in which the brine volumes obtained from the 1992 PA analyses were used as brine flow estimates, and were input directly into STAFF3D (i.e., specified boundary nodes).

Results from the 1992 PA indicate that for the E2 scenario the cumulative volume of water entering the Culebra from the borehole ranges from negative values in which brine flowed from the Culebra into the borehole to 16,300 m<sup>3</sup> of Salado brine flowing up the borehole and discharging into the Culebra (Figure 5.14). Similarly, the cumulative volume of water entering the Culebra under the E1E2 type scenario is between 156 and 9.8 x 10<sup>5</sup> m<sup>3</sup> (Figure 4.3.3). The absence of a Castile brine source in the E2-type scenario did not require that any adjustments be made to the STAFF3D simulations to account for the Castile brine. However, the STAFF3D simulations did need to account for the Castile brine source in the E1-type scenarios. To accomplish this task a number of constant flux nodes were placed directly in the repository and assigned flux values that would equal a cumulative volume of 4 x 10<sup>5</sup> m<sup>3</sup> over the 10,000-year simulation period following the intrusion of the borehole. This value lies toward the upper end of the high range of flux values that were obtained during the 1992 PA (Figure 4.3.3).

The rationale for assigning flux nodes rather than explicitly model the Castile brine source is that the overall effect on the volume of water and curies that reach the Culebra will be very similar between the two approaches. This more simplified approach is justified, because the primary focus of this study is to determine the relevant flow and transport processes that most affect the number of curies that could potentially reach the Culebra rather than perform

a detailed evaluation of the flow and transport processes within the repository.

Figure 5-14. E2 scenario, intrusion at 1000 yr: cumulative brine flow up borehole (m<sup>3</sup>).  
(Docket: A-93-03, Ref#563, Vol 4 p. 5-17)

In the 1992 PA, BRAGFLO performs only flow calculations from which a brine flux rate up the borehole is determined. This flux rate is subsequently used as input to PANEL which computes a radionuclide release rate from the repository to the Culebra. This approach eliminates the need to explicitly determine the effects on radionuclide transport of the various components of the brine flux (i.e., Castile, Salado). However, because STAFF3D solves a fully coupled flow and transport equation the distribution of the brine flux introduced to the repository will have strong influence on the number of curies released to the Culebra. Therefore, a sensitivity analysis was performed with STAFF3D to evaluate the effect that the positioning of the flux nodes in the repository have on the release rates.



Figure 5-15. Nodal flux locations and cumulative curves exiting from the well into the Culebra.

Three sets of flow and transport simulations were made with 2, 4, and 10 prescribed flux nodes in the repository (Figure 5.15). The Castile brine influx rate was set to either 4, 10 or 20 m<sup>3</sup>/y per node to total 40 m<sup>3</sup>/y in all these runs, but the locations of the nodes in the repository are varied to determine the nodal arrangement that produced the highest quantity of radioactivity moving up the borehole to the Culebra. Increasing the number of the nodes beyond 10, produced less than 5% increase in the cumulative curies arriving in Culebra. When two nodes are used, they are placed at the top and bottom of the repository along the borehole. This placement would be most representative of an E1-type scenario (i.e., single intrusion into the Castile brine). An increase in the number of nodes to 4, is analogous to an E1E2 scenario with two intrusions into the Castile brine, as the nodes are placed in the frontal plane of the repository and at the corners. Similarly, the assignment of 10 flux nodes into the repository simulates an E1E2 scenario with 5 intrusions into the Castile brine. The placement of the nodes in this case is also in the frontal plane, with 5 nodes at the top and 5 nodes at the bottom of the repository. Figure 5.15 shows the cumulative curies arriving at the borehole in Culebra Formation for the runs made with 2, 4, and 10 flux nodes. The cumulative curies released to the Culebra are about 9,000, 18,000, and 25,000 respectively for the above three nodal arrangements.

Both the number of nodes in the repository and their respective locations have considerable impact on the quantity of radionuclides that move out of the repository through the borehole. When two nodes are placed along the borehole, the brine contributed to the flow system by these nodes rushed up through the borehole, immediately after it was opened, leaving behind radionuclides that are located further away from the borehole. On the other hand, with 4 gradient nodes placed at corners of the repository, the brine is in contact with larger portions of the waste and is able to drive greater quantities of radionuclides up the borehole. One consequence of the four corner nodal arrangement is that and since flow originating from the flux nodes is radial, some of the brine moves into the adjacent parts of the Salado carrying with it a certain number of radionuclides. These radionuclides, therefore, will be will not be available for transport to the Culebra. Distributing the brine flux uniformly in 10 nodes (4 m<sup>3</sup>/y each) allows brine to be in contact with the largest surface area of the waste of the three nodal distributions examined, and also creates a flow field that is very amiable to transport the waste to the intrusion borehole. Thus, maximizing the migration of radionuclides from the repository. All of the remaining STAFF3D simulations that assume the borehole penetrates the Castile brine reservoir use the 10 node arrangement.

## *RELEVANCE TO CCA*

As indicated above, the computer simulations performed in the 1992 PA did not account for radionuclide transport within the repository. However, for the CCA, DOE did couple the flow fields calculated with BRAGFLO to the transport mechanisms simulated with the computer code NUTS (see Section 4.4.10 of EPA's TSD for 194.23: Models and Computer Codes, A-93-02, V-B-6). EPA's conclusions regarding DOE's work, with respect to this issue, is that it is adequate to support the CCA.

### 5.2.3 1992 PA Issue 3 - Decoupling of Repository from Culebra

In the 1992 PA, the flow and transport processes active in the repository have been effectively decoupled from those in the Culebra. That is, the output from PANEL consists of radionuclide concentrations which are subsequently input into SECO, which in turn simulates flow and transport through the Culebra to calculate cumulative releases at the WIPP land withdrawal boundary. The flux, however, that is calculated to move up the borehole by BRAGFLO is not introduced into the Culebra. Therefore, the influence of water flowing out of the borehole on the ambient flow field of the Culebra is not considered in the 1992 PA analysis. The effect that this perturbation may have on the flow field could impact the estimates made in the 1992 PA regarding the cumulative mass reaching the accessible environment over the 10,000-year simulation.

In the STAFF3D simulations the brine entering the repository is transported up the borehole and discharged into the Culebra, thereby affecting the flow field in the Culebra. In the 1992 PA this brine flow into the Culebra is considered insignificant and is ignored. The output from all of the STAFF3D simulations includes a concentration breakthrough curve at the borehole in the Culebra (Figure 5.16).

To determine whether the flow up the borehole would have a significant effect on the transport of radionuclides in the Culebra, a simulation was performed with STAFF3D in which the concentration breakthrough curve at the borehole from simulation Pu-k7 is used as a transient boundary condition for a steady state version of the same analysis. That is, the radionuclide mass exiting the borehole was injected into the Culebra as a function of time, however, the brine that was predicted to exit the borehole was not introduced to the Culebra. This essentially maintains the release history of the radionuclides into the Culebra but effectively removes any brine flow that would normally exit the borehole and enter the Culebra.

Figure 5.17 shows a comparison between the breakthrough curves of the steady-state versus transient flow and transport simulations at the WIPP boundary. The steady state flow field results in much lower concentrations and slower velocities. It is important to note, however, that these results need to be further substantiated in that both the stability of the problem formulation (e.g., grid spacing, time stepping) and data input needs to be further checked before these results can be fully supported. Furthermore, in the course of performing a number of similar simulations it was noted that borehole permeabilities and Culebra storativities have a significant impact on the calculated Culebra gradients. These relationships should also be further investigated as the Culebra gradient has a major effect on travel times. The Addendum in Appendix S to this report further addresses some of these issues.

#### *RELEVANCE TO CCA*

As indicated above the computer simulations performed in the 1992 PA decoupled the flow fields of the repository and the Culebra. EPA's initial concern was that the volume of flow up the borehole would perturb the Culebra flow system. However, the volume of water predicted to flow up the borehole in a human intrusion scenario is relatively small and is significantly less in the CCA, than that which was predicted in the 1992 PA. Therefore, steady-state assumptions on the flow field appear to be reasonable because the volume of flow up the borehole and therefore in the Culebra member will be relatively small with respect to the flow field (Docket: A-93-02, II-G-1, Reference # 542, Reeves et al 1991, page 3-12). Furthermore, the contaminant introduced into the Culebra is immediately dispersed into the fractures over a grid block that is 50 m<sup>2</sup>. DOE's approach artificially introduces instantaneous advection over this area which should approximate the initial fast advection adequately (Docket: A-93-02, II-G-11, *Analysis Package for Culebra Flow and Transport*, WPO #40516, page 26).

#### 5.2.4 1992 PA Issue 4 - Mass Balance and Discretization

In the 1992 PA, the model domain for BRAGFLO has a relatively coarse discretization. Recently, DOE sponsored an independent analysis on the sensitivity of the BRAGFLO results to grid convergence. However, the findings of this analysis are not yet available to EPA. To provide some perspective on the mass balance problems to which BRAGFLO may be subject, a general discussion of the STAFF3D mass-balance results with respect to the model domain discretization is presented.

Image Not  
Available

Figure 5-16. Breakthrough curve of Pu-239 concentration at the well in Culebra (single porosity simulations).

Figure 5-17. Breakthrough concentration of Pu-239 at the Boundary of the WIPP site for steady-state and transient flow runs.

The STAFF3D modeling raises a number of issues related to the mass balance considerations for the performance assessment modeling. First, it was discovered that the spacing of the nodal blocks in the repository had to be considerably finer in STAFF3D than those used in BRAGFLO to obtain a reasonable mass balance. For example, to keep mass balance errors less than 5 percent it was necessary in STAFF3D to discretize the waste region 528 nodes, whereas, BRAGFLO used 256 nodes to discretize the entire panel. It is unknown whether BRAGFLO experienced mass balance errors, at this point the first step in resolving this issue would be to review the grid convergence studies that have already been completed on BRAGFLO.

A second source of mass balance error in STAFF3D found to originate with the assumptions regarding the very high repository pressures and the non-deformable mesh used in STAFF3D. More specifically, at the high initial pressures there is a significant amount of brine released from storage within the wastes. The following equation describes the total brine volume in the repository:

$$V_T = V\theta + S_s V \Delta h$$

Where

- V = volume of the repository
- $\theta$  = porosity of the repository
- $S_s$  = specific storage of the repository
- $\Delta h$  = hydraulic head drop in the repository over the simulation period

The first term on the right hand side of the equation is equal to the total void volume of the repository if the repository were not subject to any confining pressure. However, because in

the STAFF3D simulations the repository starts off under high pressures a significant amount of brine is stored due to the expansion of the repository matrix material and some is stored by the compression of the brine itself. Therefore, to account for all of the brine in the repository a second term is added to the right hand side of the equation which is equal to the volume of brine that would be released from storage as pressure decreases due to the collapse of the matrix to a 20% porosity and the subsequent expansion of brine.

Since BRAGFLO simulations are initiated at atmospheric pressures BRAGFLO should not experience mass balance problems related to the specific storage of the wastes. It is known, however, that in the 1992 BRAGFLO simulations a certain mass of brine is lost in

BRAGFLO as the waste matrix porosity surfaces are input from SANCHO. It is unclear how much impact this "lost" mass has on the BRAGFLO results. As the PA review proceeds, this topic needs to be further reviewed.

The above equation is also used to calculate the concentration of radionuclides within the repository. That is, the total number of curies is equal to the following:

$$\text{Mass (\# curies)} = CV\theta + S_s V \Delta h C$$

Where

$$C = \text{initial concentration in the repository}$$

As shown in Section 4.2, the total number of curies in the repository after 1000 years of radioactive decay is  $3.34 \times 10^4$ . Depending on the value of  $\Delta h$ , each scenario will have a different initial concentration even though the mass is the same for each simulation as shown below and in Figures 5.18 and 5.19.

### Single Porosity Simulations

#### Base Case

$$\begin{aligned} 3.34 \times 10^4 &= [C \cdot 17556 \cdot 0.2] + [10^{-3} \cdot 17556.0 (1243.6 - 921.0)C] \\ \Delta h &= 1243.6 - 921 = 322.6 \\ \therefore C &= 3.8 \text{ Ci/m}^3 \end{aligned}$$

#### Pu-k20a

$$\begin{aligned} \Delta h &= 1643.6 - 996.0 = 247.6 \text{ m} \\ \therefore C &= 4.249 \text{ Ci/m}^3 \end{aligned}$$

Image Not  
Available

Figure 5.18. Breakthrough curve of Pu-239 concentration at the well in the repository (single porosity simulations)

Image Not  
Available

Figure 5.19. Breakthrough curve of Pu-239 concentration at the well repository (dual porosity simulations).

## **Pu-k20 and pu-k7**

$$\Delta h = 1243.6 - 1071 = 172.6 \text{ m}$$

$$\therefore C = 5.104 \text{ Ci/m}^3$$

## Dual Porosity Simulations

### **Pud-1**

$$\Delta h = 1243.6 - 996 = 247.6 \text{ m}$$

$$\therefore C = 4.249 \text{ Ci/m}^3$$

### **Pud-2**

$$\Delta h = 1243.6 - 1071. - 172.6 \text{ m}$$

$$\therefore C = 5.104 \text{ Ci/m}^3$$

### **Pud-4**

$$\Delta 1243.6 - 1021 = 222.6 \text{ m}$$

$$\therefore C = 4.5 \text{ Ci/m}^3$$

A result of the initial concentrations being variable is that, at higher concentrations, less brine has to flow out of the borehole for the same cumulative release.

## *RELEVANCE TO CCA*

To address this issue of whether the grid used for BRAGFLO was fine enough to attain a converged solution, EPA requested that DOE perform a detailed grid convergence study on the same grid as that used for the CCA calculations (A-93-02, II-I-16). DOE completed this work ( "Sensitivity of Flow, Transport, and Direct Brine Release to Grid Refinement Using the BRAGFLO and NUTS Computer Models") and a subsequent review by EPA indicated that the grid spacing used in the CCA will adequately characterize the problem and the numerical solution produced adequate results.

## 5.2.5 1992 PA Issue 5 - Treatment of Fracture Hydraulic Conductivities

The SECO flow and transport modeling performed in the 1992 PA appears to have randomly adjusted the effective porosities of the fractures, independently of the fracture spacing or of the Culebra transmissivity. The failure for the fractures to properly account for a change in transmissivity could significantly bias the modeling results.

To illustrate this point the following example is provided. If the thickness of the Culebra is 7.7 m and the hydraulic conductivity is 7 m/y the transmissivity is about 53 m/y. Now if the Culebra is treated as a dual porosity system as is assumed in the 1992 PA, all of the transmissivity must be assigned to the fractures as there is no advective flow within the matrix. Therefore, if a single fracture is assumed, it must have a sufficient hydraulic conductivity to pass the same amount of water through it as would an unfractured system with the same transmissivity. Intuitively this would suggest that if two fractures are in the Culebra their hydraulic conductivity would be less than one fracture as both fractures are capable of transmitting water. As shown in Section 4.4.1 the fracture aperture (i.e., effective porosity) may be used to translate the transmissivity of the Culebra into an equivalent fractured medium. From these relationships it is evident that to maintain an equivalent transmissivity the fracture aperture decreases with the number of fractures or fracture spacing. As one would expect, the hydraulic conductivity of the fractures ( $K_f$ ) also decreases as the number of fractures increases. If this relationship is not maintained, mass is not conserved with respect to the volume of water flowing through the system.

In the 1992 PA, the thickness of the Culebra is held constant at 7.7 m, and a series of 70 transmissivity fields are used for modeling the Culebra dolomite. Each of these fields is divided into a number of regions of varying hydraulic conductivities. As discussed above, to conserve mass each of the various transmissivity regions would need different fracture properties depending on the hydraulic conductivity assigned to the region. Not only does the 1992 PA not take this approach, but it also assumes a single fracture hydraulic conductivity (i.e., effective porosity/ aperture) regardless of the Culebra transmissivity. Furthermore, the fracture aperture is independently sampled from the fracture spacing which means that single fractures could have very small apertures or many fractures could have very large apertures. This approach to the assignment of fracture properties and the effect of this random sampling on dependent variables should be further reviewed.

## *RELEVANCE TO CCA*

As indicated by EPA's concern, one might suspect the possibility of some correlation between sampled Culebra transport parameters. Culebra physical transport parameters for which values are used in performance assessment consist of Culebra thickness, matrix tortuosity, diffusive porosity, advective porosity, matrix block length, and dispersivity. To test this possibility of correlation, DOE prepared scatter plots of interpreted results from the hydopad test sites which yielded the physical transport parameters used to develop the PA parameters distributions (H-3, H-11, and H-19) (Docket: A-93-02, II-G-1, Volume X, Appendix MASS, Attachment MASS 15-10, Figures 1 and 2). Figure 1 shows plots, constructed using transmissivity and physical transport parameters inferred from hydraulic and tracer test results at the H-3, H-11 and H-19 hydopads Beauheim 1987, Beauheim 1989, Docket: A-93-02, II-G-1, Reference #41, Reference #44 and Holt (1997). A review of the plots presented in Figure 1 of MASS Attachment 15-10 reveal no obvious correlations between transmissivity and the physical transport parameters. It has been noted that in some cases plotting scattergrams of the serial ranks of the parameters can reveal correlations which are unapparent from scattergrams of parameter values Helton et. al., (1992) - (Docket: A-93-02, II-G-1, Reference # 563, Volume 4). Therefore, DOE also plotted the serial rank of both the advective porosity and the matrix block length against the serial rank of transmissivity and against each other. These scatter plots are presented as Figure 2 in MASS Attachment 15-10, and again no correlations are apparent. Furthermore, no trends or zoning patterns are apparent in the distribution of physical transport parameters across the WIPP site. Based on these results DOE and EPA have concluded that no correlations exist between transmissivity and physical transport parameters for the Culebra dolomite. EPA also required DOE to ensure that the uncertainty ranges placed on the parameters would not result in unrealistic combinations (Docket: A-93-02, II-G-1, Volume XI, Appendix PAR, page PAR-189). EPA believes that the work documented by DOE has adequately evaluated potential correlations between porosity and transmissivity and that none exist.

### 5.2.6 1992 PA Issue 6 - Travel Time Analysis

In the 1992 PA a travel time discussion was presented that was intended to characterize the transmissivity fields (Docket: A-93-02, Ref#563; Vol 4 p. 6-28). The 1992 PA travel-time analysis assumed that the Culebra dolomite was unfractured and only advective flow was considered. Furthermore, the 1992 PA travel time analysis assigned an effective porosity of 16% rather than the median value of 13.9%. The results from this analysis are summarized as follows..." that 90 percent of the travel times were longer than 12,000 yr, 50 percent of the travel times were longer than 18,000 yr and 10 percent of the travel times were longer than 27,000 yr."

To evaluate the 1992 PA travel time conclusions, several STAFF3D travel time/transport simulations were performed. Prior to presenting the results from these simulations, it is necessary to provide relevant background information. The particle paths that are taken by the radionuclides in the 1992 PA were previously shown in Figure 4.1.6. Of particular interest are the hydraulic conductivities that were measured in the wells along these paths to the WIPP Land Withdrawal boundary. The wells that fall along these paths are H-3, DOE-1 and H-11. The hydraulic conductivities for each of these wells, as measured in the field are shown in Table 5.3. Well H-1 does not fall directly on the travel path, however, it has been included primarily because the measured hydraulic conductivity is lower than the three other wells and thus, the median hydraulic conductivity from the four wells (i.e. 22 m/y) should not be is unjustifiably high.

The 1992 PA incorporates a transmissivity field to describe the hydraulic properties of the Culebra Dolomite for each of the 70 realizations. The transmissivity is defined as the hydraulic conductivity multiplied by aquifer thickness. The 1992 PA assumes a uniform Culebra thickness and assumes the hydraulic conductivity varies within the field. The 1992 PA also indicates that the median hydraulic conductivity for the Culebra is 7 m/y.

Table 5.3. Hydraulic Property Data for the Culebra Dolomite

Well No.	Transmissivity		Hydraulic Conductivity m/y
	m <sup>2</sup> /sec	m <sup>2</sup> /yr	
H-1	9.4 x 10 <sup>-7</sup>	29.64	3.85
H-3	2.5 x 10 <sup>-6</sup>	78.84	10.24
DOE-1	1.2 x 10 <sup>-5</sup>	378.40	49.14
H-11	3.1 x 10 <sup>-5</sup>	977.6	126.9
Median Hydraulic conductivity			22.2
Average Hydraulic conductivity			47.5

This suggests that the net effect on travel time that the varying hydraulic conductivities would have on a radionuclide moving through one of the transmissivity fields would be similar to those effects caused by a transmissivity field with a uniform hydraulic conductivity of 7 m/y.

To check this 1992 PA assumption, a STAFF3D transport simulation was performed with a value of 7 m/y assigned to the hydraulic conductivity of the Culebra, and as was done in the 1992 PA travel-time analysis, an effective porosity of 16%. It was expected that the STAFF3D results would be similar to the 1992 PA results mentioned above.

The STAFF3D simulation was performed and the results are shown in Figure 5.20 (Pu-k7.dat). It appears from this simulation that the peak concentration of Pu-239, which is most representative of advective flow, reaches the boundary around 10,000 years. However, the distance a particle travels in STAFF3D simulations is 2415 m, whereas, the 1992 PA particle path is closer to 3,600 m. Therefore, under similar gradients it would take an additional 5000 years to travel an equivalent distance for a total of 15,000 years. Fifty percent of the travel times in the 1992 PA were greater than 18,000 years. This means that in 50 percent of the 1992 PA simulations the transmissivity field was characterized by an average hydraulic conductivity of less than 7 m/y, which does not appear to be supported by the field data.

As indicated in Table 5.3 the median hydraulic conductivity measured along the radionuclide travel path is 22.2 m/y. To determine the effect on travel times that an increase in hydraulic conductivity to 20 m/y, would have on the STAFF3D results, an additional simulation was performed. This simulation is identical to the previous simulation with the

exception that the hydraulic conductivity in the Culebra was increased to 20 m/y. The results are shown in Figure 5.21, and indicate that the travel time to the boundary is 5000 years. This translates to a velocity of .483 m/y. Therefore, if a radionuclide were to take a more circuitous route of 3,600 meters as was assumed in the 1992 PA it would take approximately 7,450 years to reach the WIPP Land Withdrawal Boundary. The transmissivity fields that are generated through the pilot point method and are used to support the 1992 PA appear to significantly underestimate the median hydraulic conductivities as measured in the field.

#### *RELEVANCE TO CCA*

To address these issues, the Agency asked DOE to perform the following end-to-end-test in order to address EPA's concerns (A-93-02, II-I-17, bottom of page 3):

- Generate a synthetic data set that is statistically similar to the WIPP-site data to be used to evaluate the statistical validity of GRASP\_INV results.
- Process the synthetic data with GRASP\_INV to produce 100 calibrated transmissivity fields, input the fields to SECOFL2D to produce velocity fields, and input the velocity fields to TRACKER to produce travel paths from 20 release points to a compliance boundary.

The response to the need for an end-to-end functional requirement and test is provided by the test presented in Lavenue, 1997 (A-93-02, II-I-19; WPO #44199). The response presented in Lavenue, 1997, addressed the issues raised above. As discussed in detail in Section 5.6 of the TSD for Section 194.23: Models and Computer Codes (A-93-02, V-B-6), EPA finds that the results of this test indicate that DOE's treatment of the transmissivity fields is adequate.

#### 5.2.7 1992 PA Issue 7 - Permeability of Culebra Specified in BRAGFLO

The modeling that was performed with BRAGFLO in the 1992 PA included the Culebra in the model domain. The Culebra was modeled as a single porosity porous media with no fractures and an assumed mean permeability of 7 m/y. The overall effect these assumptions

had on the brine volumes introduced into the Culebra was not presented in the 1992 PA. That is, if the permeability of the Culebra was set too low it would limit the amount of brine that could move up the borehole regardless of how high the permeability of the borehole material, which in turn, would result in lower flux values being input from BRAGFLO into PANEL and would ultimately result in lower release rates. This Culebra permeability value assigned in BRAGFLO was not statistically sampled as part of the LHS procedures in the 1992 PA, and no analyses were presented to demonstrate the lack of sensitivity of the modeling results to this parameter.



Image Not Available

Figure 5.20. Breakthrough concentration of Pu-239 at the boundary of WIPP site (single porosity simulations)



Figure 5.21. Travel time results with Culebra hydraulic conductivity at 20 m/y (Pus-K20)

A comparison of simulation results obtained from Pus-K20 and Pus-K7 of the single porosity simulations and output from Pud-2 and Pud-4 of the dual porosity simulations provide the best insight into the overall sensitivity of the Culebra permeability to the BRAGFLO borehole flux output.

As shown in Figure 5.22 the results from the single porosity simulations indicate that the volume of water leaving the borehole and entering the Culebra is indistinguishable between the simulation where the hydraulic conductivity of the Culebra is 7 m/y (Pus-K7) versus 20 m/yr (Pus-k20). Furthermore, Figure 5.23 indicates similar results with the dual porosity simulations. The negligible effect that the permeability of the Culebra has on the transport of radionuclides up the borehole to the Culebra is also shown in Figure 5.24.

These results suggest that the brine volumes predicted by BRAGFLO to move up the borehole are insensitive to the range permeabilities assigned to the Culebra. This is because, under the range of hydraulic conductivities tested, the transmissivity of the Culebra is high enough to allow all of the brine move easily into the Culebra under the existing gradients. If, however, the transmissivity of the Culebra was significantly reduced (i.e. order of magnitude), the modeling results may indicate some sensitivity to the Culebra hydraulic conductivity.

#### *RELEVANCE TO CCA*

As noted above, the STAFF3D modeling indicated that DOE's approach in the 1992 PA was adequate. Furthermore, since their approach has not fundamentally changed in the CCA, with respect to the treatment of the Culebra properties in BRAGFLO, EPA has determined that DOE's approach is appropriate and it is unnecessary to statistically sample the Culebra properties in the BRAGFLO simulations.

#### 5.2.8 1992 PA Issue 8 - Borehole Permeability

The modeling in the 1992 PA indicated that the results were very sensitive to the assumed permeability of the borehole. The sampled range in the 1992 PA is  $1 \times 10^{-14} \text{ m}^2$  to  $1 \times 10^{-11} \text{ m}^2$ , with the median at  $3.16 \times 10^{-12} \text{ m}^2$ . The permeability value that will ultimately be used to support the PA may not be based on empirical data but may be derived from regulatory

guidance. All of the STAFF3D simulations used twice the mean permeability value with the exception of one simulation where the permeability was increased by an additional 50 percent (i.e., Pud-4).

Pud-3 and Pud-4 are identical STAFF3D simulates (Table 5.2) except that the permeability of the borehole has been increased from 1200 m/y to 1800 m/y (Table 5.2). Figure 5.25 provides a comparison of STAFF3D output in cumulative curies from simulations Pud-3 and Pud-4. Although there is some difference, it does not appear that the borehole would make a significant difference unless the permeability of the borehole was changed more drastically.

#### *RELEVANCE TO CCA*

The EPA undertook several activities that investigated the effect that borehole permeability has on the CCAPA results. First, the EPA performed a parameter sensitivity analysis (A-93-02,V-B-13) and second the EPA required DOE to perform a Performance Assessment Verification Test (PAVT) in which the borehole permeability was one of the parameters that was varied (A-93-02,V-G-26). The Agency has determined that the combined results of these analyses indicate that DOE's approach is adequate.



Figure 5.22. Cumulative volume of water exiting out of the well (single porosity simulations)

Image Not  
Available

Figure 5.23. Cumulative volume of water exiting out of the well into culebra (dual porosity simulations)

Image Not  
Available

Figure 5.24. Cumulative curves exiting out of the well into culebra (single porosity mode with 10 boundary flux nodes)

Image Not  
Available

Figure 5.25. Cumulative curies exiting out of the well into culebra (dual porosity mode with 10 boundary flux nodes)

## 6. Non-Docketed References

- Brinster, K.F. 1991. *Preliminary Geohydrologic Conceptual Model of the Los Medanos Region Near the Waste Isolation Pilot Plant for the Purpose of Performance Assessment*. SAND 89-7147. Albuquerque, NM: Sandia National Laboratory.
- Cauffman, T.L., A.M. LaVenue, J.P. McCord. 1991. *Ground-Water Flow Modeling of the Culebra Dolomite; Volume II: Data Base*. SAND 89-7068/2. Albuquerque, NM: Sandia National Laboratory.
- Huyakorn, P.S., Panday S.P., Sinha, A., 1992. STAFF3D: A Three-dimensional Finite Element Code for Simulating Fluid Flow and Transport of Radionuclides in Fractured Porous Media With Water Table Boundary Conditions, Version 2.0.
- Kaufmann, D.W., ed. 1960. *Sodium Chloride, The Production and Properties of Salt and Brine*. Monograph No. 145. Washington, DC: American Chemical Society
- Leigh, C.D., B.M. Thompson, J.E. Campbell, D.E. Longsine, R.A. Kennedy, and B.A. Napier. 1993. *User's Guide for GENII-S: A Code for Statistical and Deterministic Simulations of Radiation Doses to Humans from Radionuclides in the Environment*. SAND 91-0561. Albuquerque, NM: Sandia National Laboratory.
- SAND92-7306, A Modeling Approach to Address Spatial Variability Within the Culebra Dolomite Transmissivity Field, Sandia National Laboratories, December 1992.
- SAND89-7069, Regional Double-Porosity Solute Transport in the Culebra dolomite Under Brine-Reservoir-Breach Release Conditions: An Analysis of Parameter Sensitivity and Importance, Sandia National Laboratories, February 1991.
- SAND89-7068/1, Ground-Water Flow Modeling of the Culebra Dolomite, Volume I: Model Calibration, Sandia National Laboratories, October 1990.
- SAND88-7002, Numerical Simulation of Ground-Water Flow in the Culebra Dolomite at the Waste Isolation Pilot Plant (WIPP) Site: Second Interim Report, Sandia National Laboratories, March 1988.
- SAND89-7068/2, Ground-Water Flow Modeling of the culebra dolomite, Volume II: Data Base, Sandia National Laboratories, October 1990.
- Snow, D.T., 1969, Anisotropic permeability of fractured media, Water Resources Research, vol. 5, no. 6, p 1273-1289.

APPENDIX S

SUPPLEMENTAL STAFF3D  
MODELING AT WIPP

## Contents

S1. Introduction .....	S1-1
S2. Conceptualization of Dual-Porosity Media .....	S2-1
S2.1 Fracture Conductivity and Porosity .....	S2-1
S2.2 Culebra Fracture Hydraulic Conductivity and Porosity .....	S2-4
S2.3 Calculation of Groundwater Velocity .....	S2-6
S3. Radius of Influence Calculations .....	S3-1
S3.1 Objectives .....	S3-1
S3.2 Problem Conceptualization .....	S3-1
S3.3 Model Formulation .....	S3-2
S3.4 Description of Simulations .....	S3-7
S3.4.1 Slug Source .....	S3-7
S3.4.2 Line Slug Source .....	S3-9
S3.4.3 Constant Source .....	S3-11
S4. Grid Convergence Analysis .....	S4-1
S4.1 Objectives .....	S4-1
S4.2 Problem Conceptualization .....	S4-1
S4.3 Model Formulation .....	S4-1
S4.4 Description of Simulations .....	S4-3
S5. Repository Decoupling Analysis .....	S5-1
S5.1 Objectives .....	S5-1
S5.2 Problem Conceptualization .....	S5-1
S5.3 Model Formulation .....	S5-1
S5.4 Description of Simulations .....	S5-2
S6. References .....	S6-1

Tables

Table 3.1    Input parameters for dual porosity simulations ..... S3-5

## Figures

Figure S2.1	Fracture porosity as a function of fracture hydraulic conductivity . . . . .	S2-7
Figure S3.1	Finite-element mesh for the radius of influence simulations . . . . .	S3-3
Figure S3.2	Breakthrough curves for a slug source in the radius of influence model . . .	S3-8
Figure S3.3	Breakthrough curves for a line slug source in the radius of influence model . . . . .	S3-10
Figure S3.4	Breakthrough curves for a constant source in the radius of influence model . . . . .	S3-13
Figure S4.1	Finite-element mesh for the grid convergence model . . . . .	S4-2
Figure S4.2	Breakthrough curves for the original model from SC&A (1995) . . . . .	S4-4
Figure S4.3	Breakthrough curves for the grid convergence model . . . . .	S4-5
Figure S5.1	Breakthrough curves for the original model with the repository . . . . .	S5-4
Figure S5.2	Breakthrough curves for the repository decoupled from the Culebra . . . . .	S5-5

## S1. Introduction

The Addendum describes supplemental STAFF3D modeling conducted to further address four issues raised in the main report regarding the 1992 PA. Each of the four issues and the associated STAFF3D simulation results are described in Sections S2 through S5 of this addendum.

The supplemental simulations and discussions described in the Addendum address the following issues raised in the main report (in the order presented in this addendum):

### 1992 PA Issue 5 - Fracture Porosity and Fracture Spacing

The SECO flow and transport modeling performed in the 1992 PA appears to have randomly adjusted the effective porosities of the fractures, independently of the fracture spacing or of the Culebra transmissivity. The failure to properly account for a change in transmissivity could significantly bias the modeling results.

In the 1992 PA, a series of transmissivity fields are used for modeling the Culebra Dolomite. Each of these fields is divided into a number of regions of varying hydraulic conductivities. The thickness of the Culebra is held constant at 7.7 m, therefore, the hydraulic conductivity is heterogeneous within each of the transmissivity fields. To conserve mass, each of the various transmissivity fields would need different fracture properties depending on the hydraulic conductivity assigned to the region. Not only does the 1992 PA not take this approach but it also assumes a single fracture hydraulic conductivity (i.e., effective porosity/aperture) regardless of the Culebra transmissivity. Furthermore, the fracture aperture is sampled independently from the fracture spacing which means that single fractures could have very small apertures or many fractures could have very large apertures. This approach to the assignment of fracture properties and the effect of this random sampling on dependent variables should be further reviewed.

Section S2 presents a functional relationship between fracture porosity and fracture hydraulic conductivity, which clearly shows that these parameters may be correlated; that is, they have a covariance of 1.0. In a fractured media, the fracture spacing, fracture porosity, and fracture hydraulic conductivity may be related mathematically. Furthermore, calculations presented in Section S2 illustrate that fracture porosity

representative of the range of fracture spacings described in the 1992 PA are much lower than porosity values used in the 1992 PA.

#### *RELEVANCE TO CCA*

As indicated by EPA's concern, one might suspect the possibility of some correlation between sampled Culebra transport parameters. Culebra physical transport parameters for which values are used in performance assessment consist of Culebra thickness, matrix tortuosity, diffusive porosity, advective porosity, matrix block length, and dispersivity. To test this possibility of correlation, DOE prepared scatter plots of interpreted results from the hydropad test sites which yielded the physical transport parameters used to develop the PA parameters distributions (H-3, H-11, and H-19) (Docket: A-93-02, II-G-1, Volume X, Appendix MASS, Attachment MASS 15-10, Figures 1 and 2). Figure 1 shows plots, constructed using transmissivity and physical transport parameters inferred from hydraulic and tracer test results at the H-3, H-11 and H-19 hydropads Beauheim 1987, Beauheim 1989, Docket: A-93-02, II-G-1, Reference #41, Reference #44 and Holt (1997). A review of the plots presented in Figure 1 of MASS Attachment 15-10 reveal no obvious correlations between transmissivity and the physical transport parameters. It has been noted that in some cases plotting scattergrams of the serial ranks of the parameters can reveal correlations which are unapparent from scattergrams of parameter values Helton et. al., (1992) - (Docket: A-93-02, II-G-1, Reference # 563, Volume 4). Therefore, DOE also plotted the serial rank of both the advective porosity and the matrix block length against the serial rank of transmissivity and against each other. These scatter plots are presented as Figure 2 in MASS Attachment 15-10, and again no correlations are apparent. Furthermore, no trends or zoning patterns are apparent in the distribution of physical transport parameters across the WIPP site. Based on these results DOE and EPA have concluded that no correlations exist between transmissivity and physical transport parameters for the Culebra dolomite. EPA also required DOE to ensure that the uncertainty ranges placed on the parameters would not result in unrealistic combinations (Docket: A-93-02, II-G-1, Volume XI, Appendix PAR, page PAR-189). EPA believes that the work documented by DOE has adequately evaluated potential correlations between porosity and transmissivity and that none exist.

## 1992 PA Issue 6 -Groundwater Travel Time Analysis

In the 1992 PA, travel times in the Culebra to the accessible environment are presented. The modeling results for single porosity non-fractured media in the 1992 PA (page 6-28) are summarized by the following, "...90 percent of the travel times were longer than 12,000 years, 50 percent of the travel times were longer than 18,000 years, and 10 percent of the travel times were longer than 27,000 years." The STAFF3D modeling provides a method to determine whether these travel times are realistic and in accordance with the available field data. Further STAFF3D simulations were conducted for this report in which a 100-kilometer long grid was used to provide a bounding approach to computing travel times and to determine the extent to which radionuclides may travel in the Culebra.

The transmissivity field(s) used for the 1992 PA are comprised of multiple blocks or zones of various dimensions which are assigned uniform permeability values within each block. Transmissivity, however, can vary between blocks. The 1992 PA assumes that the mean hydraulic conductivity for the Culebra Dolomite is 7 m/yr. STAFF3D travel-time analyses suggest that the overall combined effect of these composite permeabilities yield travel times far shorter than that which would be expected had the mean hydraulic conductivity of 7 m/yr been used over the entire field. Furthermore, the assumption that 7 m/yr is the mean value of hydraulic conductivity is not supported by the measured field data over the travel path of the radionuclides.

Section S3 presents radius of influence calculations in which the Culebra is represented as a dual-porosity media with fracture spacing of 7 m, an equivalent porous medium hydraulic conductivity of 7 m/yr, no chemical retardation, and active matrix diffusion. These calculations show that radionuclides could travel at least 5 km. However, these travel times include the effects of matrix diffusion. Travel distance in the Culebra for fracture flow, in a single fracture, without matrix diffusion would be on the order of 13,480 km in 10,000 years. In a practical sense, this means that any affected groundwater would exit the system within the 10,000 year time frame.

### *RELEVANCE TO CCA*

To address these issues, the Agency asked DOE to perform the following end-to-end-test in order to address EPA's concerns (A-93-02, II-I-17, bottom of page 3):

- Generate a synthetic data set that is statistically similar to the WIPP-site data to be used to evaluate the statistical validity of GRASP\_INV results.
- Process the synthetic data with GRASP\_INV to produce 100 calibrated transmissivity fields, input the fields to SECOFL2D to produce velocity fields, and input the velocity fields to TRACKER to produce travel paths from 20 release points to a compliance boundary.

The response to the need for an end-to-end functional requirement and test is provided by the test presented in Lavenue, 1997 (A-93-02, II-I-19; WPO #44199). The response presented in Lavenue, 1997, addressed the issues raised above. As discussed in detail in Section 5.6 of the TSD for Section 194.23: Models and Computer Codes (A-93-02, V-B-6), EPA finds that the results of this test indicate that DOE's treatment of the transmissivity fields is adequate.

#### 1992 PA Issue 4 -Grid Convergence Analysis

In the 1992 PA, the model domain for BRAGFLO has a relatively coarse discretization. Recently, DOE sponsored an independent analysis on the sensitivity of the BRAGFLO results to grid convergence (Palmer Vaughn, personal communication). However, the findings of this analysis are not yet available. The issue of grid convergence is an important one with any numerical model, such as BRAGFLO. A discretization that is too coarse can produce results with unacceptable levels of error.

Only qualitative results from the STAFF3D analyses pertaining to grid spacing versus the acceptability of the mass balance errors were presented in the main report. The grid that was ultimately used for STAFF3D resulted in reasonable mass balance errors (less than 5%) and was far more finely discretized than the grid used for BRAGFLO in the 1992 PA. The STAFF3D grid used 528 nodes to define the waste region in a panel, whereas, BRAGFLO incorporated 256 nodes to discretize the entire panel.

An analysis of grid convergence for the STAFF3D modeling presented in the main report is provided in Section S4. Only the Culebra was simulated, however, the mesh contained 54,000 nodes in 3 layers. Results show that travel times were somewhat higher using the finer mesh than used in earlier STAFF3D simulations presented earlier in the main report. This analysis is intended to demonstrate that grid convergence should be an important consideration for the application of a numerical model.

#### *RELEVANCE TO CCA*

To address this issue of whether the grid used for BRAGFLO was fine enough to attain a converged solution, EPA requested that DOE perform a detailed grid convergence study on the same grid as that used for the CCA calculations (A-93-02, II-I-16). DOE completed this work ( “Sensitivity of Flow, Transport, and Direct Brine Release to Grid Refinement Using the BRAGFLO and NUTS Computer Models”) and a subsequent review by EPA indicated that the grid spacing used in the CCA will adequately characterize the problem and the numerical solution produced adequate results.

#### 1992 PA Issue 3 - Repository/Culebra Decoupling Analysis

In the PA, the flow and transport processes active in the repository have effectively been decoupled from those in the Culebra. That is, the output from PANEL consists of radionuclide concentrations which are subsequently input into SECO, which in turn simulates flow and transport through the Culebra to calculate cumulative releases at the WIPP Land Withdrawal Boundary. The flux, however, that is calculated to move up the borehole by BRAGFLO is not introduced into the Culebra. The main report evaluated coupled flow in the repository and Culebra. This Addendum further describes the effect of decoupling the repository from the Culebra.

The STAFF3D analyses described in the main report indicate that if the flux from the repository was introduced to the Culebra there would be a significant increase in radionuclide velocities to the WIPP Land Withdrawal Boundary.

These findings are substantiated in Section S5 by comparing the previous STAFF3D modeling with a simulation in which the repository was decoupled from the repository.

In the original simulation with borehole flux injected into the Culebra flow system, the time at which relative concentrations (relative to an initial concentration of 1.0) exceeded  $1 \times 10^{-5}$  at a downgradient distance of 1 km occurred at about 300 years. In the decoupled simulation, where borehole flux does not disturb the flow system, the groundwater travel-time increased to about 2000 years. The maximum contaminant concentration after 10,000 years at 1 km from the borehole decreased from  $1 \times 10^{-3}$  in the original simulation to  $2 \times 10^{-4}$  in the decoupled simulation. In this analysis, the Castile brine source was not included. Addition of flow from the Castile would make the differences even greater.

#### *RELEVANCE TO CCA*

As indicated above the computer simulations performed in the 1992 PA decoupled the flow fields of the repository and the Culebra. EPA's initial concern was that the volume of flow up the borehole would perturb the Culebra flow system. However, the volume of water predicted to flow up the borehole in a human intrusion scenario is relatively small and is significantly less in the CCA, than that which was predicted in the 1992 PA. Therefore, steady-state assumptions on the flow field appear to be reasonable because the volume of flow up the borehole and therefore in the Culebra member will be relatively small with respect to the flow field (Docket: A-93-02, II-G-1, Reference # 542, Reeves et al 1991, page 3-12). Furthermore, the contaminant introduced into the Culebra is immediately dispersed into the fractures over a grid block that is  $50 \text{ m}^2$ . DOE's approach artificially introduces instantaneous advection over this area which should approximate the initial fast advection adequately (Docket: A-93-02, II-G-11, *Analysis Package for Culebra Flow and Transport*, WPO #40516, page 26).

## S2. Conceptualization of Dual-Porosity Media

### S2.1 FRACTURE CONDUCTIVITY AND POROSITY

In the 1992 PA, it is assumed that the Culebra dolomite behaves as a dual porosity system. At this time, it is unknown whether this conceptualization is more appropriate than other conceptual models (e.g., dual permeability or channeling). In light of this 1992 PA assumption, the following discussion is focused on the theory describing dual porosity groundwater flow and radionuclide transport.

Darcy's law relates the movement of water in a porous medium to the hydraulic gradient and the hydraulic conductivity. The hydraulic conductivity is a measure of the transmissive capacity of the medium coupled with the density and viscosity of the fluid (water in this case). The hydraulic gradient is simply the slope on the water table (unconfined aquifers) or the potentiometric surface for a confined system. The equation for Darcy's law is

$$q = K \, dh/dl$$

where  $q$  is the Darcy velocity (m/yr),  $K$  is the hydraulic conductivity (m/yr) and  $dh/dl$  is the hydraulic gradient (dimensionless - m/m). Hydraulic conductivity is actually a property of both the physical media (the aquifer) and the fluid. Darcy's law may also be written using intrinsic permeability ( $k$ ) which is a property of the media alone, as shown below:

where:

- $k$  = intrinsic permeability ( $m^2$ )
- $\rho$  = fluid density ( $kg/m^3$ )
- $\mu$  = viscosity ( $Pa \cdot s$ )
- $g$  = gravitational constant ( $m/s^2$ )

The rate at which a conservative contaminant (i.e., non-sorbing and nonreactive) migrates through a porous medium is computed by dividing the Darcy velocity given above, by the effective porosity.

The effective porosity for a porous medium is the ratio of the connected void space divided by the total volume of the medium.

In a fractured medium, Darcy's law still applies, however, the hydraulic conductivity (K) is more difficult to determine. If the fractures are conceptualized as a series of parallel plates (with the fractures being the gaps between adjacent plates), mathematical equations can be derived to determine the equivalent hydraulic conductivity that would be used in Darcy's law. These equations are presented later in this section.

The porosity of the fracture system actually should be viewed as two components, fracture porosity and matrix porosity. Using the parallel plate analogy, the porosity of the fractures is the number of fractures times the fracture aperture (gap thickness) divided by the thickness of the aquifer. The matrix porosity is the porosity of the blocks of rock between the fractures. In a fractured system such as granitic rock, the matrix porosity may be effectively zero because there is no intergranular void space. However, there is some measurable void space within the Culebra matrix (Docket: A-93-02, Ref#563). As will be discussed in Section 3, the matrix porosity temporarily traps contaminants moving through the fractures through the process of diffusion between the fracture and the matrix. The contaminant concentrations are initially higher in the fracture than in the matrix. Diffusion causes the contaminants to move into the matrix where it remains until the concentration in the fracture falls below that of the adjacent matrix. This process, termed matrix diffusion, causes the effective contaminant velocity for a dual-porosity medium (fracture plus matrix) to be much less than for a system of fractures alone.

The hydraulic conductivity of a system of horizontal fractures is determined by the fracture aperture and the spacing between fractures. Given an equivalent porous medium hydraulic conductivity (i.e., determined through aquifer testing) and fracture spacing, it is possible to compute the fracture hydraulic conductivity. The calculation is based upon moving the same flux of groundwater through the fracture system as through the porous medium. The derivation of this equation is developed below.

The fracture conductivity equation is derived in two steps. First, the hydraulic conductivity for a single fracture is defined and then this is related to the flow rate through the fracture. The hydraulic conductivity of a single fracture is given as:

(1)

where:

$b$  = half-fracture aperture (m)

$K_f$  = fracture hydraulic conductivity (m/yr)

This equation is presented in a number of papers by Snow (1969) and by Gale (1982). The equation is often rewritten in terms of the full fracture aperture, as follows:

(2)

where:

$w$  = full fracture aperture ( $b^2 = w^2/4$ ) (m)

The second step in computing aperture from an equivalent porous medium K value is to equate the flow rates through the porous and fractured systems. The flow through a set of N horizontal fractures of identical aperture is:

(3)

where:

$Q_f$  = flow rate through the fractures ( $m^3/yr$ )

$L$  = length of fractures perpendicular to flow (m)

$N$  = number of fractures

The term ( $N w L$ ) is the area term in a traditional Darcy's law equation. The equation for flow through an equivalent porous medium would be:

(4)

where:

$K$  = equivalent porous medium hydraulic conductivity (m/yr)

$D$  = aquifer thickness (m)

$L$  = length perpendicular to flow direction (m)

As mentioned above, equation 4 may also be written in terms of intrinsic permeability and fluid properties, as show below:

(4b)

To compute an equivalent K for the porous medium, the flow rates through the two systems (porous and fractured) must be equal. Setting equation 3 equal to equation 4b yields:

(5)

with common terms canceling from the equation. This equation can then be rearranged to give an equation of fracture aperture in terms of an equivalent porous medium hydraulic conductivity:

(6)

Finally, to get the equation in terms of spacing between fractures ( $D_f = D/N$ ), the equation becomes:

(7)

After computing the fracture aperture for a given porous medium hydraulic conductivity (equation 7), the fracture hydraulic conductivity is computed from equation 1 above.

## S2.2 CULEBRA FRACTURE HYDRAULIC CONDUCTIVITY AND POROSITY

The fracture hydraulic conductivity for the Culebra was computed for two assumed fracture spacings of 0.06 m (the minimum spacing reported in the PA) and 7.7 m (Note that half the fracture spacing is used in STAFF3D or 3.85 m in this case) and a given equivalent porous media hydraulic conductivity of 7 m/yr. Note that the fracture spacing of 7.7 m results in one fracture within the Culebra. These fracture hydraulic conductivity values computed from equation 1 are 16,560 m/yr and 421,240 m/yr, respectively. Keep in mind that the CCA assumed that the effective thickness of the Culebra is 4.0 m, rather than the 7.7 m assumed in this analysis. However, this would not change any of the conclusions based on this analysis.

As an example, to compute the fracture hydraulic conductivity for the case of a single fracture, first use equation 7 to compute fracture aperture as follows (Note that higher densities lead to higher fracture hydraulic conductivities):

$$\begin{aligned}
 K &= 7.0 \text{ m/yr} = 2.24 \times 10^{-7} \text{ m/s} \\
 D_f &= 7.7 \text{ m} \\
 \mu &= 0.001 \text{ Pa-s} \\
 \rho &= 1000.0 \text{ kg/m}^3 \\
 g &= 9.79 \text{ m/s}^2
 \end{aligned}$$

$$w = [(12 \times 2.24 \times 10^{-7} \times 0.001 \times 7.7)/(1000.0 \times 9.79)]^{1/3}$$

$$w = 0.000128 \text{ m}$$

The aperture is then used with equation 2 to compute the fracture hydraulic conductivity as follows:

$$K_f = ((0.000128)^2 \times 1000.0 \times 9.79)/(12 \times 0.001)$$

$$K_f = 0.0133 \text{ m/s} = 421,240 \text{ m/yr}$$

Given the fracture spacing and aperture (computed from equation 7), it is simple to compute the fracture porosity of the Culebra. Fracture porosity is simply the number of fractures times fracture aperture divided by aquifer thickness. In the example above, fracture porosity is computed as follows:

(8)

where

$\phi_f$	= fracture porosity	
D	= aquifer thickness	= 7.7 m
N	= number of fractures	= 1
w	= fracture aperture	= 0.000128 m

$$\phi_f = (0.000128 \times 1)/7.7$$

$$\phi_f = 1.66 \times 10^{-5}$$

In fact, fracture hydraulic conductivity and fracture porosity are related linearly on a logarithmic scale, as shown in Figure S2.1. This analysis illustrates that fracture hydraulic conductivity and porosity are functionally related (i.e., covariance = 1.0) and should not be sampled independently as was done in the 1992 PA. The plot in Figure S2.1 shows a family of curves for assumed equivalent porous media hydraulic conductivity values of 20 m/yr, 7 m/yr, and 1 m/yr. All values assume an aquifer thickness of 7.7 m. The porosity values associated with a porous hydraulic conductivity of 7 m/yr and for fracture spacings of 0.06 m and 7.7 m are 0.000423 and 0.0000166,

respectively. These values can also be obtained through inspection of Figure S2.1 (7 m/yr curve) using hydraulic conductivity values of 16,560 and 421,240 m/yr, respectively.

The 1992 PA assigned a range of fracture porosity to the Culebra of 0.0001 to 0.01. These correspond to fracture hydraulic conductivities of approximately 70,000 m/yr and 800 m/yr, respectively. These values result in much slower travel times in the Culebra compared to values computed using fracture spacing.

### S2.3 CALCULATION OF GROUNDWATER VELOCITY

The velocity at which contaminants move through a porous medium by advection may be computed from Darcy's law as:

(9)

where:

K is the hydraulic conductivity of the porous medium,

$\phi_e$  is the effective porosity, and

dh/dl is the hydraulic gradient.

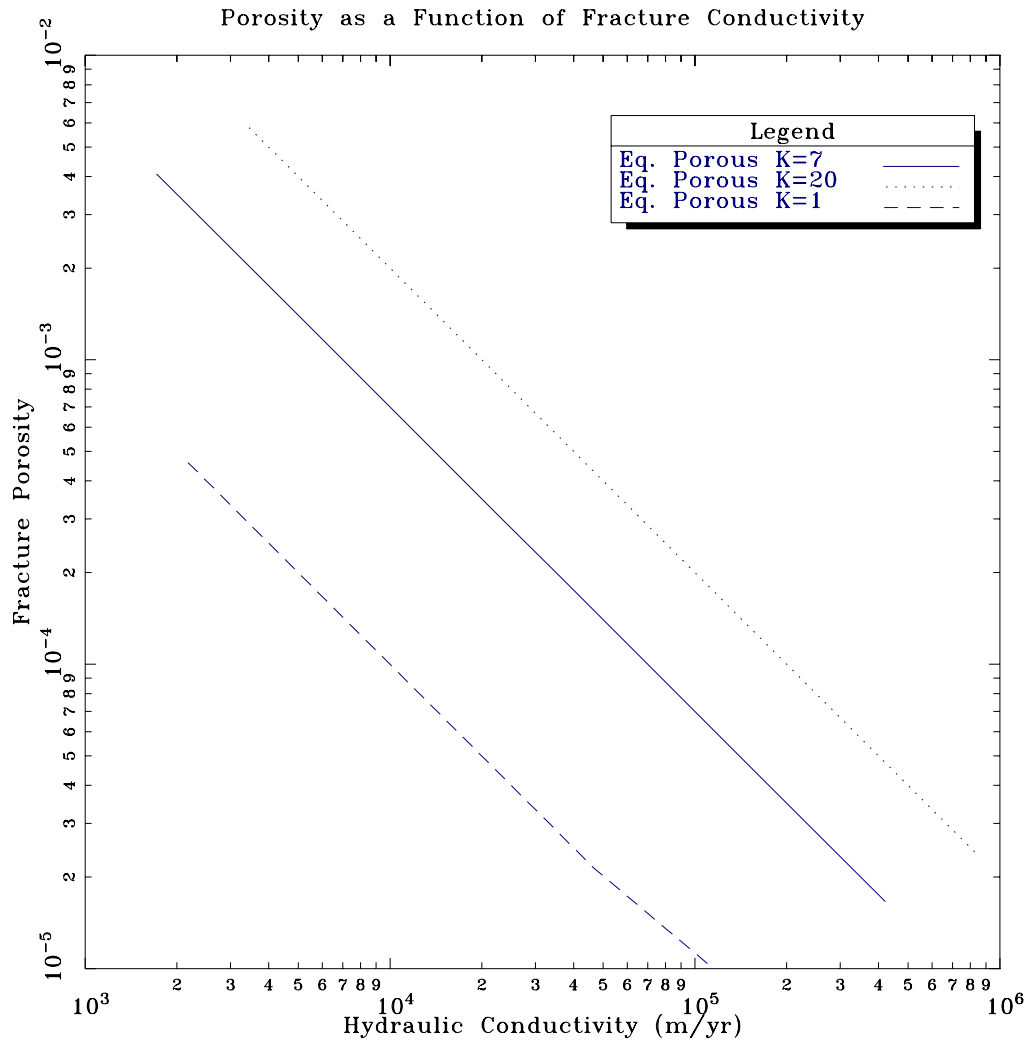


Figure S2.1 Fracture porosity as a function of fracture hydraulic conductivity.

Explanation

- Figure based on a constant equivalent porous hydraulic conductivity of 7 m/yr
- Aquifer thickness is 7.7 m
- Lower fracture hydraulic conductivities equate to more fractures
- Each fracture assumed to be of equal aperture

The same equation written in terms of intrinsic permeability ( $k$ ) and fluid properties is as follows:

(9b)

This velocity is often called the average linear or seepage velocity.

The same equation is used to compute the contaminant velocity in a fracture, except that the effective porosity ( $\phi_e$ ) is equal to 1.0. Many hydrogeologic texts (and the STAFF3D manual) refer to the velocity computed in equation 9 as the Darcy velocity.

Assuming a hydraulic gradient of 0.0032 in the Culebra and a fracture spacing of 0.06 m ( $K_f = 16,560$  m/yr as described in the previous section), the Darcy velocity in a fracture would be 53 m/yr (i.e.,  $0.0032 \times 16,560$  m/yr). The same velocity is computed for an equivalent porous medium with  $K = 7$  m/yr and porosity equal to the fracture porosity of 0.000423 (the fracture porosity computed for a fracture spacing of 0.06 m). Thus, a contaminant could travel 530 km through the Culebra in 10,000 years due to advection only. For the worst case of a single fracture in which the fracture hydraulic conductivity is 421,240 m/yr, the travel distance would be 13,480 kilometers ( $421,240$  m/yr  $\times$   $0.0032$ ). This travel distance is greatly reduced, however, when matrix diffusion processes are included, as presented in the following sections. Furthermore, at this high hydraulic conductivity, it is likely that the hydraulic gradient would be much lower than 0.0032 which would result in much lower velocities.

## S3. Radius of Influence Calculations

### S3.1 OBJECTIVES

The objective of the radius of influence calculation is to determine the maximum extent to which radionuclides could migrate within the Culebra given reasonable worst-case assumptions. As previously stated, a truly worst-case analysis would assume that flow is totally fracture controlled and that diffusion into the matrix is neglected. Under these conditions, the radionuclides would theoretically be able to travel about 13,480 km in 10,000 years. However, the Culebra Dolomite is known to be porous in some core samples and porosity has been measured in the Culebra based upon these core samples. Therefore, the extreme worst-case radius of influence of 13,480 km does not fit the conceptual model of the site. The following discussion assumes a dual-porosity conceptualization, as selected by DOE in the 1992 PA, although other conceptualizations are also conceivable.

### S3.2 PROBLEM CONCEPTUALIZATION

The conceptual model for the radius of influence calculations consists of horizontal two-dimensional steady-state flow within the Culebra as is the case for the 1992 PA. The repository has been decoupled from the Culebra; meaning that the repository is a source of contaminant mass in the Culebra but fluid flow from the repository is considered negligible. In this manner, the flow of water from the repository into the Culebra does not effect groundwater velocities in the Culebra. Simple constant and slug source terms were used in the model to introduce radionuclides (plutonium) into the Culebra. The model domain stretches for 100 kilometers downgradient of the source.

The flow system simulated to compute the radius of influence is not tied to any geographic location. The model was designed to illustrate reasonable worst-case travel distances based upon data reported for the Culebra Dolomite. The flow system is assumed to be one-dimensional with a uniform steady-state velocity parallel to the X-direction in the model. Even though a three-dimensional model was used in these analyses, there are no vertical hydraulic gradients in the system. These are the same assumptions that were used in the SECO modeling for the 1992 PA.

Three different types of source terms were simulated, as described in the following sections. These include (1) a slug source, (2) a line slug source, and (3) a constant source. In the slug

source, 27 nodes were initially set to a concentration of 1.0. A 3 x 3 block of nine nodes was specified as the source in each model layer. The center of this contaminant "slug" was located 100 km upgradient from the model boundary. The contaminant slug defined by this nodal region was released in the simulation and no additional mass was injected during the simulation. The line slug source was similar to the slug source, except that the slug was assumed to stretch from one side of the model to the other in the Y-direction. This causes the problem to reduce to a one-dimensional simulation (i.e., lateral dispersion is neglected). The final source configuration is the constant source, in which three nodes are held at a constant concentration value of 1.0. One constant concentration node is located in each of the three layers. Thus, the three nodes lie on top of each other at the same geographic location.

### S3.3 MODEL FORMULATION

The STAFF3D model for the radius of influence calculations consists of 54,000 nodes and 35,282 elements in 3 planes. The grid spacing ranges from 5 m near the source to 500 m at the outer edges of the mesh. Numerous runs were initially performed to design a stable finite-element mesh. Early simulations experienced convergence problems when the aspect ratio (ratio of the long side of a rectangular cell to the length of the short side) exceeded 100 to 1. Even the final mesh, which had an aspect ratio of 100:1, required that the number of iterations in the solution be increased from the default of 600 to 1600. The finite-element mesh is shown in Figure S3.1.

Stability problems were encountered in the radius of influence model because of the small amount of mass in the system (especially for the slug source runs), high groundwater velocities, and the large scale of the problem. The latter relates to the size of individual elements and the amount of computer memory available for the simulation. In order to make the problem practical to solve in a reasonable amount of time, the number of nodes was kept to a maximum of 54,000. This meant that grid spacings needed to be quite large away from the source.

Boundary conditions for the 100 km grid consist of fixed head boundaries at the upgradient and downgradient ends of the model. The heads were chosen to provide a gradient across the model of 0.0032 m/m. This value was computed from available water-level data measured in the Culebra in the vicinity of WIPP. The lateral edges and the bottom of the model were assumed to be no-flow boundaries. Recharge to the Culebra was assumed to be zero.

SCALE 1 inch = 3500 data units

100 Km Finite-Element Mesh

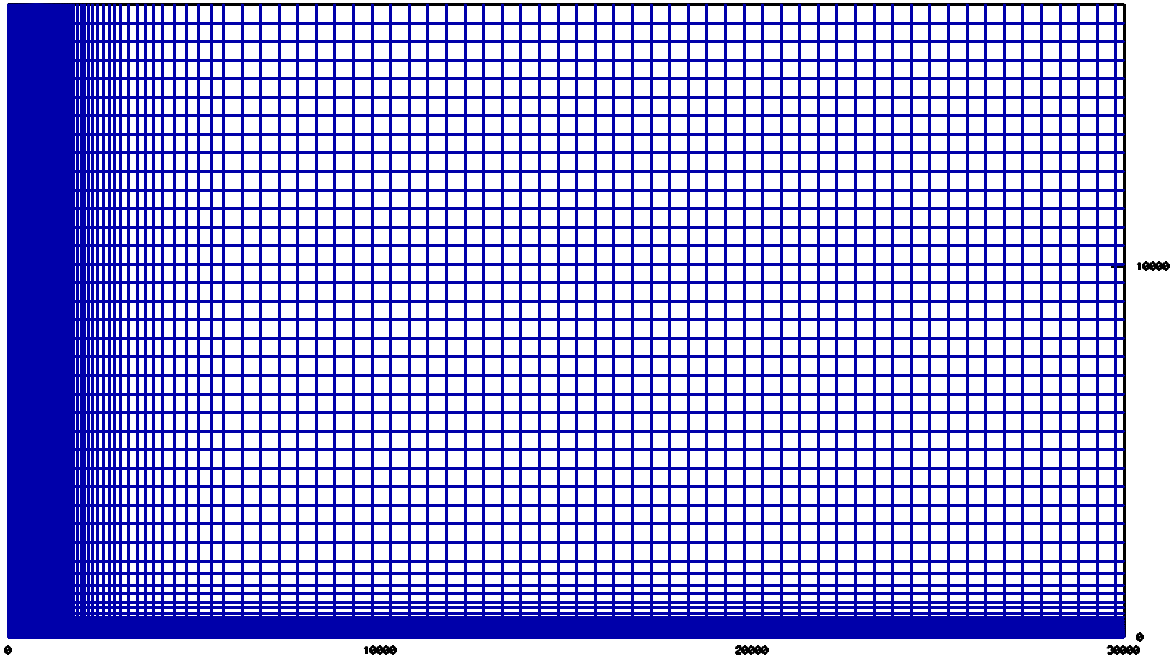


Figure S3.1 Finite-element mesh for the radius of influence simulations (NOTE: only the first 30 km of the mesh is shown).

#### Explanation

- Finite-element grid extends to 100 km (only 30 km shown)
- Source located 732.5 m from the west edge of model and along southern edge
- Heads held constant on west and east edge of model domain
- North and south boundaries are no-flow
- Two-dimensional steady-state flow assumed

Aquifer properties were assumed to be homogeneous within the Culebra. All simulations assumed a dual-porosity medium with fracture hydraulic conductivity of 421,240 m/yr, fracture porosity of 0.0000166, and fracture spacing of 7.7 m. These values were computed for the Culebra assuming a single horizontal fracture as described in Section 2. Transport parameters were also assumed to be homogeneous. To maximize physical retardation, the diffusion coefficient was chosen as the

highest value reported in the 1992 PA ( $9.46 \times 10^{-3} \text{ m}^2/\text{yr}$ ). All other parameters are summarized in Table 3.1 under the “100 Km Mesh” heading.

There are three models listed in Table 3.1, (1) 100 Km Mesh, (2) Repository/Culebra Model, and (3) Grid Convergence Model. The 100 Km Mesh refers to the radius of influence modeling reported in this section. The other two models will be described in subsequent sections of this report.

Table 3.1. Input Parameters for Dual Porosity Simulations

	100 Km Mesh	Repository/ Culebra Model	Grid Convergence Model
<b>RADIONUCLIDE — Pu-239</b>			
Kd (m <sup>3</sup> /kg)	0.0	0.0	0.0
Diff. Coeff. Pu-239 (m <sup>2</sup> /y)	9.46E-03	9.46E-03	9.46E-03
Half life Pu-239 (y)	24070	24070	24070
<b>BOREHOLE</b>			
Retardation Factor	<sup>1</sup> NA	1	NA
Hyd. Conductivity (m/y)	NA	1200	NA
Effective Porosity	NA	0.25	NA
Density (kg/m <sup>3</sup> )	NA	1230	NA
Long. Dispersivity (m)	NA	10	NA
Diameter (m)	NA	0.355	NA
<b>REPOSITORY</b>			
Retardation Factor	NA	1	NA
Initial Pressure (M Pa)	NA	15	NA
Density (kg/m <sup>3</sup> )	NA	1230	NA
Hyd. Conductivity (m/y)	NA	37.9	NA
Specific Storage (m <sup>-1</sup> )	NA	0.001	NA
Effective Porosity	NA	0.2	NA
Brine water flux rate	NA	40	NA
No. of prescribed flux nodes	NA	2	NA
Long. Dispersivity (m)	NA	10	NA
Ratio of (long/transverse) Dis.	NA	10	NA
<b>SALADO</b>			
Retardation	NA	1	NA
Fluid Density (kg/m <sup>3</sup> )	NA	1230	NA
Hyd. Conductivity (m/y)	NA	7.59E-07	NA
Specific Storage (m <sup>-1</sup> )	NA	9.58E-08	NA

Table 3.1. Input Parameters for Dual Porosity Simulations (Continued)

	100 Km Mesh	Repository/ Culebra Model	Grid Convergence Model
Tortuosity	NA	0.14	NA
Porosity	NA	0.01	NA
Long. Dispersivity (m)	NA	15	NA
Ratio of (long/transv.) Disp.	NA	10	NA
<b>CULEBRA Matrix Properties</b>			
Retardation Factor	1	1	1
Effective Porosity	0.139	0.139	0.139
Specific Storage (m <sup>-1</sup> )	1.96E-07	1.96E-07	1.96E-07
Hyd. conductivity (m/y)	7.1	7.1	7.1
Tortuosity	0.0	0.00	0.0
Fluid Density (kg/m <sup>3</sup> )	1090	1090	1090
<b>CULEBRA Fracture Properties</b>			
Retardation Factor	1	1	1
Fluid Density (kg/m <sup>3</sup> )	1090	1090	1090
Hyd. Conductivity (m/y)	421,240	16,560 421,240	16,560 421,240
Tortuosity	0.0	0.0	0.0
Fracture spacing (m) (single)	3.85	0.03 3.85	0.03 3.85
Fracture Porosity	1.66E-05	4.23E-04 1.66E-05	4.23E-04 1.66E-05
Porosity within Fractures	1	1	1
Specific Storage (m <sup>-1</sup> )	1.96E-07	1.96E-07	1.96E-07
Long. Dispersivity (m)	100	100	100
Ratio of (long/transv.) Disp.	10	10	10

<sup>1</sup> Not Applicable

#### S3.4 DESCRIPTION OF SIMULATIONS

### S3.4.1 Slug Source

The first simulation assumed the source configuration to be a 10 meter cube within the Culebra with a plutonium concentration of 1.0. The slug was released at the beginning of the simulation and tracked for 10,000 years. Concentrations were monitored at downgradient nodes in the STAFF3D model over time to determine travel distance of the contaminant slug. A plot of concentration versus time at selected downgradient nodes is presented in Figure S3.2. The plot shows breakthrough at the 2 km node but not at the 5 km node. Note that this run experienced some instability as the front moves past a given point. The instability is exhibited by the oscillation in concentration after the peak concentration is reached on each curve.

Attempts were made to alleviate the instabilities from the slug source simulations by reducing the time step size and by scaling dispersivity based upon cell size. The latter was done to keep the Peclet number at a constant value of 2. The Peclet number is computed as follows:

where:

$P_e$  = Peclet number

$V$  = Darcy velocity

$D$  = Dispersion coefficient

$x$  = grid spacing

The numerical solution of the transport equation becomes unstable if the Peclet number becomes too large. None of these attempts resulted in better stability; therefore, alternative source configurations were simulated. Note that the solution is stable until the peak concentration passes a given point. Oscillations occur at the trailing edge of the plume, probably due to very small amounts of mass in the system dispersed over a very large area.

INPUT FILE: 100KM\SLUG\S 100K.DAT

Dual Porosity - K=421,240 m/yr - Slug Source

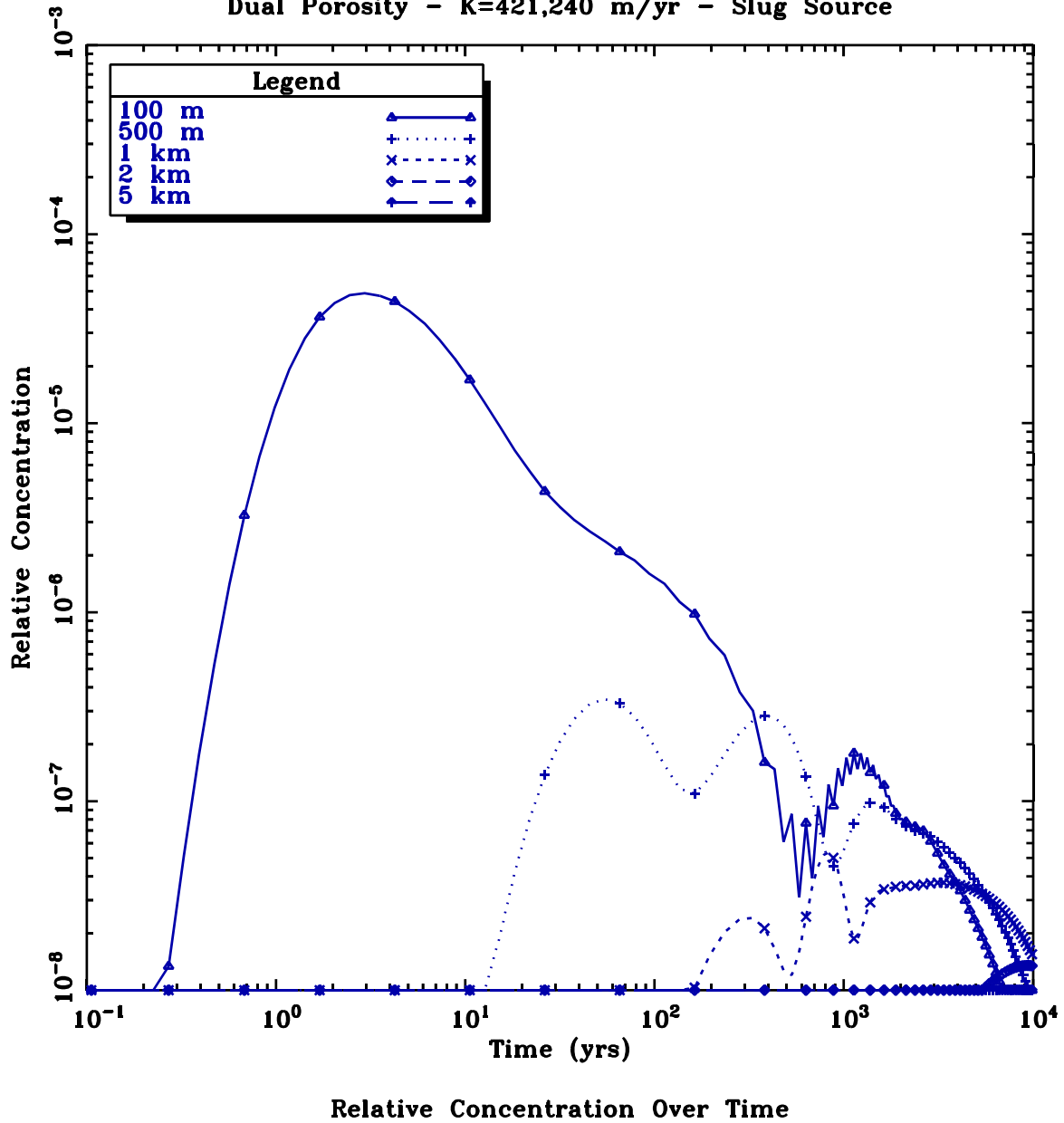


Figure S3.2 Breakthrough curves for a slug source in the radius of influence model.

Explanation

- Concentration vs. time plotted at observation nodes

- Nodes are located downgradient of the source (repository) at distances shown in legend

#### S3.4.2 Line Slug Source

The source was altered to be a linear source stretching laterally across the finite-element mesh. This type of source reduces the problem effectively to one dimension and eliminates lateral dispersion as a potential problem. The line source is not representative of the repository source but since it is designed solely to estimate the potential distance traveled downgradient of the repository, it is appropriate for the intended purpose.

The plot of concentration versus time is shown in Figure S3.3. This source configuration results in greater numerical stability than the 10 meter cubic source described in the last section. While there is some oscillation in concentration values as the front passes a given point, it is much less pronounced than with the cubic source.

The line slug source simulation shows that the maximum extent of contaminant movement is about 5 kilometers downgradient of the source. This is shown on Figure S3.3 as the breakthrough curve is just starting to rise about a relative concentration of  $1 \times 10^{-8}$  at 10,000 years. The center of mass of the plume has not reached 5 km, however, the leading edge of the plume has migrated 5 km within 10,000 years.

Each break-through curve in Figure S3.3 shows a rapid increase in concentration followed by a gradual concentration decline after reaching a peak. A typical break-through curve for a porous aquifer would show a symmetric curve. The gradual decline in concentration in the dual-porosity case is caused by matrix diffusion.

The apparent contaminant velocity may be determined from the breakthrough curves by computing the time at which the peak concentration passes a given point. The velocity is then computed as distance of the observation point from the source divided by time of peak concentration. In this case, the velocity is approximately 25 m/yr for the 100 meter observation point, but only 5 m/yr at the 500 m observation point. These apparent velocities were computed by observing the time to reach peak concentration in Figure S3.3 and dividing the time into the distance of the observation (100 and 500 m, respectively). Note that the peak at 500 meters is not as sharp as at 100 meters. Again, matrix diffusion causes apparent migration velocity to

decrease downgradient as the contaminant diffuses into the matrix and is held there until the front passes.

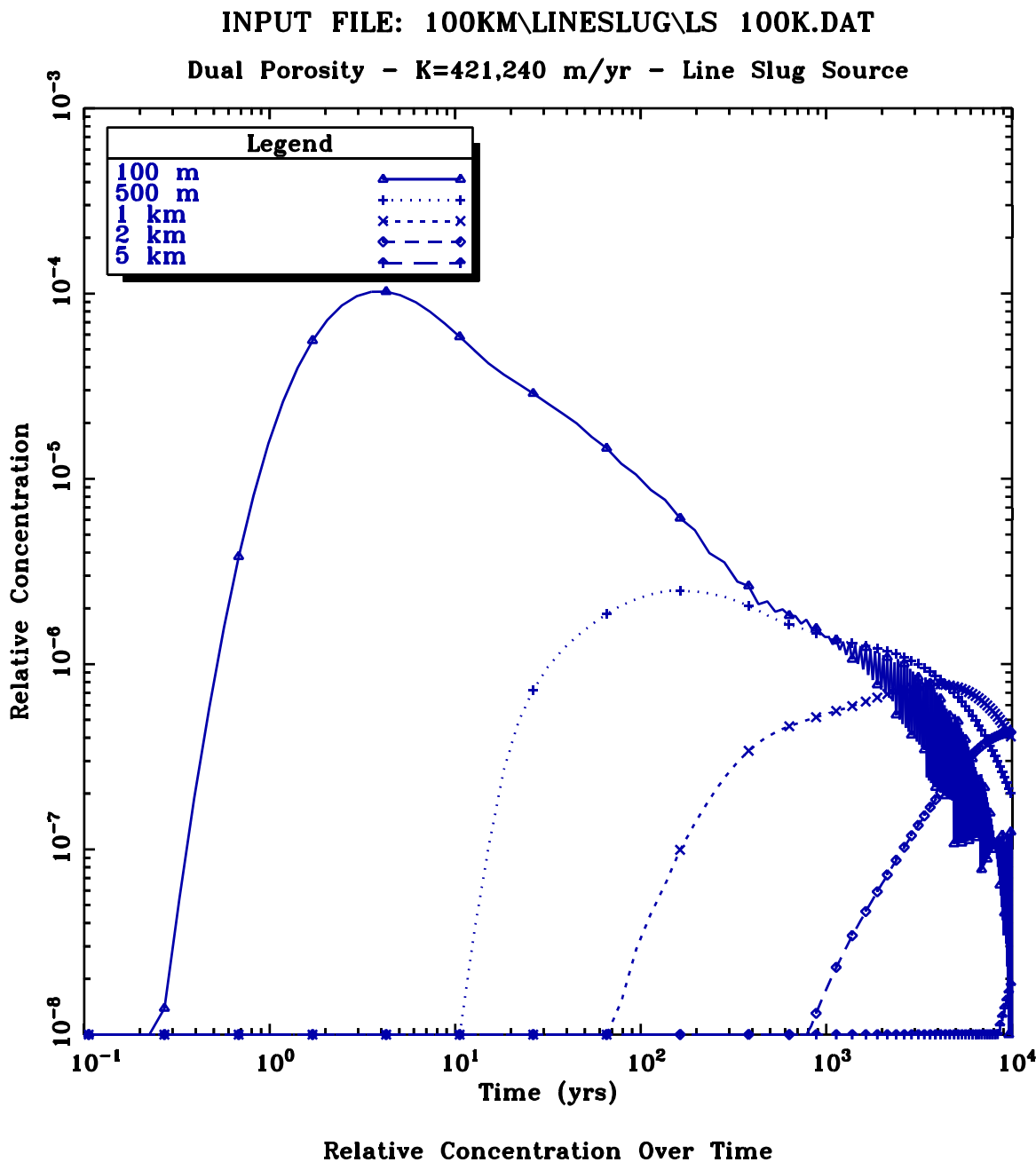


Figure S3.3 Breakthrough curves for a line slug source in the radius of influence model.

Explanation

- Concentration vs. time plotted at observation nodes

- Nodes are located downgradient of the source (repository) at distances shown in legend

Remember that the travel distance in a single fracture system without matrix diffusion would be about 13,480 km. Thus, matrix diffusion provides an effective retardation factor of over 2,700. Note that all simulations in this report assume no chemical retardation of plutonium in either the fractures or in the matrix. All apparent retardation is caused by matrix diffusion.

### S3.4.3 Constant Source

A constant source simulation was conducted to further stabilize the oscillations in the slug source runs. This approach eliminates the oscillations; however, the breakthrough curves are more difficult to interpret. There are no peaks on a constant source breakthrough curve because the source concentration is held constant for the 10,000 year simulation. This causes observed concentrations at downgradient nodes to increase over time and ultimately reach a plateau. As with the line slug source described in the previous section, this source is not meant to represent the repository, but rather is used to infer travel distance for the radius of influence analysis. The plot of concentration versus time for this scenario is shown in Figure S3.4.

The constant source simulation shows no instability compared to the slug source runs because there is more mass in the system and it is added continuously. However, determination of travel time is more difficult to interpret as there is no peak concentration. The constant source breakthrough curves are similar to the slug source at early time values. The first part of the curve where concentration increases rapidly is due to dispersion. If there were no dispersion, the contaminant concentration would arrive at the monitoring point instantaneously for both the slug and constant sources and determination of travel time would be simple. Dispersion causes a smearing of the contaminant front as shown at early time values for both the slug and constant sources.

The conclusion from the constant source run is the same as for the slug source runs. The maximum extent of downgradient migration is about 5 kilometers. Obviously, there is a significant difference between this value and the travel distance computed based upon purely fracture flow. Some of this difference could be due to the fact that all of the current simulations and those presented in the main report assumed that there was no resistance or skin effect along the fracture walls. This assumption allows for the maximum amount of contaminant to migrate into the matrix. Mineral and clay deposits along fracture walls could lower the rate at which

contaminants may diffuse into the matrix. The 1992 PA assumes that the fracture walls are clay-lined, however, it appears that this was done to allow for different distribution coefficients to be assigned to the fracture and the matrix. It is not known whether a skin resistance factor was used in the SECO modeling. It appears, however, that modeling results will be very sensitive to the value chosen for skin resistance. Additional simulations should be performed to assess the sensitivity of skin resistance and discretization of matrix elements in STAFF3D on travel times.

INPUT FILE: 100KM\CSOURCE\C 100K.DAT

Dual Porosity - K=421,240 m/yr

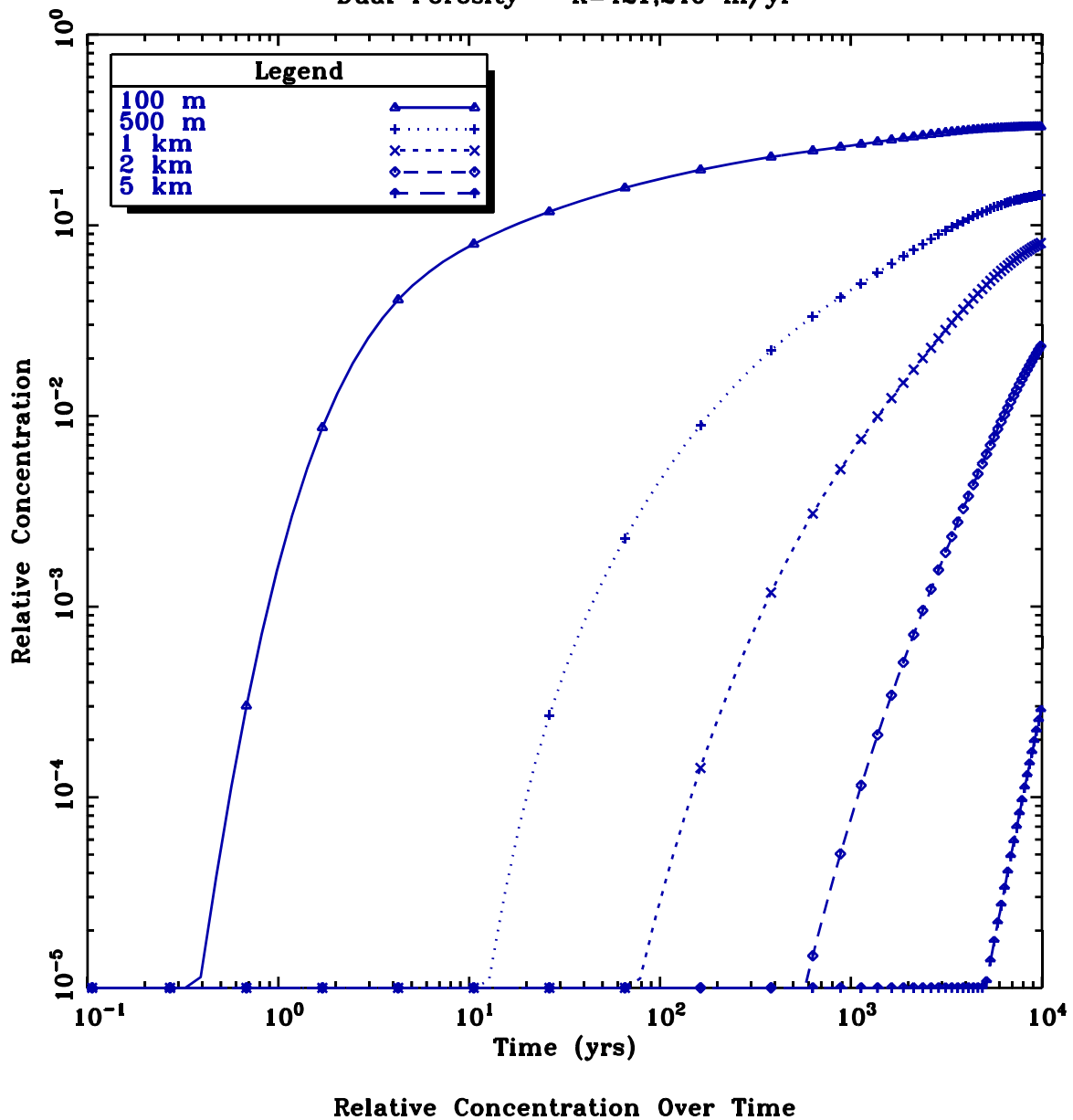


Figure S3.4 Breakthrough curves for a constant source in the radius of influence model.

Explanation

- Concentration vs. time plotted at observation nodes

- Nodes are located downgradient of the source (repository) at distances shown in legend

## S4. Grid Convergence Analysis

### S4.1 OBJECTIVES

The objective of the grid convergence analysis is to determine the effect of grid refinement on the results of the STAFF3D modeling presented in the main report. Grid convergence is an issue for all numerical codes being applied at WIPP. If the BRAGFLO modeling presented in the PA was based upon a grid that was too coarse, the results could be inaccurate or misleading. Numerical models are approximations of the mathematical equations where the dependent variable (e.g., concentration or head) is computed at discrete points. The approximation becomes more accurate as the spacing between points (often called discretization) becomes smaller. It is unclear to what extent grid convergence studies have been performed by SNL in support of the WIPP modeling. However, grid convergence studies should be an integral component in numerical modeling analyses to assure that the necessary accuracy is achieved.

### S4.2 PROBLEM CONCEPTUALIZATION

The conceptual model for the grid convergence calculations consists of horizontal steady-state flow within the Culebra. The repository has been decoupled from the Culebra. A transient source term was used in the model to introduce radionuclides (plutonium) into the Culebra at the same rate and concentration as computed from the original STAFF3D model described in the main report. The model domain stretches for 3.3 km downgradient of the source (borehole).

### S4.3 MODEL FORMULATION

The STAFF3D model for the grid convergence calculations consists of 38,346 nodes and 25,092 elements in 3 planes. The mesh measures 6400 m in the direction of groundwater flow and 3205 m perpendicular to flow. The grid spacing ranges from 5 m near the source to 50 m at the outer edges of the mesh. The finite-element mesh is shown in Figure S4.1.

SCALE 1 inch = 750 data units

### Mesh for Grid Convergence Simulation

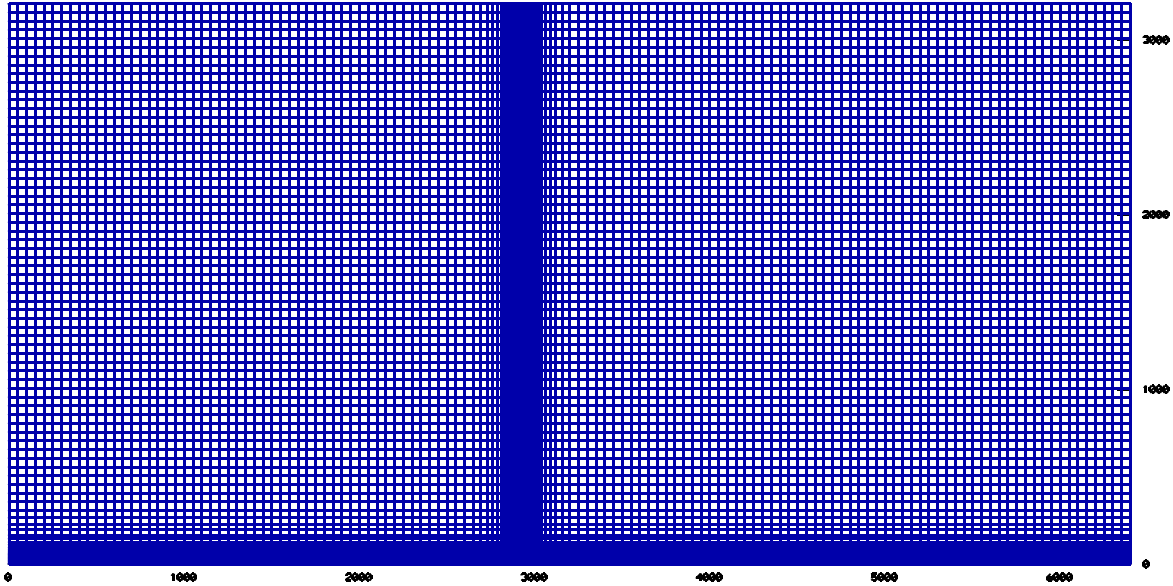


Figure S4.1 Finite-element mesh for the grid convergence simulation.

#### Explanation

- Source located 2900 m from the west edge of model domain along the southern edge
- Flow is from west to east with constant heads at the west and east boundaries
- North and south boundaries are no-flow

The original mesh described in the main report measured 6437 m by 3218 m with 4,370 nodes per layer. The Culebra was simulated with 2 planes (layers) of nodes. The minimum grid spacing in the original mesh was 15 m and the largest spacing was 150 m.

Boundary conditions for both finite-element meshes consist of fixed head boundaries at the upgradient and downgradient ends of the model. The heads were chosen to provide the same gradient (0.0032) used in the previous STAFF3D modeling (described in the main report). This value was computed from available water-level data measured in the Culebra.

Aquifer properties were assumed to be homogeneous within the Culebra for each model. All simulations assumed a dual-porosity medium with fracture hydraulic conductivity of 16,560 m/yr, fracture porosity of 0.000423, and fracture spacing of 0.06 m. Transport parameters were also assumed to be homogeneous. The diffusion coefficient was chosen as the maximum value reported in the 1992 PA ( $9.46 \times 10^{-3} \text{ m}^2/\text{yr}$ ). All other parameters are summarized in Table 3-1.

#### S4.4 DESCRIPTION OF SIMULATIONS

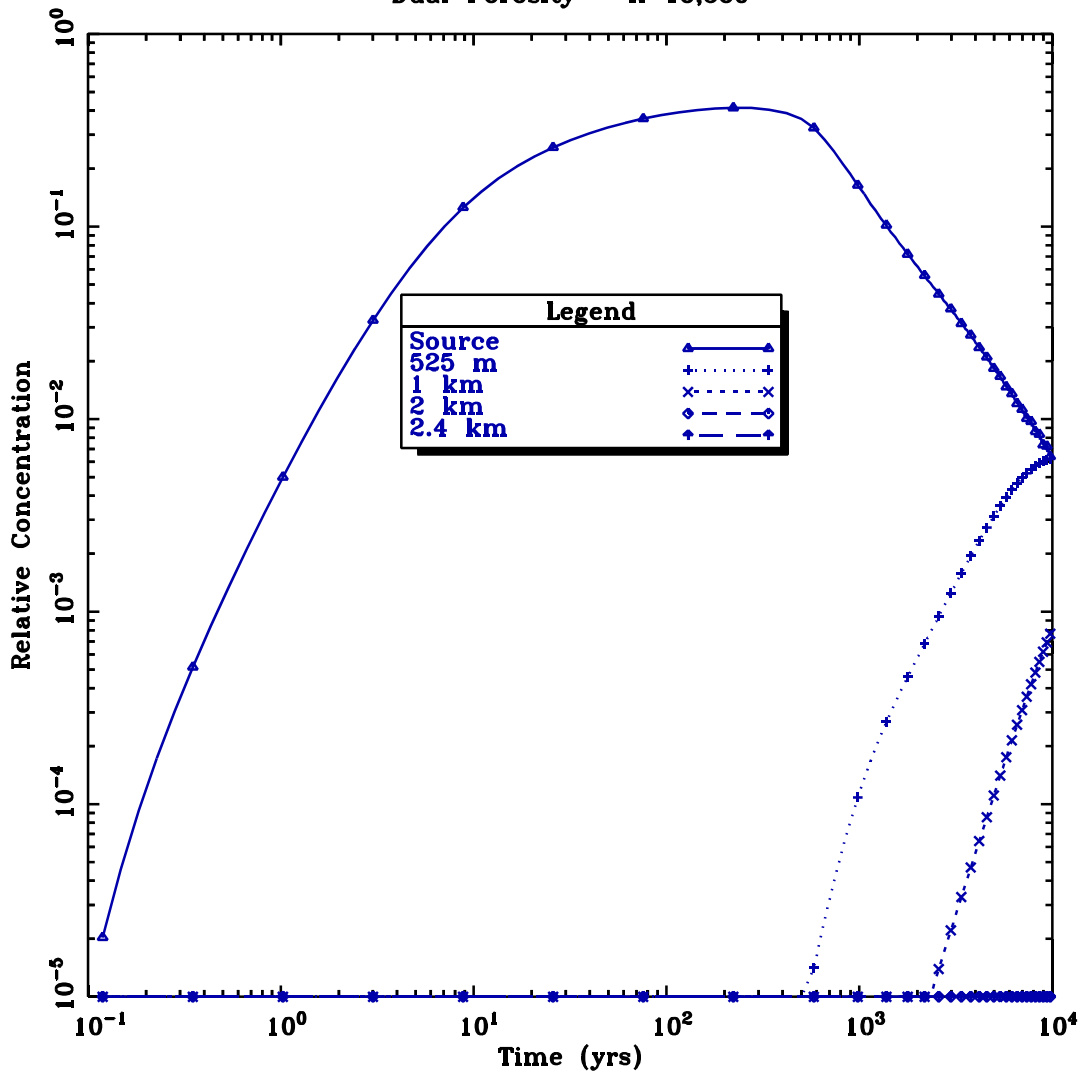
The objective of the grid convergence simulation was to check whether a finite-element mesh with a much finer discretization than the original simulation reported by SC&A (1995) would result in significantly different results. All other parameters and boundary conditions in the model were identical. Due to computer memory limitations, however, the repository could not be simulated. Therefore, the refined mesh was created for the Culebra flow system only. A transient flux boundary condition was used to simulate the borehole in order to make the two simulations as close as possible in all factors except the mesh spacing. The original finite-element mesh used 8,740 nodes in 2 planes to simulate the Culebra flow system. The refined mesh incorporated 54,000 nodes in 3 planes.

Relative concentration versus time was plotted for the original model and for the refined model, as shown in Figures S4.2 and S4.3, respectively. The parameters for both models are reported in Table 3.1. The original model (described in the main report) is referred to in Table 3.1 as the Repository/Culebra model and the refined model is the Grid Convergence model. The concentration at the borehole is also plotted to verify that the source terms for the two simulations were similar. While there are differences, the overall effect is close enough for comparison. The relative source concentration using the coarser mesh reaches a peak of about 0.4, while the relative source concentration using the finer mesh reaches a peak of about 0.6. More importantly, the time to reach the peak concentration is virtually the same in both cases.

Contaminant breakthrough times for the refined mesh are somewhat sooner than for the original mesh. Relative concentrations reach a peak at 1 km in about 3,000 years for the refined mesh, whereas the peak for the original mesh, with the larger nodal spacings, occurs sometime after 10,000 years. These differences are probably due to less numerical dispersion in the refined mesh. With less dispersion, the contaminant does not spread laterally as far as in the original

INPUT FILE: BCASE\LO K\BCASE-PU.DAT

Dual Porosity - K=16,560



Relative Concentration Over Time

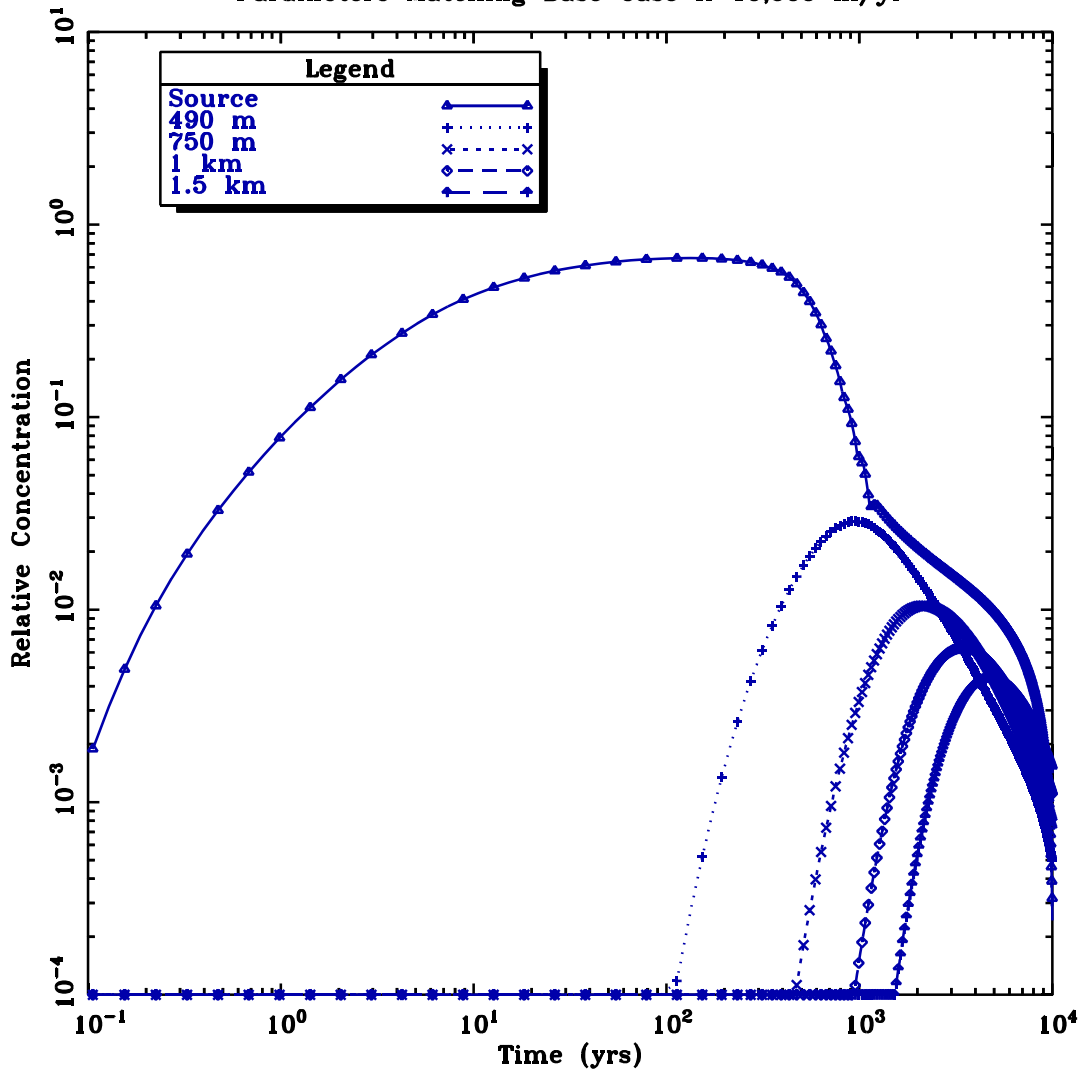
Figure S4.2 Breakthrough curves for the original model.

Explanation

- Concentration vs. time is plotted at observation nodes
- Nodes are located downgradient of the source (repository) at distances shown in legend

INPUT FILE: 4MNHID TRS1.DAT

Parameters Matching Base Case K=16,560 m/yr



Relative Concentration Over Time

Figure S4.3 Breakthrough curves for the Grid Convergence model.

Explanation

- Concentration vs. Time plotted at observation nodes
- Nodes located downgradient of the source (repository) at distances shown in legend
- Model with smaller mesh spacings than results presented in Figure S4.2.

model. Consequently, there is less matrix diffusion taking place to slow the advancement of the plume.

The results of this analysis indicate the importance of grid convergence studies in numerical modeling. Refined nodal networks can give different results when compared with coarse meshes. It is not possible to determine the optimum nodal spacing without conducting such a grid convergence study.

## S5. Repository Decoupling Analysis

### S5.1 OBJECTIVES

The repository decoupling analysis was performed to evaluate the effect of borehole flux on the flow field in the Culebra. The model used in this analysis was the same one reported by SC&A (1995).

### S5.2 PROBLEM CONCEPTUALIZATION

The conceptualization for the repository decoupling scenario is the same as described in the main report (See Section 4.0 in the main report) for the STAFF3D simulations including the repository. In this case, however, the borehole flux is not simulated by the flow model but the flux of contaminants is introduced through a transient solute flux term. Thus, the only difference between the original model and the decoupled model is the injection of fluid from the borehole into the Culebra. The difference between the two simulations is that the original simulation disturbed the Culebra flow field by injecting water and the decoupled simulation does not disturb the uniform gradient in the Culebra. Contaminant mass is introduced at approximately the same rate, however, in both models.

### S5.3 MODEL FORMULATION

The original mesh described in the main report measured 6437 m by 3218 m with 4,370 nodes per layer. The Culebra was simulated with 2 planes (layers) of nodes. The minimum grid spacing in the original mesh was 15 m and the largest spacing was 150 m.

Boundary conditions for the finite-element mesh consist of fixed head boundaries at the upgradient and downgradient ends of the model. The heads were chosen to provide the same gradient (0.0032) used in the previous STAFF3D modeling. This value was computed from available water level data measured in the Culebra (See Section 4.3.4 in the main report).

Aquifer properties were assumed to be homogeneous within the Culebra. All simulations assumed a dual-porosity medium with fracture hydraulic conductivity of 16,560 m/yr, fracture porosity of 0.000423, and fracture spacing of 0.06 m. Transport parameters were

also assumed to be homogeneous. The diffusion coefficient was chosen as the maximum value reported in the 1992 PA ( $9.46 \times 10^{-3} \text{ m}^2/\text{yr}$ ). All other parameters are summarized in Table S3.1.

#### S5.4 DESCRIPTION OF SIMULATIONS

As described above, repository decoupling removes the flux of water migrating up the borehole into the Culebra. Thus, the only difference between the original simulation and the decoupled simulation is the effect of the borehole flux on the Culebra flow field.

The repository decoupling was simulated in three steps. First, the concentration and fluid flux data were recorded at the borehole in the original repository/Culebra model described in the main report. These data were then reformatted as a transient flux boundary condition for STAFF3D. Finally, the transient flux data were added to a new data set in which groundwater flow in the Culebra was assumed to be at steady-state and the borehole source was removed. This produced a flow field with a uniform one-dimensional gradient in the Culebra (the same as in the 1992 PA).

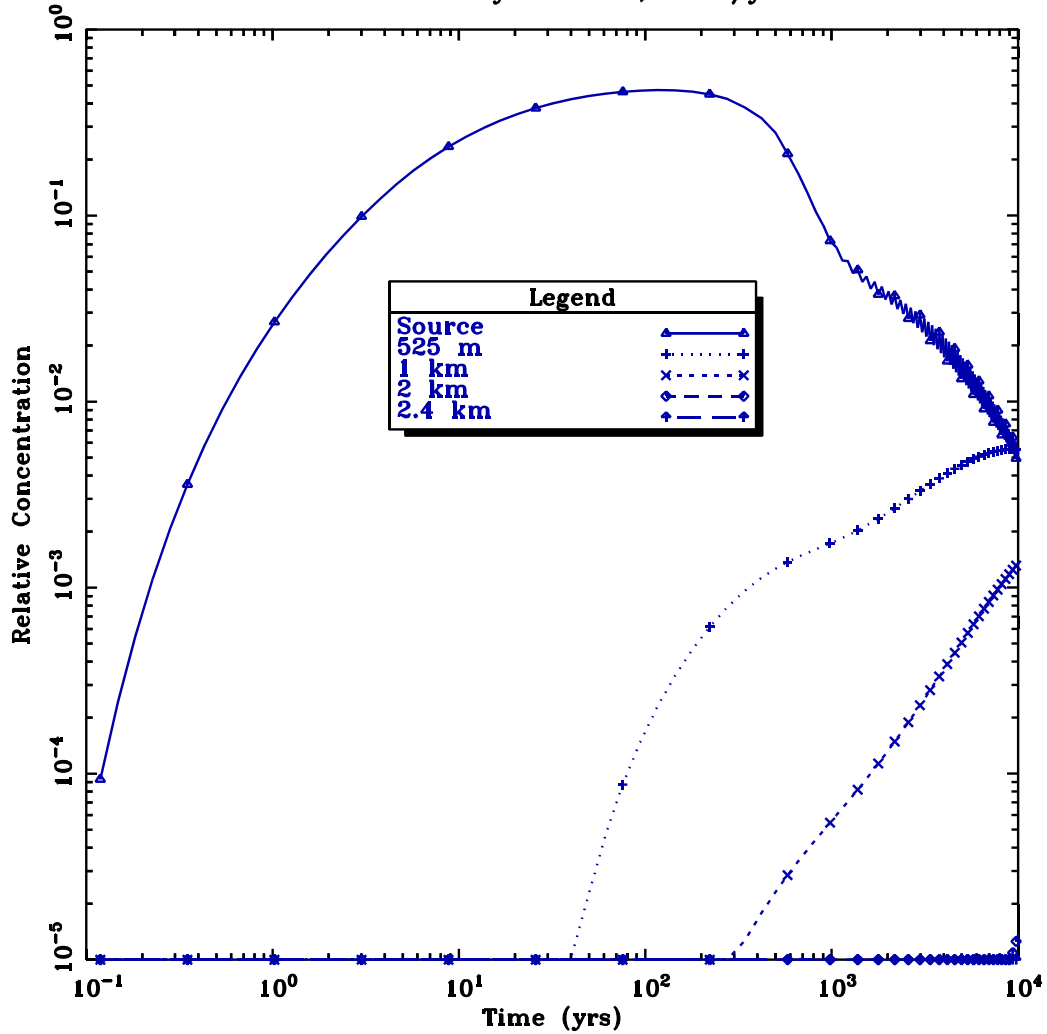
The repository decoupling simulation shows that flux from the borehole can have a significant impact on contaminant transport. Breakthrough curves of concentration versus time were plotted for the original simulation (Figure S5.1) and for the scenario with the repository decoupled (Figure S5.2). In the original simulation with borehole flux injected into the Culebra flow system, the time at which relative concentrations exceeded  $1 \times 10^{-5}$  at a downgradient distance of 1 km occurred at about 300 years. In the decoupled system, where borehole flux does not disturb the flow system, the time increased to about 2000 years. The maximum contaminant concentration after 10,000 years at 1 km from the borehole decreased from  $1 \times 10^{-3}$  in the original simulation to  $2 \times 10^{-4}$  in the decoupled simulation. The cumulative mass leaving the downgradient boundary in the decoupled model was also an order of magnitude lower than the original simulation. These simulations indicate that the flux from the borehole can be an important component in the Culebra flow system and should not be neglected, as it was in the 1992 PA.

The repository decoupling analysis was conducted without the additional brine flux potentially derived from the Castile. Addition of this flux, as in the E1-type simulations described in the main report, would cause even larger differences between the two

simulations. Additional simulations should be performed with the refined mesh described in Section 4 and adding the brine flux from the Castile.

INPUT FILE: BCASE\HI K\BCASE-PU.DAT

Dual Porosity - K=421,240 m/yr



Relative Concentration Over Time

Figure S5.1 Breakthrough curves for the original model with the repository.

Explanation

- Concentration vs. time plotted at observation nodes
- Nodes located downgradient of the source (repository) at distances shown on legend

INPUT FILE: BCASE\DECOUPL\BCASE-PU.DAT

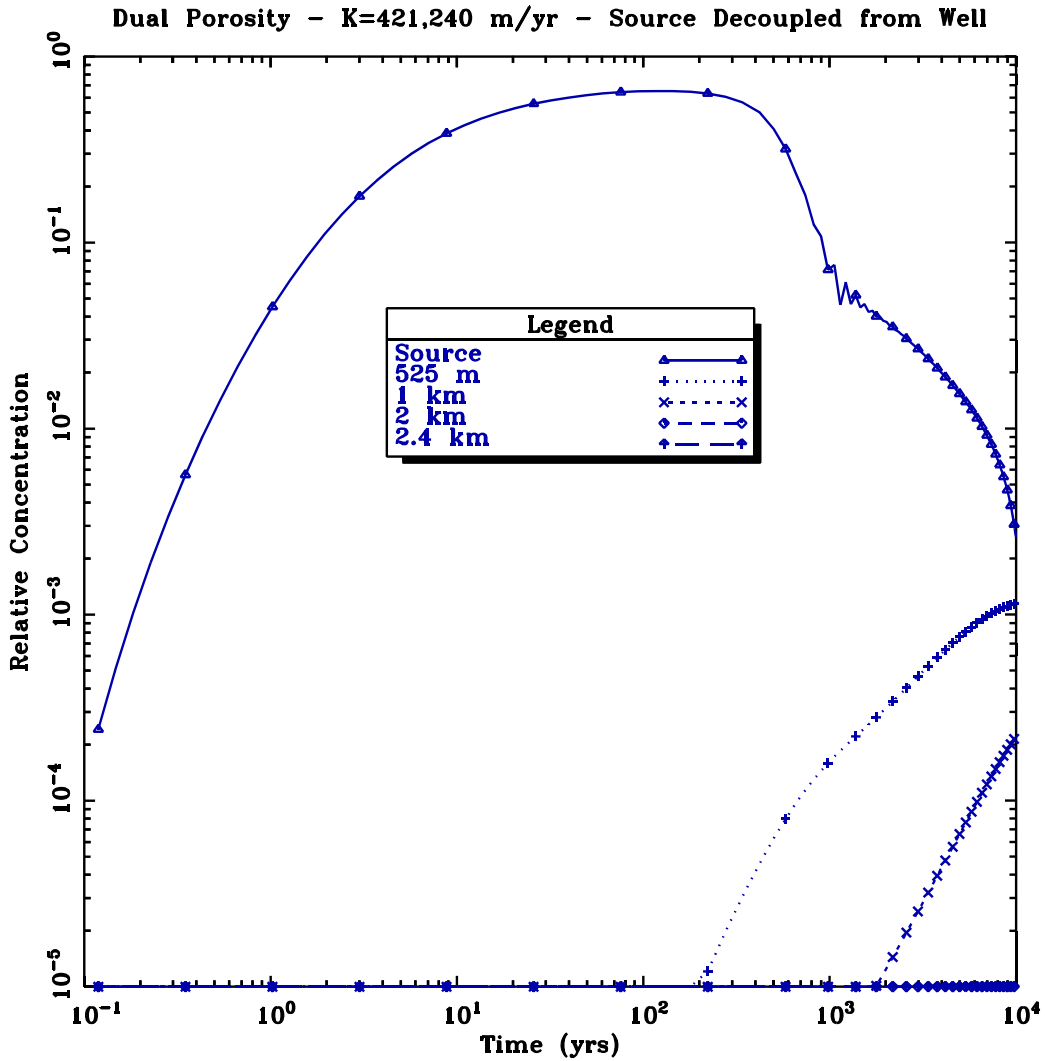


Figure S5.2 Breakthrough curves with the repository decoupled from the Culebra.

Explanation

- Concentration vs. time plotted at observation nodes
- Nodes located downgradient of the source (repository) at distances shown in legend

## S6. References

- Gale, J.E., 1982, Assessing the permeability characteristics of fractured rock, Geological Society of America, Special Paper 189, in Recent Trends in Hydrogeology, edited by T.N. Narasimhan, p. 163-181.
- Snow, D.T., 1969, Anisotropic permeability of fractured media, Water Resources Research, vol. 5, no. 6, p 1273-1289.